The nucleoplasmic reticulum form, formation, and function

A thesis submitted for the degree of Doctor of Philosophy

Lior Pytowski



Hilary term 2022

Investigation executed in the laboratory of

Prof. David J.T. Vaux,

Sir William Dunn School of Pathology,

And

Lincoln College, University of Oxford



SIR WILLIAM DUNN SCHOOL OF PATHOLOGY

Abstract

Many primary cells, cell lines and cells *in situ* in tissues may have under certain circumstances a network of invaginations of the nuclear envelope. This network called the nucleoplasmic reticulum (NR) brings deep within the nucleus the conventional functions of the nuclear envelope such as anchorage and regulation of genetic material and transport of ions and macromolecular cargo. Abundant NR is a hallmark of cancer cells and senescence.

We hypothesised that the NR may be involved in the exchange of material across the nuclear boundary. To investigate that, we had a tripartite approach where we (i) study NR assembly and disassembly; (ii) investigate the NR structure and explore whether there is bidirectional nucleocytoplasmic exchange of material; (iii) explore the changes in gene expression leading to or resulting from the induction of NR formation.

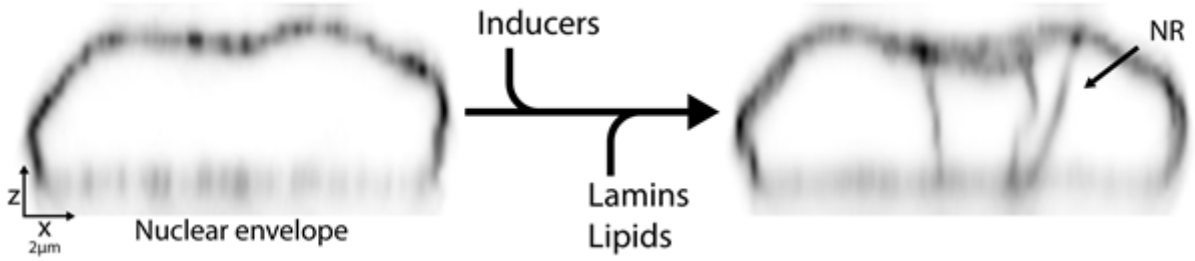
We tagged endogenous Lamin A and Lamin B1 with fluorophores and found that this enables the acquisition of long time-courses, in live cells, with minimal phototoxicity. We demonstrated that the addition of a fluorophore to the N-termini of both lamins does not affect the toxicity of saquinavir. We observed that the assembly and disassembly of NR can occur in interphase without the nuclear envelope reassembly step of mitosis. Moreover, we established that the membrane curvature-associated reticulon, RTN4, can be found on NR and NE, but that it is not required for NR assembly.

To address whether the NR is involved in the exchange of material across the nuclear envelope we explored its structure. We found that the invaginations of the nuclear envelope may contain a cytoplasmic core and nuclear pore complexes. Using photocleavable proteins we detected import of fluorophores across the NR. Finally, we explored NR abundance relative

to the cell cycle and nuclear volume. We found that immediately after mitosis nuclei have abundant NR but that, although some are disassembled, there is a net increase in NR abundance if the nuclei become more voluminous or polyploid. We also found that when colonies are derived by clonal expansion from single cells there is a correlation between the slowest growing colonies, with the fewest cells, and the highest abundance of NR per cell.

Finally, we investigated the changes in gene expression leading to or resulting from inducing the NR physiologically or pathologically, and identified five genes that are significantly changed in both conditions. Changes in specific pathways have also been identified and include a reduction in some lipid related pathways. In parallel we observed that cells from patients with dysfunctional CCTα have increased NR abundance indicating that a reduction in the canonical lipid pathways may lead to an increase in NR abundance caused by the scavenger pathways.

Overall, we have demonstrated that the NR is a structure that is formed by a highly regulated and dynamic machinery that incorporates newly synthesised elements and that it is involved in the exchange of material across the nuclear envelope.



Acknowledgments

Doing this thesis has been a lifelong endeavour that was only possible thanks to all the people and experiences that shaped me - both directly and indirectly. This obviously begins with no other than my parents and family that laid down the foundations to who I am today.

Throughout my academic career many have contributed to my development: my friends, my colleagues, my mentors, and my supervisors all gave me what I needed to achieve this.

More recently within the lab, department, college, and university many more have contributed to my development thought both minor and major contributions that all let to the completion of this project.

Undeniably one of the contributors to the success of this endeavour were those of you that I interacted with on a daily basis during this DPhil and provided me with the guidance, support and supervision necessary to its completion.

This project would have not been possible without the developers, maintainers and supporters of open-source software, free courses, and free virtual assistance.

This project has been enabled by all the people, institutions and organisations that provided assistance and funding throughout my whole academic path.

And for this I am grateful to you all.

Table of Contents

Abstract III
Acknowledgments V
List of figures IX
Contributions XII
Abbreviations XIII
1. Introduction 1
1. Introduction 1
2. Architecture and function of the nuclear envelope 3
The nuclear envelope 3
The Lamina 4
The Nuclear Pore Complex 7
The LINC complex 10
Biophysical properties of lipids in the nuclear membrane 12
3. A diverse range of invaginations of the nuclear envelope 13
4. NR structure 15
5. NR formation 17
"Pushing in" 17
"Pulling in" 18
Dedicated machinery 18
6. NR Function 20
7. Hypothesis and aims of the thesis 22
2. Materials & Methods 23
1. Chemicals, reagents, materials 23
Key chemicals, reagents 23
Plasmids 23
DNA purification 24
Cell culture products 25
Antibodies 25
Microscopy 26
2. DNA amplification, purification, and cloning 26
Bacterial cell culture 26

Competent bacteria preparation 27
Bacterial cell transformation 27
Purification of plasmid DNA from bacterial cells 27
DNA cloning 28
3. Mammalian cell culture 28
Cell lines and their origin 28
General cell culture technique 29
NR formation induction of cells in culture 29
Plasmid transfection of mammalian cells in culture 29
4. Generation of cell lines by CRISPR 30
Overall strategy 30
gRNA plasmid generation 30
Donor plasmid generation 31
Transfection and cell sorting 31
5. NGS 32
mRNA isolation 32
mRNA-seq library construction 32
Data analysis: 33
6. Light microscopy 33
Immunolabelling of cultured cells 33
Light microscopy 34
Image analysis 35
3. NR assembly and disassembly in interphase 38
1. Introduction 38
2. Results 44
NR formation 52
NR disassembly 55
Role of membrane-curvature proteins in NR biogenesis 59
3. Discussion 63
4. Role of NR in bidirectional nucleocytoplasmic transport 68
1. Introduction 68
2. Results 73

3. Discussion 91
5. Global transcriptome analysis of NR induction 96
1. Introduction 96
2. Results 100
Links between lipid metabolism and NR formation 112
3. Discussion 120
6. Perspective and future directions 124
7. References 134

List of figures

Figure 1-1: Invaginations often appear as spots in the XY axis of the nucleus but when observed on the XZ axis their tubular shape becomes apparent **2**

Figure 1-2: Post-translational modifications of Lamin A and Lamin B..... **6**

Figure 1-3: Diagram of the nuclear import machinery **9**

Figure 1-4: Diagram of the LINC complex structure displaying the positions of Nesprin2 relative to the whole complex..... **11**

Figure 1-5: Three non-exclusive models for NR formation..... **17**

Figure 1-6: The nuclear envelope is highly dynamic..... **19**

Figure 3-1: Tagging of the lamina allows us to observe the nuclear envelope and nucleoplasmic reticulum in live cells..... **45**

Figure 3-2: Cell survival vs Saquinavir concentration. WT and mNeonGreen Lamin A expressing cells are equally sensitive to Saquinavir..... **46**

Figure 3-3: Denoising allows accurate low SNR (low magnification) nuclei counting..... **48**

Figure 3-4: The NR is enriched in both Lamin A and Lamin B1 compared to the rest of the nuclear envelope..... **49**

Figure 3-5: NR formation in endometrial cells is reversible and cell cycle independent **51**

Figure 3-6: NR Formation with nucleoplasmic leak **54**

Figure 3-7: NR disassembly. U-2 OS cells with endogenous labelled Lamin A-mNeonGreen. **56**

Figure 3-8: montage of a nucleus in 3D where one invagination's is disassembled while another is not **57**

Figure 3-9: Quantification of NR disassembly..... **58**

Figure 3-10: Perinuclear RTN4-GFP abundance and intensity within foci does not change when NR formation is induced with Saquinavir **60**

Figure 3-11: Reticulon 4 is present in the proximity of nuclear envelope infoldings and invaginations **61**

Figure 3-12: Reticulon 4 knockdown by siRNA reveals that it is not essential for NR formation **62**

Figure 4-1: NR abundance is correlated to nuclei volume and DNA content **74**

Figure 4-2: Advanced analysis of NR count vs volume and DNA density from previous figure **76**

Figure 4-3: NR contains a cytoplasmic core **77**

Figure 4-4: Nups and LINC are found in the nucleoplasmic reticulum **79**

Figure 4-5 When NR formation is pharmacologically induced with oestrogen and progesterone, invaginations are first formed then NPC and LINC are recruited to the NR **80**

Figure 4-6: Synchronous release of a cargo targeted to the nucleus can be achieved by photocleaving the fusion protein CD2-Photocleaveable protein-FP-NLS with UV light in HCT cells **82**

Figure 4-7: The LEXY system allows export of material from cytoplasm to nucleoplasm **84**

Figure 4-8: H4-mCherry intensity profile is steeper than LEXY mCherry across the nuclear envelope **86**

Figure 4-9: Colonies resulting from single cells can have very different resulting sizes **88**

Figure 4-10: Analysis of the U-2 OS colonies resulting from single cells **89**

Figure 4-11: Further analysis of data in Figure 4-10 revealing the relationship between nuclear area versus DNA content, nuclear area versus nuclear circularity and mean Lamin A mNeonGreen brightness and DNA content **90**

Figure 5-1: Number of genes with p-adj<0.02 when NR formation is induced with either Saquinavir or Hormones **100**

Figure 5-2: qPCR validation of the RNA-Seq experiments **101**

Figure 5-3: RNA expression changes in cancer versus healthy tissue **106**

Figure 5-4: No specific chromosome is significantly changed by Saquinavir in Ishikawa cells **108**

Figure 5-5: No specific chromosome is significantly changed by Oestrogen and Progesterone in Ishikawa cells **109**

Figure 5-6: Venn diagram of miRNA expression changes in Saquinavir and Hormones treatment **111**

Figure 5-7: NR abundance increased in patients with some mutations in the PCYT1A gene. **113**

Figure 5-8: Electron microscopy of PCYT1A mutant cells **114**

Figure 5-9: NanoSIMS analysis of Ishikawa cells with NR formation induced with hormones and pulse chased with deuterated choline for 12 hours **116**

Figure 5-10: NanoSIMS analysis of HeLa cells with NR formation induced with Saquinavir and pulse chased with deuterated choline for 12 hours **117**

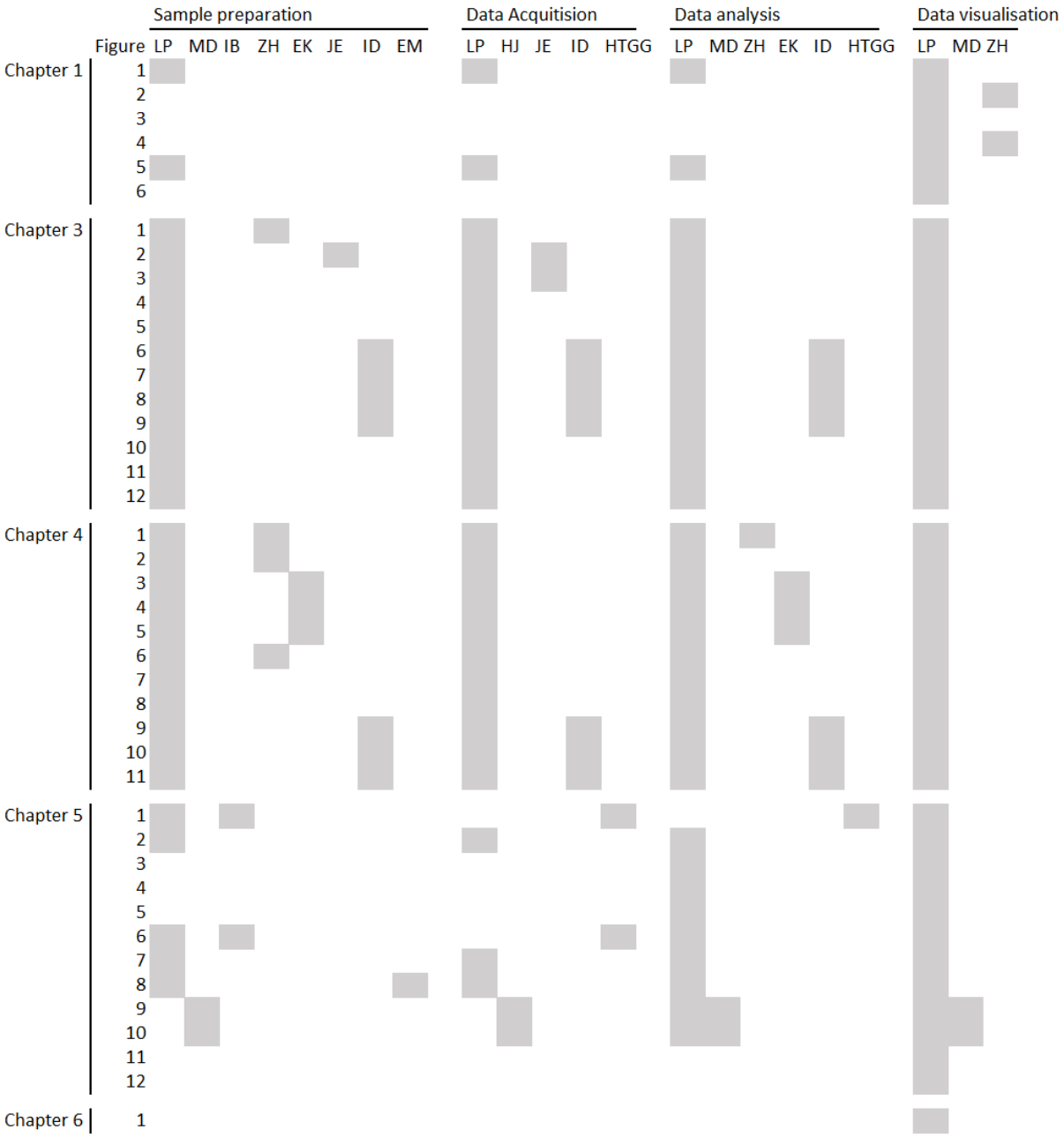
Figure 5-11: Synthesis pathway for Phosphatidylcholine, Phosphatidylethanolamine, Phosphatidylserine and Sphingomyelin in mammalian cells **118**

Figure 5-12: Synthesis pathway for Diacylglycerol, and Phosphatidylinositol in mammalian cells **119**

Figure 6-1: Graphical summary illustrating structure-function **133**

Contributions

Many people contributed to the work presented in this thesis. Their contributions are summarised below:



LP: Lior Pytowski, MD: Marek Drozdz, IB: Ivan Boubriak, ZH: Zayra Hernandez,

EK: Emily Knot*, JE: James Elwell*, ID: Isaac Dennis*, HJ: Haibo Jiang,

EM: Dunn School Electron Microscopy Facility (Errin Johnson, Anna Pielach)

HTGG: High-Throughput Genomics Group at the Wellcome Trust Centre for Human Genetics, Oxford.

Not present in the table but absolutely essential: **David J.T. Vaux** for conceptualization, funding acquisition, guidance and contribution to experiment design, data analysis, reviewing.

*EK, JE, ID: Visiting students under LP's supervision.

Abbreviations

AF: Alexa Fluor

BB: Backbone

BD: Becton & Dickinson

CA: California

CCT-α: CTP:phosphocholine-cytidylyltransferase-a

CD2: Cluster of Differentiation 2

CDKN1C: Cyclin-dependent kinase inhibitor 1C

CFSE: Carboxyfluorescein succinimidyl ester

CMV: Cytomegalovirus

CRISPLD2: Cysteine-Rich Secretory Protein LCCL Domain-Containing 2

CRISPR: clustered regularly interspaced short palindromic repeats

CTP: Cytidine triphosphate

CV-1: Cercopithecus aethiops-1

DAPI: 4',6-diamidino-2-phenylindole

DEP domain: Dishevelled, egl-10 and Pleckstrin domain

DEPTOR: DEP Domain Containing MTOR Interacting Protein

DESeq2: Differential gene expression analysis based on the negative binomial distribution

DMEM: Dulbecco's Modified Eagle's Medium

DMSO: Dimethyl Sulfoxide

DNA: Deoxyribonucleic Acid

EGR1: Early Growth Response 1

ER: Endoplasmic Reticulum

FACS: Fluorescence-Activated Cell Sorting

FBS: Foetal Bovine Serum

FCS: Foetal Calf Serum

FIJI: Fiji Is Just ImageJ

FKBP: FK506 binding protein

FRB: FKBP–rapamycin binding FSG: Fish Skin Gelatine

GFP: Green Fluorescent Protein

GO: Gene Ontology

HA: Homology Arm

HCT: Human Colorectal Carcinoma

HDF: Human Dermal Fibroblasts

IF: Immunofluorescence

INM: Inner Nuclear Envelope

KO: Knock Out

LB: Lysogeny Broth

LCCL: Limulus Clotting Factor C

LINC: Linker of Nucleoskeleton And Cytoskeleton

LBR: Lamin B Receptor

LSM: Light Scanning Microscope

MEF: Mouse Embryonic Fibroblasts

MHC: Major Histocompatibility Complex

MIT: Massachusetts Institute of Technology

MTOR: Mechanistic Target Of Rapamycin

NA: Numerical Aperture

NCBI: National Center for Biotechnology Information

NCS: Nucleolar Channel System

NE: Nuclear Envelope

NEB: New England Bioloabs

Nets: Nuclear Envelope Transmembrane Proteins

mNG: monomeric Neon Green

NGS: Next Generation Sequencing

NLS: Nuclear Localisation Signal

NOGO: Neurite Outgrowth Inhibitor

NPB: Nucleolar Precursor Bodies

NPC: Nuclear Pore Complex

NR: Nucleoplasmic Reticulum

NRK: Normal Rat Kidney Epithelial Cells

NSC: Neural Stem Cells

ONM: Outer Nuclear Membrane

PBS: Phosphate-Buffered Saline

PCR: Polymerase Chain Reaction

PCYT: Choline-Phosphate Cytidylyltransferase A

PECS: Parietal Epithelial Cells

PFA: Paraformaldehyde

RCC1: Regulator Of Chromosome Condensation 1

RFP: Red Fluorescent Protein

RNA: Ribonucleic Acid

ROI: Region Of Interest

RT: Room Temperature

RTN: Reticulon

SD: Sample Deviation

SEM: Standard Error Of The Mean

SIRNA: Small Interfering RNA

SNR: Signal-To-Noise Ratio

SOC: Super Optimal Broth

SUN: Sad1p, UNC-84

TE: Tris-EDTA

UV: Ultraviolet

WT: Wild Type

1. Introduction

"Caminante no hay camino
se hace camino al andar"

Antonio Machado (1875 - 1939)

"Wanderer, there is no path
the path is made by walking"

1. Introduction

The nuclear envelope (NE) was once seen as a simple barrier separating the genomic DNA from the rest of the cell. Many textbooks depict the nucleus as a continuously convex structure, often spherical in form, but it is now well known that the nuclear envelope is a tremendously complex structure that can contain deep infoldings and or branching tubular invaginations (**Figure 1-1**). Given the resemblance of this structure to branched endoplasmic reticulum (ER) networks in the cytoplasm, this

structure has been called the nucleoplasmic reticulum (NR). While it is clear that NR invaginations have the potential to increase nuclear-cytoplasmic interactions in the deep nuclear interior, little is yet known about the formation or function of these invaginations.

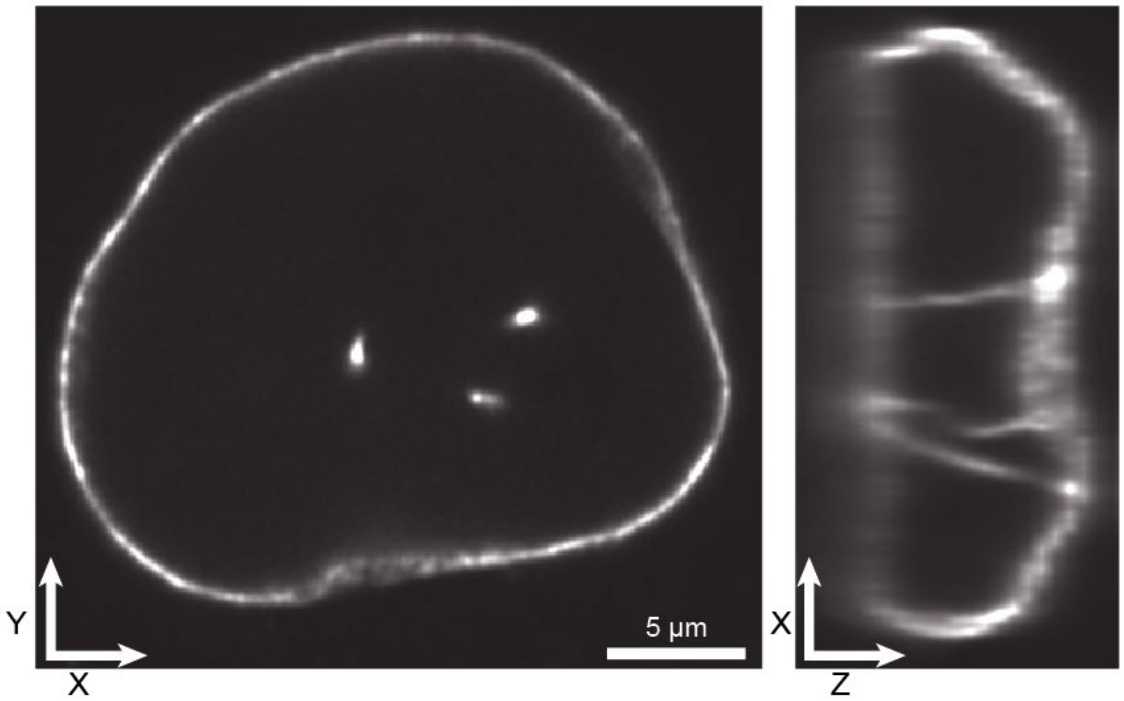


Figure 1-1: Invaginations often appear as spots in the XY axis of the nucleus but when observed on the XZ axis their tubular shape becomes apparent

The nuclear envelope comprises two phospholipid bilayers enclosing an intermembrane space between the inner nuclear membrane (INM) and the outer nuclear membrane (ONM). The nuclear envelope is punctuated with nuclear pore complexes (NPCs) that allow highly regulated exchange of material between the nucleoplasm and the cytoplasm. Between the INM and the chromatin resides a meshwork of intermediate filament proteins called lamins, some with prenylated

carboxy termini affording hydrophobic membrane anchoring, which acts as a scaffold for the nucleus.

Despite the lack of information about NR function, some clues exist. For example, morphological changes of the nuclear envelope, abundance of tubular invaginations and infoldings or nuclear grooves are associated with cancers such as breast cancer and Papillary thyroid cancer (Chow et al., 2012; Fischer, 2014) and can be used as a tool for scoring nuclear pleomorphism and cancer grading (Bussolati, 2008; Kinsella et al., 2013). Whether this association is because NR abundance is causal in some aspect of tumorigenesis, or a consequence of other changes during this process remains to be determined.

2. Architecture and function of the nuclear envelope

The nuclear envelope

The nuclear envelope is a porous structure that separates the nucleoplasm from the cytoplasm. In the animal kingdom, the inner face of the nuclear envelope is covered by a ~25 nm wide meshwork of ~10.5 nm filaments called the Lamina (Aebi et al., 1986). The heterochromatin or condensed chromatin is mostly present in close proximity to the inner nuclear membrane while transcriptionally active euchromatin is further way from the nuclear envelope. The outer nuclear envelope and its 30 to 50 nm wide perinuclear space (Franke et al., 1981; Berrios, 1998) are continuous with the rough endoplasmic reticulum and its lumen such that ribosomes are also present decorating

the outer nuclear membrane, and ER content fills the intermembrane space of the nuclear envelope.

The lipid bilayers are 4 to 5 nm thick (Agrawal and Lele, 2019) and contain dozens of proteins that can be associated in various ways (Korfali et al., 2016; Schirmer and Gerace, 2005). Nuclear envelope transmembrane proteins (NETs) can have one or multiple hydrophobic transmembrane domains (α-helix or β-barrels) that anchor them to the lipid bilayer or amphiphilic domains partially inserted in the surface of the lipid bilayer. Other proteins are coupled to the lipid bilayers by covalently bound lipid chains or oligosaccharides linkers. Finally, membrane-associated proteins can be non-covalently bound to other NETs (Schirmer, 2003; Alberts, 2015).

The overall nuclear envelope thickness varies within the same nucleus, tissues, and species but it is thought to be between 60 to 100 nm wide.

The Lamina

The lamina meshwork provides structural support to the lipid bilayer and chromatin, is a substrate for the anchorage of various proteins that tether specific chromatin domains at sites called LADs (lamin-associated domains; (Briand and Collas, 2020) and regulate gene expression either though chromatin accessibility or sequestration of transcriptions factors (Boubriak et al., 2017; Malhas et al., 2009) and anchoring and positioning of NPC (Burke and Stewart, 2013; Gruenbaum et al., 2000).

The lamina is a 10-20 nm thick meshwork of intermediate filaments divided in two types based on its structure: A-type lamins and B-type lamins (Aebi et al., 1986;

Burke and Stewart, 2013; Dittmer and Misteli, 2011; Gerace and Huber, 2012; Hutchison, 2014). The lamina is composed of B-type lamins (LMNB1 and LMNB2) in most tissues and stages of development while A-type lamins (LMNA and LMNC) are not. The *LmnA* gene encodes primarily the LMNA and LMNC proteins in somatic cells. *LmnA* also encodes for LMNC2 in testis and LMNAΔ10 protein in somatic cells but at variable levels. The Lamin C proteins are derived from Lamin A but with an alternative splicing. The *LmnB1* and *LmnB2* genes respectively encode LMNB1 and LMNB2 in somatic cells. LMNB3 is an alternative splicing of LMNB2 found in testis. All lamins are formed by 3 main sub-units: (i) a head in the N-termini, (ii) a central α-helical rod domain, followed by a nuclear localisation sequence, (iii) a tail in the C-termini with a CaaX motif before maturation.

After translation LMNA, LMNB1 and LMNB2 undergo multiple post-translational modifications (**Figure 1-2**, Burke and Stewart, 2013). The first post-translational modification step is the farnesylation of the C-terminal CaaX motif at the cysteine residue by a farnesyltransferase. This is followed by the cleavage of the aaX motif by FACE2 (farnesylated proteins-converting enzyme 2) for the Lamin B proteins and ZMPSTE24 (zinc metallopeptidase STE24) for pre-Lamin A (Kitten and Nigg, 1991; Sinensky, 1994). The last step for the B Lamins is a carboxy methylation of the C-termini. Pre Lamin A also undergoes prenylation and carboxy methylation of the endoproteolytically cleaved C-terminus but this processing is followed by an additional cleavage of a site 14 residues upstream of the modified C terminus by the endoprotease ZMPSTE24/FACE1 after being incorporated in the lamina (Corrigan, 2005).

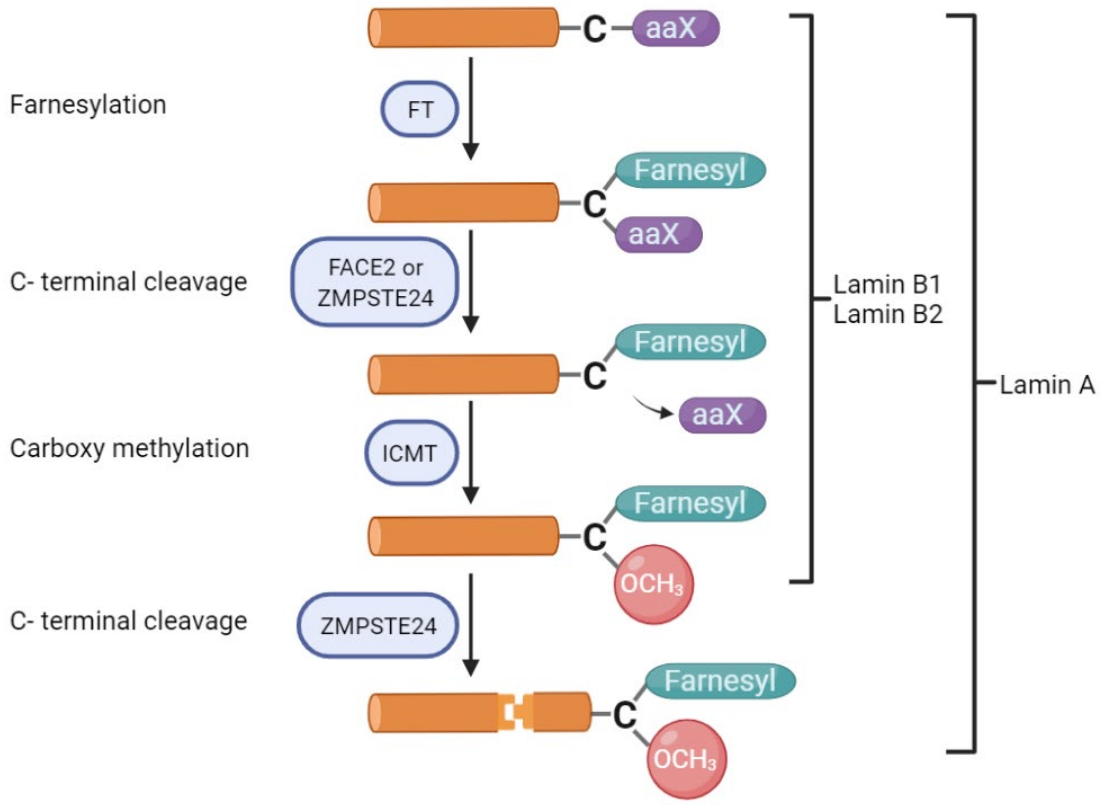


Figure 1-2: Post-translational modifications of Lamin A and Lamin B. *FT: Farnesyltransferase; FACE: farnesylated proteins-converting enzyme 2;* ZMPSTE24*: Zinc Metallopeptidase STE24; ICMT: isoprenylcysteine carboxylmethyltransferase. Figure inspired from Burke and Stewart, 2013.*

The lamina is a meshwork of intermediate ~10 nm intermediate filaments but individual Lamin monomers are 1.75 nm thick. Lamin monomers dimerise by intercalating their rod-domains and form 3.5 nm thick dimers held by hydrophobic interactions (Ahn et al., 2019). Linear head-to-tail polymers of dimers follow. Anti-parallel association of polymers form protofilaments that themselves form another anti-parallel association that makes the final ~10 nm wide intermediate filaments (Dittmer and Misteli, 2011). Lamin B and A are anchored to the nuclear envelope by the Lamin B receptor protein (Olins et al., 2010; Ye and Worman, 1994). Likewise, Emerin anchors

LMNA to the inner nuclear envelope (Bengtsson and Wilson, 2004). Both Lamin B receptor (LBR) and Emerin are involved in gene expression regulation.

Mutations in lamins are responsible for over 17 diseases termed Laminopathies (Worman, 2011). The main diseases are muscular dystrophies, lipodystrophies, and premature aging. There are over 350 *LmnA* mutations associated with all Laminopathies (Dittmer and Misteli, 2011) while only two diseases (lipid dystrophy and leukodystrophy) are associated with mutations of the *LmnB1* or *LmnB2* (Hegele et al., 2006; Padiath, 2006).

The Nuclear Pore Complex

The nuclear envelope has pores (known as nuclear pore complexes, NPC) that regulate the exchange of proteins between the cytoplasm and nucleoplasm (Callan and Tomlin, 1950). The NPC is a complex that forms a ~120 nm wide, ~40 nm long channel with a ~50 nm aperture across the nuclear envelope made up of ~30 structural proteins known as nucleoporins (Nups). The central pore of the channel has 3 layers: (i) the membrane layer that holds the NPC in the lipidic bilayer, (ii) a scaffold layer, (iii) a phenylalanine-glycine (FG) Nups, forming a low complexity filamentous layer prone to hydrogel formation that serves as a filter in the central channel. The cytoplasmic face of the channel has a ring with ~50 nm long filaments that capture proteins of the import machinery to be imported into the nucleus. The nuclear face of the channel has also a ring with filaments that form a ~75 nm long basket with a distal ring at the end (Goryaynov et al., 2012; Hampoelz et al., 2019; Kabachinski and Schwartz, 2015).

Small molecules < ~40 kDa can passively diffuse thought the NPC but larger ones need to be actively shuttled though the nucleoporin diffusion barrier. Proteins are imported to the nucleus if they have a nuclear localisation signal (NLS) exposed on their surface. Importin α, from the cytoplasmic pool, binds to these nuclear localisation signals then Importin β binds to Importin α. This cargo with the Importin α -β complex sequentially displaces low complexity FG domain interactions in the barrier nucleoporins of the channel to permit nuclear import via the NPC channel without compromising the overall diffusion barrier for macromolecules. Once in the nucleoplasm, RanGTP displaces Importin β and Nup 50 from the nuclear basket and binds to Importin α which leads to the release of the cargo in the nucleoplasm. A CAS-RanGTP displaces Importin α from Nup 50 (**Figure 1-3**). RCC1 phosphorylates RanGDP into RanGTP. Both importins are exported to the cytoplasm and are released and the cycle can repeat (Marfori et al., 2011; Stewart, 2007).

Proteins with nuclear export signals (NES) bind to exportins that form a complex with RanGTP. This trimeric complex is then exported to the cytoplasm and dissociates releasing its cargo. And the cycle can repeat. Both import and export can happen simultaneously through the same NPC (Weberruss and Antonin, 2016).

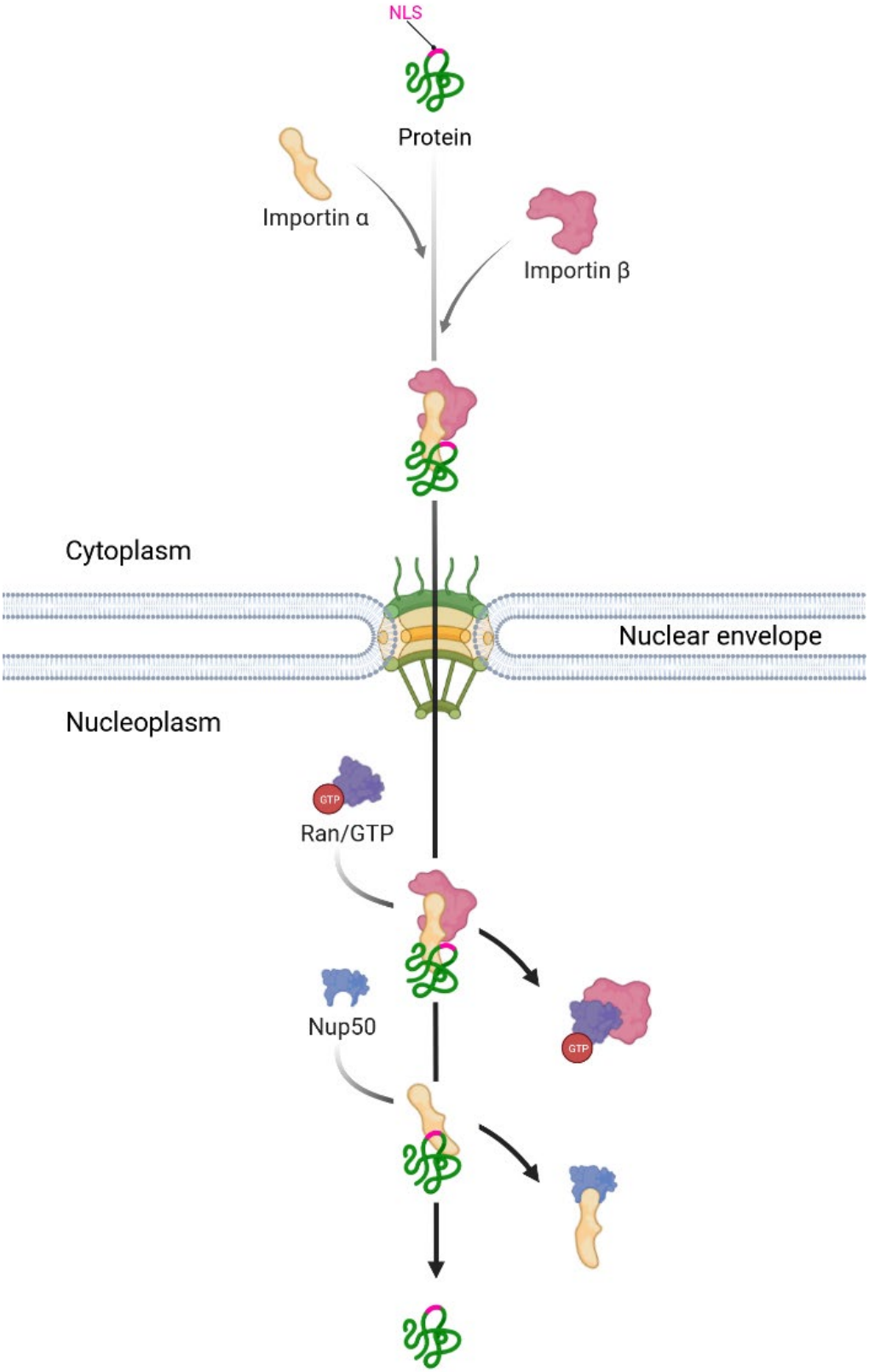


Figure 1-3: Diagram of the nuclear import machinery. *Diagram created in BioRender, with inspiration from "TRPS1 Transport into the Nucleus".*

The LINC complex

Another set of proteins contribute to the structural integrity of the double layer membrane of the nuclear envelope by providing linkages between the inner and outer nuclear membranes. In so doing, they also provide anchor points for cytoplasmic cytoskeletal attachment to the nuclear envelope, and a mechanism for transmission of force to the inner side of the nuclear envelope. In this way, the LINC complex (Linker of Nucleoskeleton and Cytoskeleton) connects the cytoskeleton to the nucleoskeleton (including the lamina). The LINC complex contributes to the mechanical integrity of the nuclear envelope and is involved in mechanotransduction (Liu et al., 2016; Wong et al., 2021).

SUN trimers' span the perinuclear space, and their transmembrane domains are anchored in the INE and interact with the nuclear lamina. In the outer nuclear membrane, KASH domains bridge the cytoplasmic Nesprins with the perinuclear SUN domains. The Nesprins connect the KASH domains to the cytoskeleton. Motor proteins can bind to the cytoskeleton and LINC's KASH proteins and displace or deform the nucleus (**Figure 1-4**).

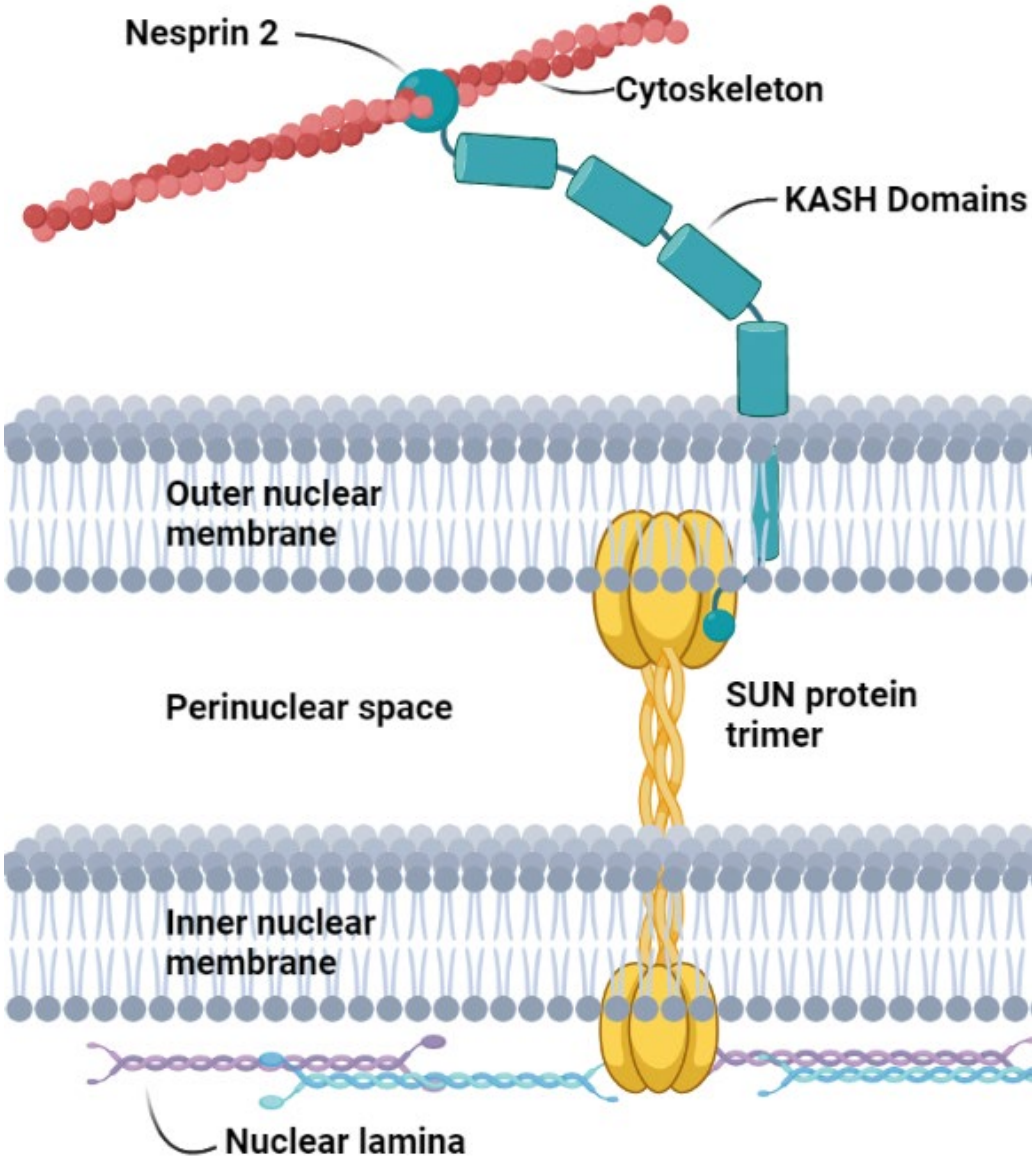


Figure 1-4: Diagram of the LINC complex structure displaying the positions of Nesprin2 relative to the whole complex. *Diagram created in BioRender.*

Evidence for the role of these proteins in the organisation of the nuclear envelope comes from knockout experiments. For example, knockdown of SUN leads to the dilation of the perinuclear space to 100 nm or more (originally 30 to 50 nm wide) (Crisp, 2006).

Biophysical properties of lipids in the nuclear membrane

The main component of the nuclear envelope are the lipids that compose the bilayers. Hydrophobic forces naturally make the lipids create sheets and membranes, but the lipid composition also influences how thick or thin and how flat or curved the membranes are. The effect of a certain lipid on the curvature of a membrane will depend on its shape and is defined by the relative steric size of the hydrophilic head group versus the hydrophobic fatty acyl chains (Cooke and Deserno, 2006; Domart et al., 2012; Chung et al., 2018). Additionally, this will be affected by the electric charges of the lipid (Dickey and Faller, 2008) and the hydration radius (Hirama et al., 2017). Due to their conical shape - with larger tails than heads-, Phosphatidic acid (PtdOH), Cholesterol, Phosphatidyl-ethanolamine (PtdEth) and diacylglycerol (DAG) induce negative curvatures in membranes. Phosphatidyl-choline (PtdCho) and phosphatidyl-serine induce no curvature as they are cylindrical in shape. Finally, Lyso-PtdOH, Lyso-PtdCho and Phosphatidyl-inositol (PtdIns) inverted conical shape - with larger heads than tails - induce positive curvature in membranes (Cooke and Deserno; Larijani et al., 2022). Additionally, the changes in lipid density themselves can alter membrane curvature (de Jesus et al., 2014).

The curvature of a membrane is defined by its lipid and protein composition. In order to create a tube made of a lipid membrane, each leaflet would need to have a combination of lipids with larger tails than heads plus lipids having larger tails than heads. The abundance of cylindrical lipids will determine the diameter of the tube. The inner leaflet will have more negative than positive curvature inducing lipids while the

outer leaflet will have more positive than negative inducing lipids. Each leaflet needs both types of lipids so that there are no voids between the lipids that would create lipid-packing defects. However it is in the sites with high tension or packing defects that proteins may be inserted (Peeters et al., 2022).

The focal accumulation of either proteins that have a particular interaction with specific lipids or the delivery/consumption of specific lipids may induce curvature in the membrane. Accumulation of enzymes that are rate-limiting in the lipid synthesises, accumulation of flippases, accumulation of proteins that self-interact with curvature inducing lipids may all contribute to development of local membrane shape changes (Graham and Kozlov, 2013). This is elaborated in more details in the general discussion.

3. A diverse range of invaginations of the nuclear envelope

There are two types of invaginations of the nuclear envelope. Invaginations comprising only the INM are called type I invaginations and invaginations comprising the INM and the ONM are called type II invaginations (Malhas et al., 2011). Type II invaginations contain a cytoplasmic core that has been shown to have diffusional connectivity to the bulk cytoplasm (Fricker et al., 1997). Invaginations may penetrate partially the nucleoplasm, or they may traverse the nucleus from side to side. The invaginations may have branches that extend in multiple directions. This network of invaginations is called the nucleoplasmic reticulum (NR).

Different kinds of invaginations were reported in a variety of healthy and pathogenic tissues as well as in primary and immortalised cells in tissue culture. Tubular

invaginations were reported in HeLa (Fricker et al., 1997; Peddie et al., 2014), HDF, mouse pre-adipocytes (Drozdz et al., 2017); in NSC34 neural cell line (Mavlyutov et al., 2017); in breast carcinoma and stromal cells (Rappa et al., 2017); in human mammary epithelial cells (Jorgens et al., 2017), ventricular myocytes (Plačkić et al., 2016), 3T3 cells and MEFs (Legartová et al., 2014), G8, Vero, PHK, NRK, PECS, CV-1 (Fricker et al., 1997) muscle cells (Avedanian et al., 2011) (additional references in (Malhas et al., 2011). Deep and wide infoldings of the nuclear envelope were found in frog gonocytes (Haczkiewicz et al., 2017). These invaginations are not restricted to the animal kingdom as both protrusions and invaginations containing various organelles have been reported in plants such as in *Silene involucrate* mesophyll cells (Giełwanowska et al., 2014), and onion epidermal and tobacco cells (Collings et al., 2000) .

Nuclear envelope invaginations are found in every stage of development as embryonic nuclei may have invaginations as well. The properties of invaginations are species dependent; for example, bovine embryonic nuclei have invaginations containing small cytoplasmic cores while rabbit embryo cells have both nuclear invaginations with small and large cytoplasmic cores (Popken et al., 2016).

The NR may show dynamic physiological regulation, by hormones, for example. Human endometrial cells contain in midluteal phase a nucleolar channel system (NCS). This NCS is a membranous organelle formed of several layers of tubular cisternae emerging from the nuclear envelope (Guffanti et al., 2008; Kittur et al., 2007). This NCS is absent in female patients using oral contraceptives and in infertile women (Dockery et al., 1997; Nejat et al., 2014).

Of another kind, intranuclear vesicles connected to the nuclear envelope with a cytoplasmic core enriched with the RNA-binding protein Unr were described in trophoblast giant cells (Saltel et al., 2017).

The invaginations are found in every phase of cell cycle: from G1 and S to G2 as well as in prophase prior to the nuclear envelope breakdown (Beaudouin et al., 2002; Hebbar et al., 2008; Salina et al., 2002; Turgay et al., 2014).

Wrinkles of the nuclear envelope are found in countless tissue culture cells, often depending on the confluency of the cells, and are sometimes mis-identified as NR in low resolution imaging or when visualising grazing sections of the nuclear envelope. For this reason, great care is necessary when identifying, and especially when quantifying, these structures.

4. NR structure

The NR, being continuous with the nuclear envelope, and by extension the ER, has a similar composition to the rest of the nuclear envelope. Type II NR contains NPCs connecting the cytoplasm to the nucleoplasm in its double-membraned wall while type I NR having only the INM does not (Avedanian et al., 2011; Fricker et al., 1997; Goulbourne et al., 2011; Legartová et al., 2014; Malhas et al., 2011). It has been observed that the cytoplasmic core of type II NR may contain cytoskeletal elements (including actin, cytokeratin, intermediate filaments and microtubules) mitochondria, and ribosomes (Jorgens et al., 2017). Both types of NR are in contact with A and B type

lamins (Legartová et al., 2014) and are associated with electron dense heterochromatin (Jorgens et al., 2017).

There are multiple non-exclusive mechanisms that could lead to the formation of the NR. One possibility would be that NR simply represents mistiming between chromosome decondensation at the end of mitosis and nuclear envelope reformation by fusion of fragments re-bound to chromatin surfaces. In this view, NR formation would be the consequence of an error leading to premature fusion of chromosome-bound NE fragments before decondensation, leading to a convoluted NE shape, with NR channels defined by interchromosomal non-contact zones. Such a random process would not be consistent with a specific function for the NR dependent on its morphology or distribution.

Simple models of NR formation consistent with functionally significant morphology might include physical deformation of an existing nuclear envelope by forces originating in the cytoplasm and locally pushing into the nucleoplasm, or by forces emanating from the nucleoplasm locally drawing in the nuclear envelope (**Figure 1-5**). While some evidence exists to support these mechanisms, we note that neither of these offer a simple explanation for the genesis of branched structures. Finally, there is evidence to support an active morphogenic machinery, akin to the budding of tubulovesicular structures from the surface of organelles in the cytoplasm. There is evidence supporting the idea that there is a dedicated machinery, but there are some grounds that may support that NR invaginations may be formed by mechanical forces enforcing towards the nucleoplasm or pulling in from the nucleoplasm.

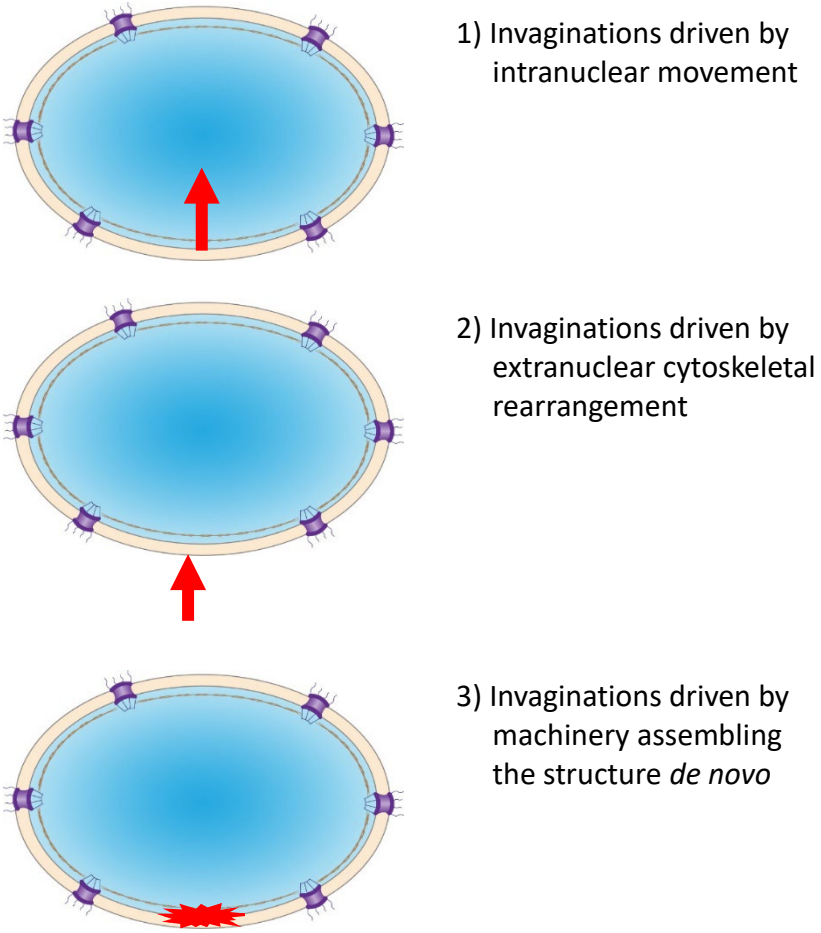


Figure 1-5: Three non-exclusive models for NR formation.

5. NR formation

"Pushing in"

Multiple electron microscopy observations of the NR show that the invaginations may contain cytoskeletal filaments (Clubb and Locke, 1998; Collings et al., 2000; Jorgens et al., 2017). Early spindle microtubules can also cause formation of invaginations of the nuclear envelope prior to nuclear envelope breakdown (Beaudouin et al., 2002; Hebbar et al., 2008; Salina et al., 2002; Turgay et al., 2014). This leads to the hypothesis that the polymerisation of the cytoskeleton towards the nuclear envelope

can potentially induce the invaginations. However, not every invagination contains cytoskeletal filaments. Therefore, without excluding the possibility that the pushing inward forces can form invaginations, there must be other mechanisms for their formation.

"Pulling in"

Another hypothesis is that through condensation and movement of chromatin focal points the nuclear envelope is pulled inwards. Knockdown of LINC proteins that physically bind INM and ONM (e.g. SUN proteins) increases the abundance of type I NR (Ohsaki et al., 2016). This observation implies that a "pulling force" of chromatin condensation may be decoupled from counterbalancing stabilisation created by the cytoskeleton.

While these observations suggest possible mechanisms whereby NRs may form, neither condensin hyperactivity nor the absence of functional LINC complexes are normal in cells, implying that there should be other mechanisms for NR formation.

Dedicated machinery

NR development depends on phosphatidylcholine synthesis and notably on function of the rate-limiting enzyme for the PC synthetic pathway CTP:phosphocholine-cytidylyltransferase-α (CCT-α). When CCT-α is knocked down by siRNA, NR formation does not occur (Gehrig and Ridgway, 2011; Gehrig et al., 2008; Goulbourne et al., 2011; Lagace and Ridgway, 2005). Moreover, it has been shown that cells incorporate newly synthesised phospholipids into nascent tubular invaginations of nuclear envelope as

well as newly synthesised Lamin B1 (Drozdz et al., 2017; Pytowski et al., 2019). These observations suggest that deformation of a pre-existing NE without addition of new material cannot account for NR formation.

The newly synthesised components and the fact that the NR can be formed during interphase without nuclear envelope reassembly after mitosis (Fricker et al., 1997; Goulbourne et al., 2011) implies that there is a specific machinery dedicated to the NR formation (**Figure 1-6**).

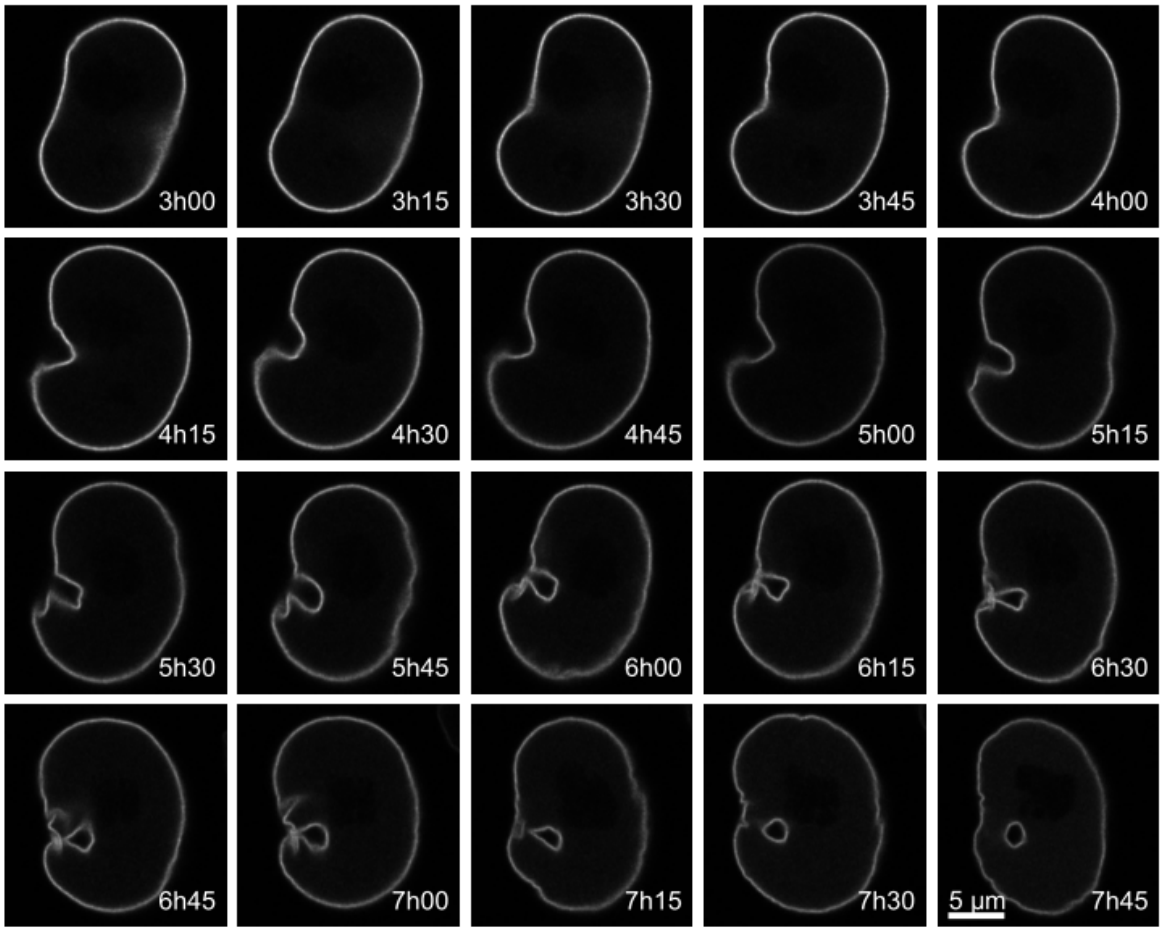


Figure 1-6: The nuclear envelope is highly dynamic. *Hela cells were transfected with Lamin A-mNeonGreen. 24 h after transfection NR formation was induced with Saquinavir at T=0. Z-stacks were acquired every 15min. Midplanes are displayed.*

6. NR Function

The first function of the NR that one might think is that NR increases the nuclear-cytoplasmic interactions. The folding and invaginations of the nuclear envelope bring deep within the nucleus the standard functions of the nuclear envelope. It increases transport of regulatory molecules to their nuclear targets. This includes the passive diffusion of compounds through the nuclear envelope and the active transport of macromolecular cargo through the NPCs. Indeed in bovine embryos invaginations containing NPCs mainly in proximity of condensed DNA may be involved in import-export functions (Legartová et al., 2014; Popken et al., 2015). Also subdomains of late endosomes are found in nuclear envelope invaginations (Rappa et al., 2017). Large-volume invaginations being associated with nucleolar precursor bodies (NPBs) in rabbit embryos is possibly the result of the acute need of NPBs in the nucleus during embryogenesis (Popken et al., 2016), and the Unr-containing intranuclear vesicles connected to the nuclear envelope in trophoblast giant cells are sites of active translation (Saltel et al., 2017) further supports the idea that NR enhances nucleus/nucleoli interaction with the ER/cytoplasm.

It is also thought that NR contributes to the regulation of transcription by the lamina associated domains of chromatin and the sequestration of transcription factors (Boubriak et al., 2017; Malhas et al., 2009). Moreover, invaginations can contain ER cisterns with ribosomes and polysomes so NR may increase protein synthesis activity. The fact that NR may contain mitochondria may provide a faster energy transfer between cytoplasm and nucleoplasm.

Another role of the NR may be in calcium regulation, indeed tubular invaginations were found to contain calcium, express InsP3 and ryanodine receptors and can give rise to local calcium signals in the nucleoplasm (Echevarría et al., 2003; Guatimosim et al., 2008; Lee et al., 2006; Lui et al., 2003; Mauger, 2012; Plačkić et al., 2016). However, this is expected because the NE and hence the NR are continuous with the ER which is a major (regulated and re-loadable) calcium store in cells. However, the calcium regulation function of NR is controversial as is has been shown that NR is not essential in calcium signalling in primary neurons (Bezin et al., 2008).

7. Hypothesis and aims of the thesis

We hypothesise that the NR is a functional structure whose abundance is regulated (that it is neither a post-mitotic remnant nor random). We postulate that the nucleoplasmic reticulon is involved in the exchange of material between the cytoplasm and nucleoplasm and that it may be present in nuclei with larger volumes or DNA contents than most cells. We also hypothesised that its formation can be induced and observed in interphase in live cells.

In summary, the aim of this project is to:

1. Further understand how and when the nucleoplasmic reticulum is assembled.
2. Identify how it is structured and if/how it differs from the nuclear envelope.
3. Evaluate its function in terms of exchange or material between the cytoplasm and nucleoplasm.
4. Elucidate what are the gene expression changes that occur when the nucleoplasmic reticulum formation is induced.

For this, various plasmids and cell lines were engineered, and advanced light microscopy plus image analysis including state of the art machine learning tools were employed.

2. Materials & Methods

1. Chemicals, reagents, materials

Key chemicals, reagents

- Saquinavir: Sigma, S8451, ≥98%
- Oestradiol: Sigma, E1024
- Progesterone: Sigma, P8783, ≥99%

Plasmids

We generated plasmids used in this work by combining dsDNA from other plasmids or from genomic DNA (Table 2-1). Parental plasmids used are the following:

- CMV-mNeonGreen-Lamin A
- CMV-CD2-Photocleavable protein-tdTomato-NLS
- pBluescript II SK(+)-Lamin A HA Nt-mNeonGreen-Lamin A HA Ct (for generation of cell lines by CRISPR)
- pBluescript II SK(+)-Lamin B1 HA Nt-mScarlet-Lamin B1 HA Ct (for generation of cell lines by CRISPR)
- U6-gRNA-CMV-pSpCas9n-NLS

Table 2-1: Origin of dsDNA used in this work

Plasmid DNA	Origin
Lamin A	Vaux Lab stocks
mNeonGreen	Addgene, (Shaner et al., 2013)
CD2	Dr Marion Brown Lab stocks
Photocleavable protein	Addgene, (Zhang et al., 2017)
tdTomato	Addgene, (Shaner et al., 2004)
Lamin A Homology Arms	Genomic DNA from HeLa cells
Lamin B1 Homology Arms	Genomic DNA from HeLa cells
mScarlet	Addgene, (Bindels et al., 2017)
U6-gRNA-CMV-pSpCas9n-NLS	Addgene, (Ran et al., 2013)

All sequences available in Genbank (Benson et al., 2012) and Addgene.

DNA purification

DNA purification procedures used for this work are based on the Monarch® Plasmid Miniprep Kit and Monarch® DNA Gel Extraction Kit from NEB, used according to the manufacturer's instructions.

Cell culture products

Reagents used for tissue culture were DMEM from sigma or Thermo Fisher Scientific. FBS from Sigma. Non-essential amino acids, penicillin streptomycin solution, Tryple Express, Lipofectamine 2000, from Life Technologies. Plasticware was from Greiner, Started or Costar.

Antibodies

Primary antibodies and dilutions used for this work are listed in Table 2-2. Secondary antibodies and dilutions used for this work are listed in Table 2-3.

Table 2-2: Primary antibodies used in this work

Antibody	Source	Supplier	Dilution
Anti-lamin A/C (4C11)	Mouse monoclonal	Active Motif	1:100
Anti-lamin B1 (C-20)	Goat polyclonal	SantaCruz	1.5:50 IF
Anti-lamin B1 (8D1)	Mouse monoclonal	Own	Undiluted hybridoma supernatant
Anti-Nesprin 2 clone 20-478	Mouse monoclonal	Merck	1:50
Anti-Nup153 (ab84872)	Rabbit polyclonal	Abcam	1:500
Anti-Nup98 [2H10] abc50610)	Rat monoclonal	Abcam	1:100

Table 2-3: Secondary antibodies used in this work

Antibody	Source	Supplier	Conjugate	Dilution
Anti-mouse IgG	Donkey polyclonal	Invitrogen	Alexa Fluor 594	1:300
Anti-mouse IgG	Donkey polyclonal	Invitrogen	Alexa Fluor 488	1:300
Anti-goat IgG	Donkey polyclonal	Invitrogen	Alexa Fluor 488	1:300
Anti-Goat IgG	Donkey polyclonal	Jackson Immunoresearch	Cy-5	1:300
Anti-Rat IgG	Donkey polyclonal	Jackson Immunoresearch	Alexa Fluor 594	1:300
Anti-Rabbit	Donkey polyclonal	Invitrogen	Alexa Fluor 568	1:300

Microscopy

Microscopy related materials were 76x26 mm microscope Slides from Thermo Scientific, 1,5 Borosillicate glass coverglass from VWR, ProLong™ Glass Antifade Mountant from Invitrogen, Optical bottom plates from PerkinElmer, air dusters from Office Depot.

2. DNA amplification, purification, and cloning

Bacterial cell culture

E. coli was grown in LB at 37°C in with 250 rpm in a rotary shaker. Appropriate selection antibiotics were used (kanamycin at 50 µg/mL or ampicillin at 100 µg/mL).

Glycerol stocks were made by mixing a fresh *E. coli* solution with the same volume of a 50% glycerol solution and stored in cryotubes at -80°C.

All bacterial work was done using appropriate aseptic technique.

Competent bacteria preparation

Competent bacteria were prepared following the *Mix & GO E. Coli* transformation kit (Zymo Research) following manufacturer recommendations. Bacteria origin was NEB® 5-alpha Competent E. coli. Bacteria were grown at 20°C for higher transformation efficiency. The genotype is *fhuA2 Δ(argF-lacZ)U169 phoA glnV44 Φ80 Δ(lacZ)M15 gyrA96 recA1 relA1 endA1 thi-1 hsdR17.*

Bacterial cell transformation

Competent cells were transformed following Cohen et al. 1972 protocol (Cohen et al., 1972). Frozen competent bacteria were thawed for 5 minutes on ice than plasmid DNA was added to the bacteria. After a gentle mixing, bacteria were left for 1h on ice followed by a heat shock at 42°C for 30 s and finally back on ice for 2 minutes. SOC was added to the bacteria and left for 1h at 37°C with 250 rpm in a rotary shaker before being plated on the appropriate LB-agar plates. Plates were then placed at 37°C overnight before colony-picking.

Purification of plasmid DNA from bacterial cells

Plasmid DNA purification from bacterial cells was carried out using a Monarch® Plasmid Miniprep Kit following manufacturer's instructions with the exception of DNA

being finally resuspended in water instead of TE buffer. DNA concentration was determined using a *NanoDrop*™ spectrophotometers and DNA was stored at -20°C.

DNA cloning

Plasmids were constructed with the NEBuilder® HiFi DNA Assembly Cloning Kit (modified version of Gibson assembly) from NEB following manufacturer instructions. All PCR were performed with Q5 polymerase following manufacturer instructions and gel purified with Monarch® DNA Gel Extraction Kit from NEB following manufacturer's instructions. When necessary, DNA sequences were retrieved from NCBI and GenBank. PCR primers were manually designed using SnapGene with and overlap for HiFi assembly of 25bp. Newly constructed plasmids were sequence verified by Sanger sequencing.

3. Mammalian cell culture

Cell lines and their origin

HeLa, Ishikawa and HCT cells were part of Vaux Lab collection. PCYT1A wild type and mutant primary cells were provided by Prof. David Savage - Cambridge University Hospitals. U-2 OS Cells traceable from ATCC were a gift from Fumiko Esashi, University of Oxford.

General cell culture technique

All tissue culture related manipulations were carried out in a laminar flow hood. Cells were maintained in vented flasks at 37°C, 5% CO_2 with adequate humidity in an incubator.

Adherent cells were passaged when they reached confluency after release with Tryple Express. HeLa, HCT and PCYT1A cells were cultured in Dulbecco's Modified Eagle Medium (DMEM) supplemented with 10% foetal calf serum (FCS), 1% non-essential amino acids, and penicillin and streptomycin antibiotics (100 units/mL). Ishikawa cells were grown in the same medium, with the exception that it is phenol free and with charcoal-striped FCS.

NR formation induction of cells in culture

NR formation was induced by either 20 µM Saquinavir for 48 h or by 150 pg/mL oestradiol and 10 ng/mL progesterone for 24 or 48 h.

Plasmid transfection of mammalian cells in culture

Cells were transfected using Lipofectamine 2000 using manufacturer's instructions.

4. Generation of cell lines by CRISPR

Overall strategy

In order to tag the Lamin A and Lamin B1 with fluorophores by CRISPR we need to generate a plasmid containing RNA guides that will enable the Cas protein to cut the genomic DNA. We choose to use a modified Cas9 that only cuts one strand of the genomic DNA at a time. This reduces the off-targets effects because two nickase Cas9 are required to create a double strand break thus the probability of having both guides binding in an unintended location close enough to each other is greatly reduced. Simultaneously with the guide RNA and the Cas9n, a template for the repair of the genomic DNA is provided; this template contains homology arms for the target insertion site plus the sequence coding the insert of our choice. After transfecting the cells with both guide RNAs and the donor template, cells are left to recover then single cell sorted in 96-well plates, grown, and finally validated first by microscopy and then by Sanger sequencing.

gRNA plasmid generation

gRNA and plasmid design were done following Ran et al. 2013 recommendations (Ran et al., 2013).

Guides were designed with the MIT design tool: http://crispr.mit.edu/ and inserted into Addgene Plasmid #48141 pSpCas9n(BB)-2A-Puro (PX462 was a gift from Feng Zhang). Guides RNA were 5’ ACGGGGTCTCCATGGCCGGCAGG 3’ and 5’ AGCGGCGCGCCACCCGCAGCGGG 3’ for Lamin A and 5’ CCGCCGCCCGCCATGGCGACTGC

3’ and 5’ ACCCCCGTGCCGCCGCGGATGGG 3’ for Lamin B1. Plasmid sequences available in Addgene.

Donor plasmid generation

mNeonGreen and mScarlet were inserted after the start codon of respectively Lamin A and Lamin B1 using a double-nicking strategy with the Cas9 D10A nickase mutant. The donor plasmid for Lamin A consisted of the insert enclosed in a 475 bp C term homology arm and a 483 bp N term homology arm between positions 120 and 121 of the lacZa gene of pBluescript. The donor plasmid for Lamin B consisted of the insert enclosed in a 359 bp C term homology arm and a 537 bp N term homology arm between positions 120 and 121 of the lacZa gene of pBluescript. The donor plasmids were assembled by isothermal assembly (NEBuilder® HiFi DNA Assembly). All sequences are available in Genbank (Benson et al., 2012) and Addgene.

Transfection and cell sorting

Plasmids containing the guides and donor templates were transfected in HeLa cells using Lipofectamine 2000 following manufacturer recommendations. Cells were then left to recover and to express the fusion protein for a week before proceeding with cell sorting. Cell sorting was done on a BD FACS Aria III run with the Diva software version 8.0.2; positive cells were sorted if green or red fluorescence was 10^3 times brighter that control cells. Positive cells were single cell sorted in an optical 96 well plate containing preconditioned media and adequate localisation of the fusion protein was confirmed by confocal microscopy. After expansion of clones, correct insertion was confirmed by Sanger sequencing.

5. NGS

mRNA isolation

NR formation was induced in Ishikawa cells for 6 hours with either Saquinavir or oestradiol and progesterone. mRNA was extracted with Agilent's Absolute RNA - miRNA kit following manufacturer instructions.

mRNA-seq library construction

This was carried out by the High-Throughput Genomics Group at the Wellcome Trust Centre for Human Genetics, Oxford:

Total RNA quantity and integrity were assessed using Quant-IT RiboGreen RNA Assay Kit (Invitrogen, Carlsbad, CA, USA) and Agilent Tapestation 2200 RNA Screentape. Purification of mRNA, generation of double stranded cDNA and library construction were performed using TruSeq® Stranded mRNA (RS-122-2103) with minor modifications to manufacturer specifications. The following custom primers (25 µM each) were used for the PCR enrichment step, which includes in-house unique dual indexing (based on Lamble et al., 2013):

5'AATGATACGGCGACCACCGAGATCTACAC [index-i5] ACACTCTTTCCCTACACGACGCTCTTCCGATCT

5'CAAGCAGAAGACGGCATACGAGAT [index-i7] AGTGACTGGAGTTCAGACGTGTGCTCTTCCGATC*T

Amplified libraries were analysed for size distribution using the Agilent Tapestation 2200 D1000. Libraries were quantified using Picogreen and relative volumes

were pooled accordingly. Sequencing was performed as 75 bp paired end reads on a HiSeq4000 according to Illumina specifications.

Data analysis:

Untrimmed reads were mapped using HiSat2 (carried out by the High-Throughput Genomics Group at the Wellcome Trust Centre for Human Genetics, Oxford). Gene counts were processed with DESeq2 (Love et al., 2014) and the Gene-set Enrichment was done with the gage package (Luo et al., 2009).

6. Light microscopy

Immunolabelling of cultured cells

Cells were seeded on coverslips 24 h before fixation or before beginning of any treatment. Cells were rinsed in PBS and fixed for 10 min in 4% PFA. Free aldehyde groups were quenched with 25 mM Glycine for 5 min and cells were permeabilized for 10 min with 0.5% Tx-100. Cells were blocked with 0.5% w/v fish skin gelatine (FSG) for 30 min at RT. Antigens were labelled for 1 h with the primary antibody at the appropriate dilution followed by 3 times 5 min PBS washes. Appropriate secondary antibodies were incubated for 1h and excess was washed 3 times 5 min PBS washes. If necessary, DNA was counterstained with 0.5 µg/mL (0.8115 µM) Hoechst 33342 for 5 minutes. Samples were mounted on ProLong™ Glass Antifade Mountant and the exposed surfaces of coverslips were carefully cleaned with 100% methanol.

Light microscopy

Samples were imaged on a Zeiss LSM880 confocal laser scanning with Airyscan, or an Olympus SoRa spinning disc confocal or an EVOS M7000 widefield Imaging System. The EVOS microscope was used for work requiring only low magnification images that were used to count nuclei for example. The LSM880 microscope was used mostly for experiments that required 3D imaging of fixed samples to quantify NR abundance (the resolution of this microscope is up to 140 nm laterally and 400 nm axially) which provides adequate resolution for this task. The Olympus SoRa spinning disc confocal was used for live cells experiments as it enables the fastest acquisitions with the most sensitive detectors and provides 120 nm lateral resolution.

When using the Zeiss LSM880 with Airyscan, samples were imaged using a Plan Apochromat 63x 1.4 NA oil immersion lens with appropriate, lasers, filters, pixel size, pinhole size and Z interval. Images were acquired with Zen Black software. When working with live cells for time lapses care was taken to reduce photobleaching and phototoxicity.

When using the Olympus SoRa spinning disc confocal, samples were imaged either with a x40 UPlanXApo 1.4 or an x60 UPlanApo 1.5 oil immersion lenses with appropriate lasers, filters, pixel size, pinhole size and Z interval. Images were acquired with Olympus cellSens software. When working with live cells for time lapses care was taken to reduce photobleaching and phototoxicity. If necessary images were denoised with noise2void (Krull et al., 2019).

The EVOS M7000 widefield Imaging System was used only for the cell survival versus Saquinavir assay. cells were stained with Hoescht 33342 (ThermoFischer), then live samples were imaged with an UplanSApo 10x/0.40 NA objective and an EVOS DAPI light cube filter cube. Each well was fully imaged at T=0 then Saquinavir or control DMSO were added for 48 and wells were imaged again. Samples were kept at all times in a 5% CO2, with humidity. The outer wells of 96-well plates were filled with PBS to reduce evaporation. Low magnification images were denoised with noise2void (Krull et al., 2019) to improve later segmentation.

Image analysis

Every quantification was done using macros. If necessary, images were denoised with noise2void (Krull et al., 2019) or median filters when edge preservation is necessary or gaussian blurs. When necessary GPU-acceleration was used with CLIJ libraries (Haase et al., 2020a). Models for Noise2Void were created the ZeroCostDL4Mic toolbox (von Chamier et al., 2021). Typically macros were created with the macro recorder or interactive GPU-accelerated image data flow graphs (Haase et al., 2020b; Vorkel and Haase, 2020). For nuclei segmentation Stardist (Schmidt et al., 2018; Weigert et al., 2020) was used with the Versatile model; Cellpose (Stringer et al., 2020) - from within the ZeroCostDL4Mic toolbox - was used for nuclei and cytoplasm segmentation (using the Cyto2 model). When appropriate, channel registration was performed using 0.1 µm TetraSpeck™ Microspheres and images were corrected for translation, rotation, and scaling. Images were processed using FIJI (ImageJ) (Schindelin et al., 2012, 2015).

A sample macro is provided below. Its purpose is to extract measurements from a series of images that have been segmented with Cellpose and save the results. The `getDirectory` commands in line 1 to 3 will assign the directory to a variable. The `"Set Measurements..."` command in line 4 will define what measurements to extract from the image. In this case we will measure the `area` of the cells and their `mean` intensity only. The arguments "`stack`" and "`display`" are used only to keep track of the origin of the measurements. The command in line 7 will simply close all images, reset the ROI manager and clear the results that may have been present before starting the macro. The commands in line 9 and 10 will assign the list of files present in both directories to two arrays. Line 12 is the beginning of the **`for`** loop that will process all the files that have a `".tiff"` extension (line 13). The **`for`** loop ends in line 27. The command in line 14 will open the image `[i]` from the `filelist1` then the window title is assigned to a variable called `title` (line 15). Line 16 will do the same as line 14 but from the `directory2`. Both commands use the same `filelist` so that an image and its corresponding label map are opened. The `"Label image to ROIs"`, will convert the label map into individual regions of interest (line 18) that will be used on the input image (lines 21 and 22). Line 23 will close all the images so that the **`for`** loop can be repeated. The command in line 27 will save all the measurements as a .csv file.

```
1   directory1 = getDirectory("1 Choose directory with input images");
2   directory2 = getDirectory("2 Choose directory with segmentations");
3   directory3 = getDirectory("2 Choose directory to save results");
4   run("Set Measurements...", "area mean stack display redirect=None
5   decimal=3");
6
7   run("Fresh Start");
8
9   filelist = getFileList(directory1);
10
11  for (i = 0; i < lengthOf(filelist1); i++) {
12        if (endsWith(filelist[i], ".tiff")) {
```

```
13          open(directory1 + File.separator + filelist[i]);
14          title = getTitle();
15
16          open(directory2 + File.separator + filelist[i]);
17
18           run("Label image to ROIs", "rm=[RoiManager[size=0,
19    visible=true]]");
20
21          selectWindow(title);
22          roiManager("measure");
23          run("Close All");
24          }
25          }
26
27    saveAs("results", directory3 + "results.csv")
```

3. NR assembly and disassembly in interphase

"To see is to believe"

1. Introduction

The nucleoplasmic reticulum has been primarily observed and studied in micrographs of fixed samples both by light and electron microscopy. Therefore, very little is known about its assembly – or formation –, and its disassembly. Here we aim to elucidate some of the unknowns surrounding the appearance and disappearance of this structure in live cells.

The nuclear envelope is a highly dynamic structure. Its plasticity and elasticity make its study in live samples essential. This requires the use of a fluorescent label

expressed or diffused in to living cells. For these experiments this was achieved with fluorescently labelled proteins and, specifically, fluorescently labelled Lamin A or Lamin B1 so we can observe the nuclear envelope as it evolves and forms invaginations. When imaging live cells repeatedly it is essential to reduce phototoxicity to the minimum possible. This entails the use of the brightest available fluorescent proteins so that one can achieve the highest signal to noise ratio possible for a given illumination level. Use of image analysis tools permitted additional improvements in experiment duration and minimal phototoxicity by denoising of images collected with very low incident illumination.

The nuclear envelope separates the nucleoplasm from the cytoplasm. It is a double lipid bilayer, traversed by nuclear pores that allow exchange of material. The outer membrane is continuous with the endoplasmic reticulum and is studded with ribosomes. The nucleoplasm contains the active euchromatin and the repressed heterochromatin and the periphery. The nucleolus, found in the nucleoplasm, is the ribosome factory. In the inner face of the inner nuclear membrane, the nuclear lamina forms a meshwork that acts as a nucleo-skeleton.

The lamina is a network of mainly Lamin A/C and Lamin B1/B2. It anchors the heterochromatin to the nuclear envelope, and it fixes other transmembrane proteins to the inner nuclear membrane. The SUN proteins traverse the lamina and anchor the chromatin though the BAF protein to the Nesprins forming the LINC complex. The lamina binds transcriptions factors and releases them under stressors, for example, and

regulates gene expression. The lamina associated domains are chromatin regions that are associated to the lamina and thus repressed.

When studying NR formation, having a way of inducing the formation of those structures can be useful. To this date there are two distinct ways to achieve this. (i) Saquinavir is an HIV protease inhibitor used to treat and prevent AIDS (Vella and Floridia, 1998) that as a side effect blocks the enzyme responsible for the cleavage of the farnesyl group of prelamin A, ZPMSTE-24, and as a consequence leads to its accumulation (Se et al., 2008; Caron et al., 2007; Coffinier et al., 2007). This and the HIV Protease Inhibitor–Related Lipodystrophy Syndrome (Carr, 2000) lead to the formation of infoldings and invaginations of the nuclear envelope (Goulbourne and Vaux, 2010). (ii) Although its mechanism is unknown, physiological levels of oestrogen and progesterone also induces the formation in tubular invaginations of the nuclear envelope in hormone-sensitive endometrial cells such as Ishikawa cells (Pytowski et al., 2019). The Ishikawa cell line is derived from human endometrial tissue, and expresses both oestrogen and progesterone receptors (Nishida et al., 1985). In endometrial tissue, it has been found that patients have varying levels of nuclear infoldings and cisternae resembling the Golgi apparatus and named the nucleolar channel system (NCS) (Kittur et al., 2007; Terzakis, 1965). The presence of this NCS has been tied to the temporal position in the menstrual cycle, infertility, and the use of contraceptives. Both infertile and users of contraceptives had no NCS detected while patients in the mid-luteal phase of their menstrual cycle did (Ernest I. Kohorn et al., 1972; Feria-Velasco et al., 1972; Kohorn et al., 1972; Nejat et al., 2014; Pryse-Davies et al., 1979; Wynn, 1967) (although the absence of NCS in infertile women has been questioned by Rybak et al., 2011). Both the invagination induced with

Saquinavir and oestrogen and progesterone require newly synthesised lipids and lamins (Drozdz et al., 2017; Gehrig and Ridgway, 2011; Gehrig et al., 2008; Goulbourne et al., 2011; Lagace and Ridgway, 2005; Pytowski et al., 2019). Saquinavir serves as a pathological induction while oestrogen and progesterone serve as a physiological inducer of the NR in Ishikawa cells.

The nuclear envelope invaginations and the tubular endoplasmic reticulum (ER) are both highly curved structures. In the ER, regions of high curvature are associated with the presence of membrane-associated proteins that promote deformation of planar phospholipid bilayers. These proteins include the reticulons which are thought to form and maintain the curvature of those tubes. Reticulons have two to four hydrophobic domains that traverse the whole lipid membrane and are connected by short hydrophilic domains that causes the hydrophobic domains to form a V-shape and thus induce the curvature of the membranes (D'Eletto et al., 2020; Wang and Rapoport, 2019; Yang and Strittmatter, 2007). Reticulon 4 is one of those reticulons that locates to regions of high membrane curvature (in the tubular ER but not in flat ER cisternae) (Kiseleva et al., 2007) so it may have a function in the formation or maintenance of the tubular invaginations of the nuclear envelope (Illustrated in Figure 6-1 D).

When imaging repeatedly live samples is it essential to prevent phototoxicity and photobleaching by using low light doses. Despite using highly sensitive cameras, having low signal to noise ratios is inevitable. It is then essential to denoise the images so they can be interpreted. There are multiple strategies to denoise images, this can include traditional methods such as mean or median filters or the use of machine and

deep learning. Multiple networks have been developed in recent years and are divided into two categories - the supervised networks such as the content aware image restoration (CARE, Weigert et al., 2018) – and the unsupervised networks such as Noise2Noise (Lehtinen et al., 2018) or Noise2Void (Krull et al., 2019). In CARE a convolutional neural network (CNN) is used to denoise images by training the network to predict high SNR images from low SNR images, but this requires ground truths (that is, the training set includes both the experimental low SNR image and also an associated high SNR image obtained by high level illumination or exposure to serve as the target and comparator against which the denoising process is cyclically assessed, called the "ground truth"). The input is fed to the network then it predicts an output and the difference between the prediction and the ground truth is used to adjust the internal parameters of the network until it can no longer improve (plateauing the learning or validation loss). This enables the prediction of denoised images, but the acquisitions of ground-truth are difficult as one needs pairs of low and high SNR images without the sample moving at all. The Noise2Noise network has the advantage of not needing ground-truths. Here, pairs of noisy images are used to predict the denoised signal. This is possible because the true signal remains constant between the pairs of images while the noise does not (assuming the sample does not move). This method has the advantage of not needing a ground-truth, but it still needs to image the samples twice. Noise2Void on the other hand does not require ground-truths nor pairs of noisy images – it can function with single noisy images. This is possible because the noise is zero-mean and pixel-wise independent while the true signal is pixel-wise dependent on its surrounding pixels. The way that the convolutional neural network work, in this case, is

by using blind spots and then using the receptive field (the surrounding pixels) to predict the true signal with no noise. This is only possible because the noise is random while the true signal is not. We used Noise2Void to denoise low signal to noise ratio 3D time lapses. This enabled the analysis of the formation and deformation of the NR.

We hypothesised that Lamins are a good marker for the observation of the invaginations of the nuclear envelope in live cells and that their endogenous tagging would enable the observation of the NR assembly or disassembly. We also hypothesised that reticulons may be involved in the formation of the NR.

In this chapter we:

1. Demonstrated that it is possible to tag the endogenous locus of Lamin A and Lamin B1 by CRISPR (**Figure 3-1**) and ensured that it did not affect its response to Saquinavir (**Figure 3-2** and **Figure 3-3**).
2. Used the newly created cell lines to investigate the density of the lamina in the nuclear envelope versus its invaginations (**Figure 3-4**).
3. Assessed whether it is possible to assemble and disassemble the NR without going through mitosis (**Figure 3-5**).
4. Observed the assembly and disassembly of the NR with unprecedented spatial and temporal resolution (**Figure 3-6** to **Figure 3-9**).
5. Investigated whether Reticulon 4 is present and/or required for the nucleoplasmic reticulum formation (**Figure 3-10** to **Figure 3-12**).

2. Results

In order to study the assembly and disassembly of the nucleoplasmic reticulum, it is essential to use live cells that have a reasonable abundance of NR, and that the formation of this structure is readily visible. For this we used HeLa, Ishikawa and U-2 OS osteosarcoma cells with the lamina tagged with fluorescent proteins by CRISPR/Cas-9 gene editing.

Lamin A and Lamin B1 were respectively tagged with the fluorescent proteins mNeonGreen and mScarlet. Both fluorophores were chosen for their high brightness (product of extinction coefficient and quantum yield) and thus enabled frequent imaging in live cells. In order to tag the endogenous locus of both lamins, a fragment of the genomic DNA at the position of the intended insertion was amplified by PCR, then inserted in a donor plasmid and the sequences coding for the fluorescent proteins were inserted in the N-termini of the lamin sequence. The donor plasmid and guides RNAs were transfected along with nickase Cas9 in the cells. Then fluorescent cells were selected by flow cytometry and finally grown from monoclonal colonies. **Figure 3-1** shows HeLa cells with both Lamin A and Lamin B1 fluorescently labelled. This demonstrated that it is possible to tag these essential proteins without altering the morphology of the nuclear envelope or compromising cell survival. In addition, the nucleoplasmic reticulum is now visible in living cells without further labelling.

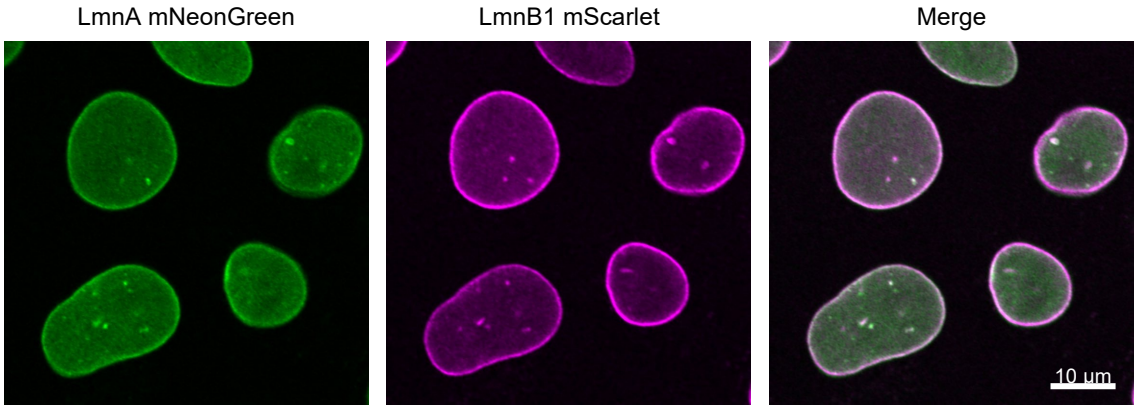


Figure 3-1: Tagging of the lamina allows us to observe the nuclear envelope and nucleoplasmic reticulum in live cells. *HeLa cells had their Lamin A and Lamin B1 endogenously tagged with mNeonGreen and mScarlet respectively by CRISPR. The cells maintain a normal looking morphology despite the addition of both fluorescent proteins.*

Not visibly altering the nuclear envelope morphology is not sufficient evidence that tagging the endogenous locus of both Lamin A and Lamin B1 doesn't affect the cells. Since we are interested in NR formation, we investigated whether having the lamina encumbered with an additional protein – the fluorescent tag protein – affects the cell toxicity due to Saquinavir (**Figure 3-2**). We treated wild type or mNeonGreen-Lamin A HeLa cells with varying amounts of Saquinavir and measured toxicity by following cell proliferation over time. We found that cells respond in the same way to both Saquinavir and the DMSO-only control in terms of cell abundance after 48 hours of treatment. Cells were cultured in 96 well plates and imaged at 0 and 48 hours. All the cells were automatically counted, and the abundance of cells is expressed relative to t 0. The data demonstrated that at the initial time point all the wells have similar abundance of cells and that both cell lines behave in the same way when exposed to Saquinavir or DMSO.

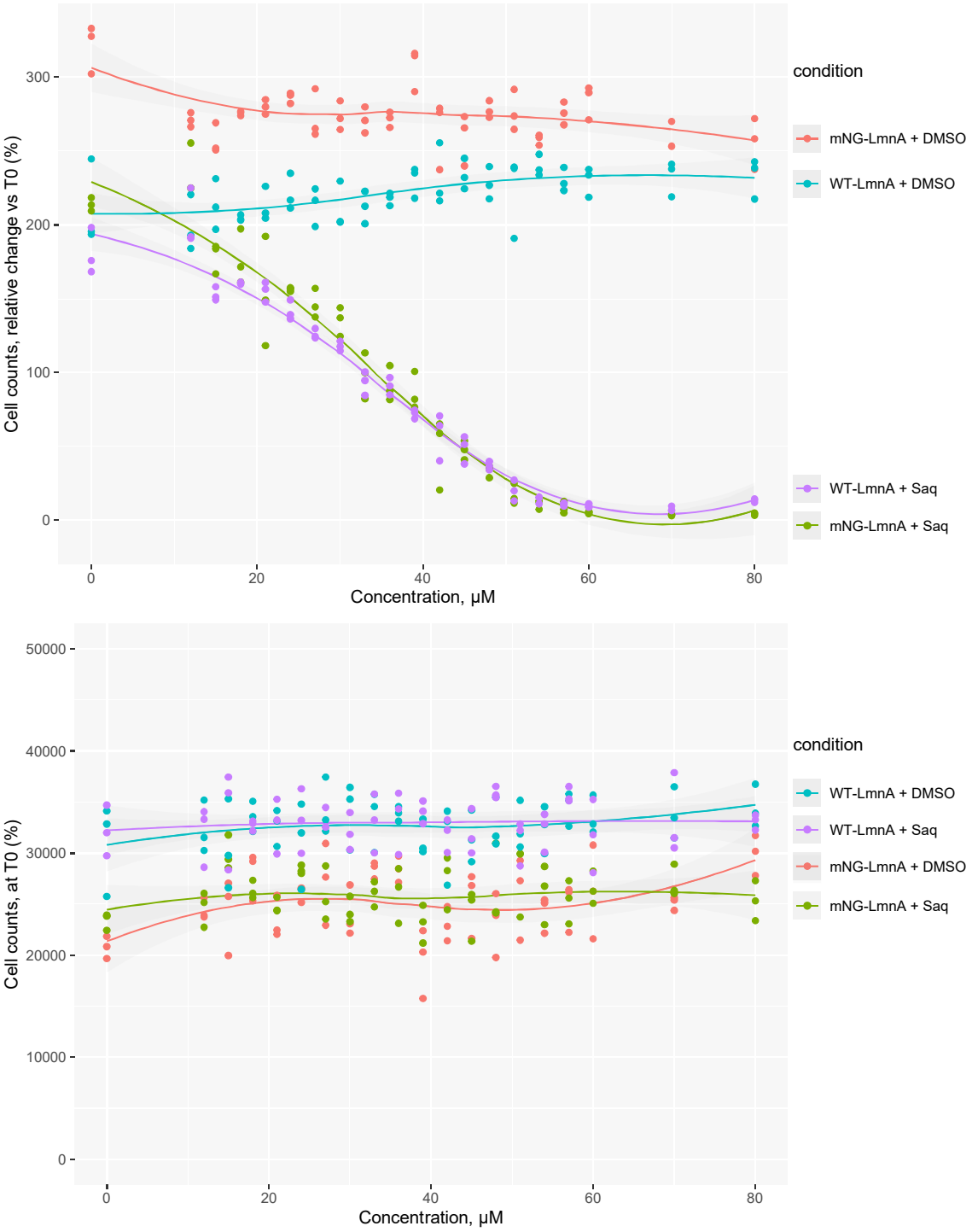


Figure 3-2: Cell survival vs Saquinavir concentration. WT and mNeonGreen Lamin A expressing cells are equally sensitive to Saquinavir. *The hypothesis that one non-linear fit fits both cell lines (top graph) is not rejected (p=0.2899) meaning that they are statically equally responsive to Saquinavir in terms of cell survival.*

In order to accurately count the cells in 240 wells of 96 well plates (two cell lines, two conditions – Saquinavir or DMSO -, twenty concentrations, triplicates: 2x2x20x3) while efficiently using the time at the microscope, cells were imaged at low magnification, with a wide field microscope. In our case, with our microscope and acquisitions settings, this led to images with low signal to noise ratios. To count accurately the number of cells in our image, images were denoised with the noise2void network. This is an efficient self-supervised method that denoised the input images without needing ground truth and allowed us to accurately count the nuclei present in each well of the 240 wells (**Figure 3-3**).

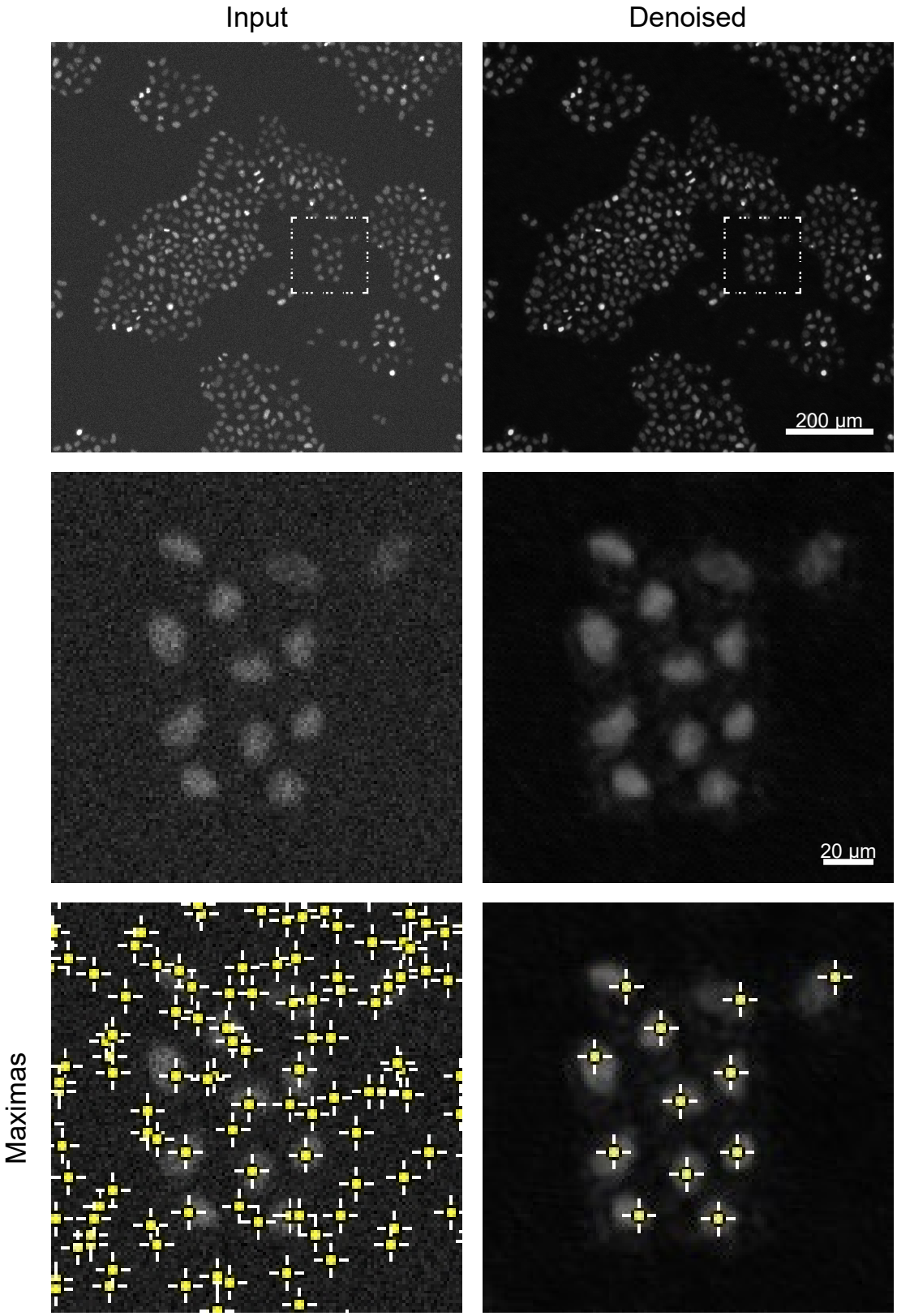


Figure 3-3: Denoising allows accurate low SNR (low magnification) nuclei counting. *Maxima with prominence of 300 for the denoised and original images. Maxima finding can be improved for the raw image, but remains of inferior quality compared to the denoised image.*

Once we ensured that the cell lines we created were suitable for the purpose of our research we investigated the lamina density of the nucleoplasmic reticulum relative to that of the nuclear envelope (**Figure 3-4**). This is possible because we tagged the endogenous locus of both Lamin A and Lamin B1 and hence the abundance of the fluorescent protein and its brightness is directly proportional to the abundance of the Lamin protein to which they are attached. We found that both Lamin A and Lamin B1 have an apparent higher density in the tubular invaginations than in the rest of the nuclear envelope of the same nucleus (the increase being larger for Lamin A than Lamin B1).

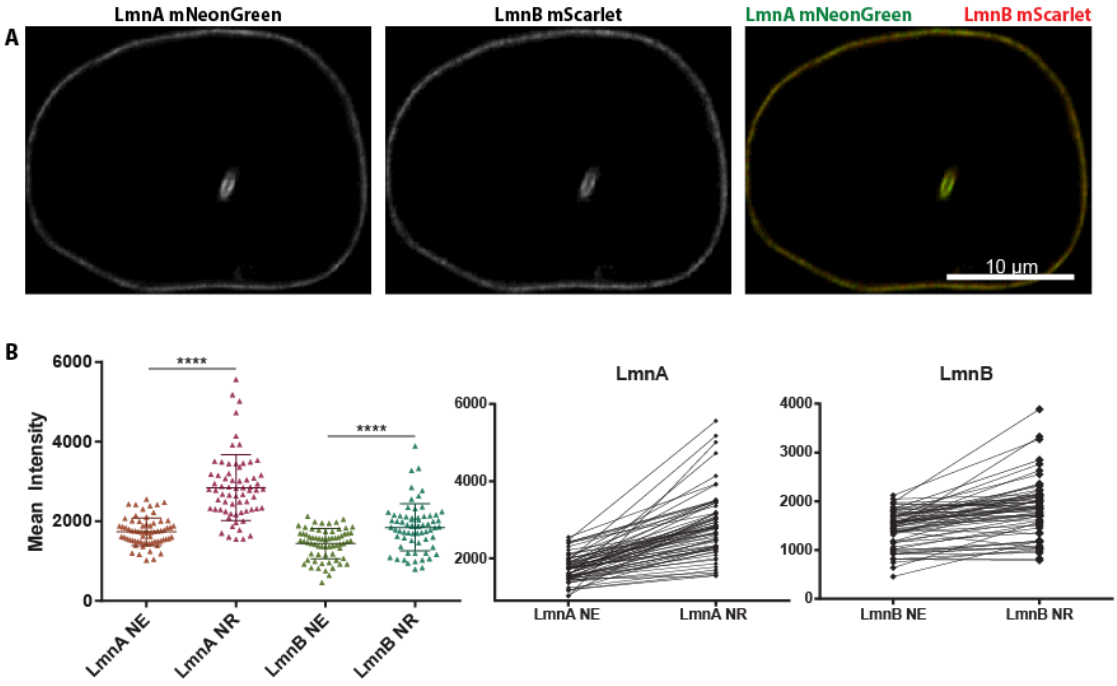


Figure 3-4: The NR is enriched in both Lamin A and Lamin B1 compared to the rest of the nuclear envelope*. (**A**) HeLa cells with endogenous Lamin A mNeonGreen and endogenous Lamin B1 mScarlet. (**B**) Mean intensities of lamins in NE and NR. n=67, paired t-test.*

We have demonstrated that it is possible to induce NR formation with Saquinavir. Here we demonstrate that NR formation in Ishikawa cells expressing tagged lamin proteins at endogenous levels can be induced with physiological levels of oestrogen and progesterone. This enabled us to address the question of the stability of these NR structures upon hormonal withdrawal, and indeed whether such structures can be lost from living cells without an intervening mitotic disassembly of the nucleus. Cells were exposed to hormones for 24 hours then the hormones were removed, and the cells were examined after 3 hours-culture in hormone-free medium. The number of invaginations per cell was quantified and we found that there is indeed an increase in the NR abundance after the treatment but once the hormones are removed the abundance of invaginations per nucleus return to the levels prior to the hormonal exposure (**Figure 3-5** A, B). To ensure that the loss (or the formation) of the invaginations was not preceded by cell division we investigated the rate of cell division using CFSE. CFSE is a fluorescent dye that covalently binds to proteins in the cell and is conserved after cell division. We found that the CFSE fluorescence halved every 30 hours for both the treated and untreated Ishikawa cells meaning that the reduction in invaginations abundance within 3 hours of the removal of the hormones could not be due to cell division (**Figure 3-5** C, D).

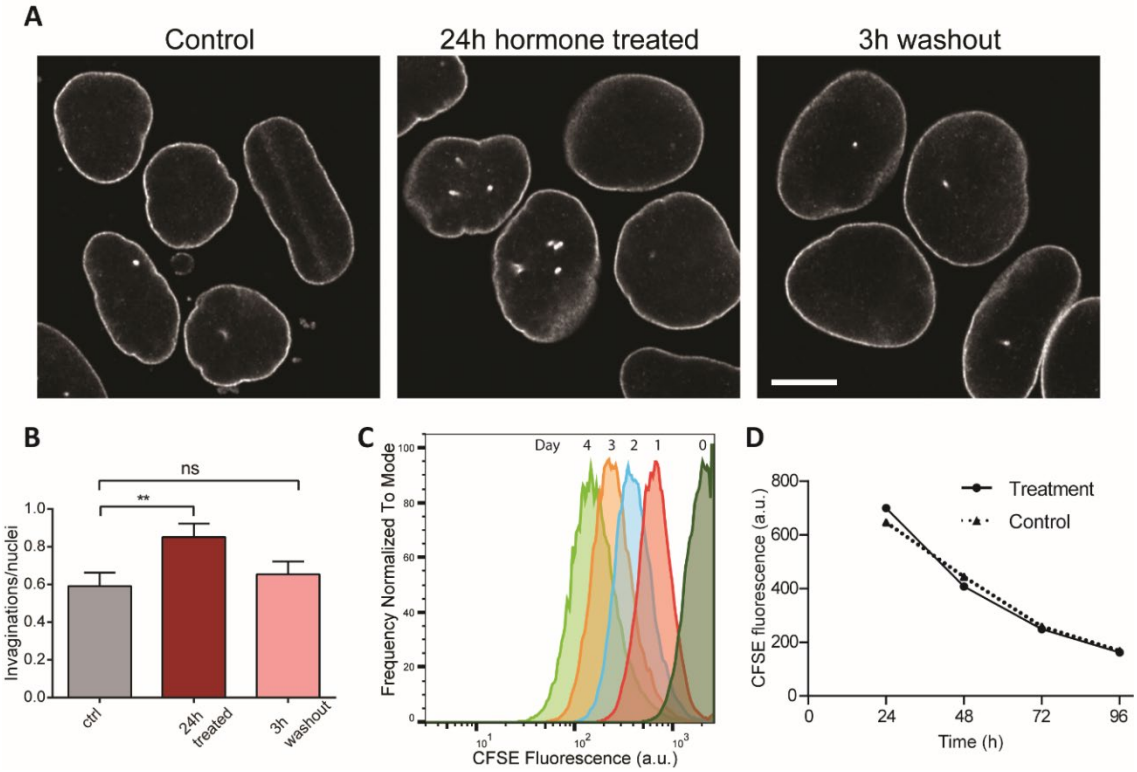


Figure 3-5: NR formation in endometrial cells is reversible and cell cycle independent. (A) *NR induction in Ishikawa cells treated with oestrogen and progesterone for 24 h and then subjected to 3 h washout in hormone-free media. Nuclei immunostained with anti-Lamin B1-Cy5. Scale bar 10 µm.* ***(B)*** *NR abundance quantification. Three replicates total, n = 242, 262, 203, respectively. ** for p < 0.01; ns for non-significant. Error bars represent SEM.* ***(C)*** *Hormone addition or removal does not affect cell division rate. Normalised frequency of CFSE fluorescence of Ishikawa cells measured by flow cytometry. Hormones were added for 48 h then removed for another 48 h. Average cell number per profile = 28,000.* ***(D)*** *Average CFSE loss over time of treated and control samples reveal non-significant difference in cell proliferation rates. Figure from Pytowski et al. Nucleoplasmic Reticulum Formation in Human Endometrial Cells is Steroid Hormone Responsive and Recruits Nascent Components. IJMS 20, 5839 (2019).*

NR formation

Creating these cells lines expressing endogenous levels of labelled Lamins allowed us, for the first time, to follow the changes in nuclear envelope morphology and nucleoplasmic reticulum formation in live cells without over-expressing any protein. We used unstimulated U-2 OS cells expressing mNeonGreen Lamin A and imaged them every minute and a half with full Z-stacks. In order to track the position and shape of the nucleus and monitor nuclear envelope integrity we used cells carrying an additional genetic modification, in this case a cassette inserted into the safe haven site AAVS1 that drives the expression of an exogenous fusion protein consisting of mCherry-SNAP-Tag with a nuclear localisation signal from a CMV promoter. In order to maintain the cell alive with no evident phototoxicity while imaging both the mNeonGreen and mCherry channels very low light doses were used and then images were denoised using noise2void.

We found multiple examples of newly formed tubular invaginations in interphase. **Figure 3-6** illustrates one such example, in minute 3 and 4.5 we can see the beginning of the formation of a new tube. The rightmost column is an orthogonal projection at the position of the new structure. We can observe in the orthogonal projection that from no later than minute 7.5 the new tube transverses the whole nucleus and that new structure remains visible for the duration of the acquisition until at least T = 78. From these observations it is clear that *de novo* formation of NR channels can occur on a timescale of minutes in cultured interphase cells, and that this can be a spontaneous behaviour not linked to external stimuli. This formally excludes the

possibility that NR exists only as an aberration of late steps in nuclear envelope reassembly at the end of mitosis.

Previous work using timelapse imaging of live cells expressing fluorescent nuclear import reporters have shown that interphase cells in culture may undergo repeated transient loss of nuclear envelope integrity, especially in cells accumulating prelamin A (Vos et al., 2011). The experiments shown here using double labelled U-2 OS cells confirmed that transient loss of nuclear envelope integrity can also be observed in cells without a lamin processing defect. The mCherry-NLS fluorescent protein is present, as expected, primarily in the nucleus of the cell. When the new invagination starts appearing at minute 3 and 4.5 a visible release of this nucleoplasmic material into the cytoplasm occurs and remains visible until minute 33 when it appears that the cytoplasmic material is imported again to the nucleus. The data is not consistent with a model in which this fluorescent cytoplasmic reporter appears due to a global cessation of nuclear import in the face of continued synthesis, since a leakage from the accumulated nuclear pool is readily apparent from the reduced intensity of the nuclear signal at the onset of this event. Moreover, this reporter pool is efficiently imported back into the nucleus over the next thirty minutes, implying that nuclear envelope integrity has been restored so that a closed compartment is recreated.

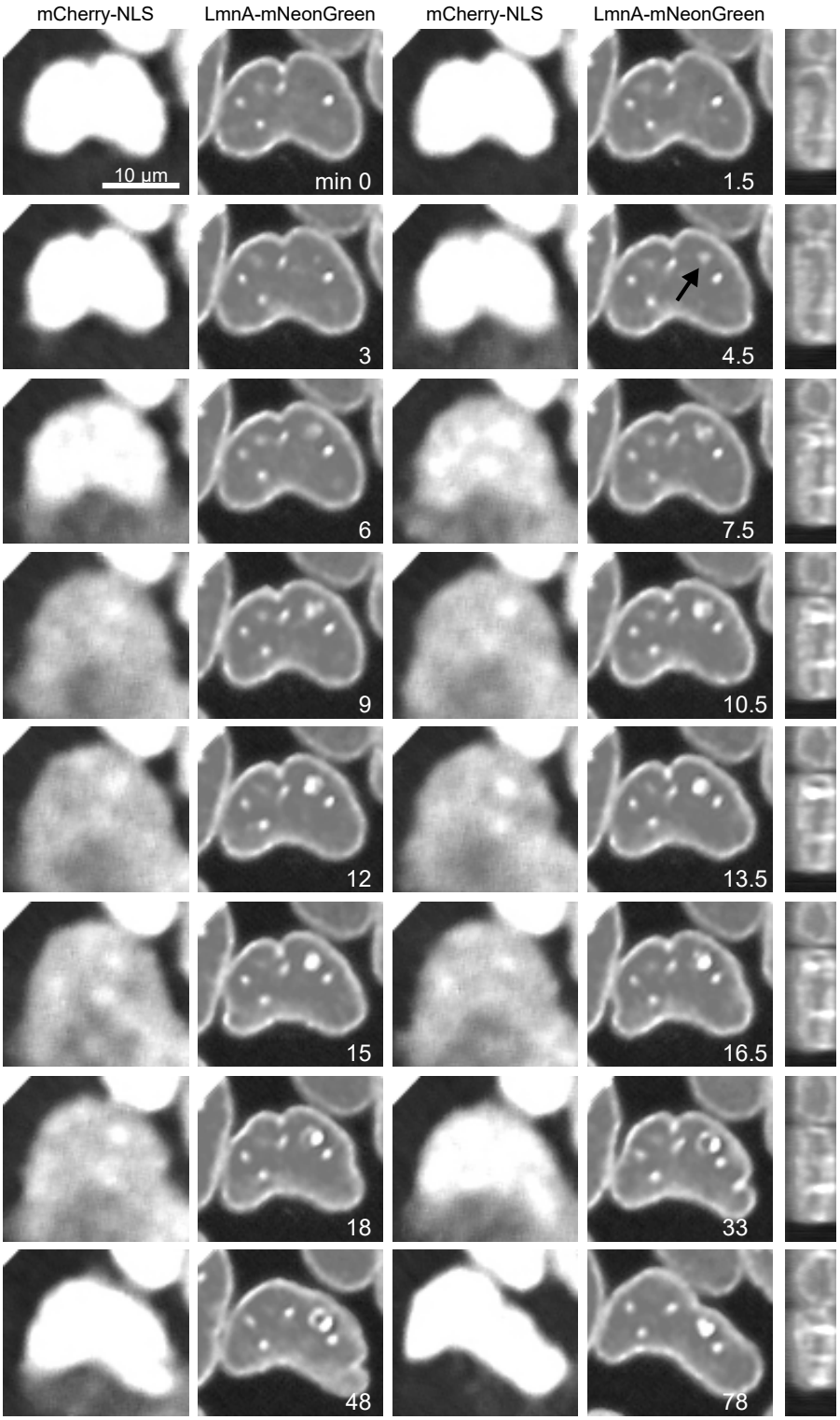


Figure 3-6: NR Formation with nucleoplasmic leak. *U-2 OS cells with endogenous labelled Lamin A-mNeonGreen and mCherry-SNAP-tag-NLS expressed from the AAVS1 locus were imaged every 1.5 minutes with z-stacks. Images were denoised with noise2void. A tube appears to start forming at minute 4.5 while mCherry-NLS appears to leak to the cytoplasm until the NR formation is complete and cytoplasmic mCherry-NLS is reimported. Rightmost images are orthogonal projections at the position of the newly formed tube. mCherry-NLS saturated on purpose so that the low-brightness cytoplasm can be visible in this static figure.*

NR disassembly

The exploration of these time courses also revealed the disassembly of these structures. In **Figure 3-7** we can see an example of a tubular invaginations that crosses the whole nucleoplasm. That tube is present and visible for about 30 minutes. It appears that the apical side becomes thinner, then the rest of the tube becomes also less bright around minute 60 and then it disappears. In **Figure 3-8** we have another example, this time we have a nucleus with two invaginations shown in 3D. We can observe that the left invagination becomes thinner in the bottom then it seems to get cut and the other side retracts to the apical surface. At the same time there is a second invagination that remains unperturbed throughout this timecourse. **Figure 3-9** is a quantification of these disassemblies. The horizontal axis are the z-slices while the vertical axis is the maximum intensity in a region of interest comprising the invagination or a region of interest of the same size in its vicinity. Each line is a time point, the red lines being the early timepoints and the blue lines being the late time points. For the first nucleus, we can observe that there are two peaks of high intensity separated by a valley. This is consistent with the fact the apparent brightness is higher in the vicinity of the nuclear envelope on either side of the nucleus, but lower in the intervening nucleoplasm. In the case of the invagination, we have in the early time points no valley because the invagination bridges both sides of the nuclear envelope and forms a continuum of high intensity values. However, after the invagination is disassembled, we have a profile consistent with that of the adjacent region of interest that did not contain an invagination. Nucleus two is an

example of a two invagination that are disassembled one after the other in a similar fashion than that of nucleus 1.

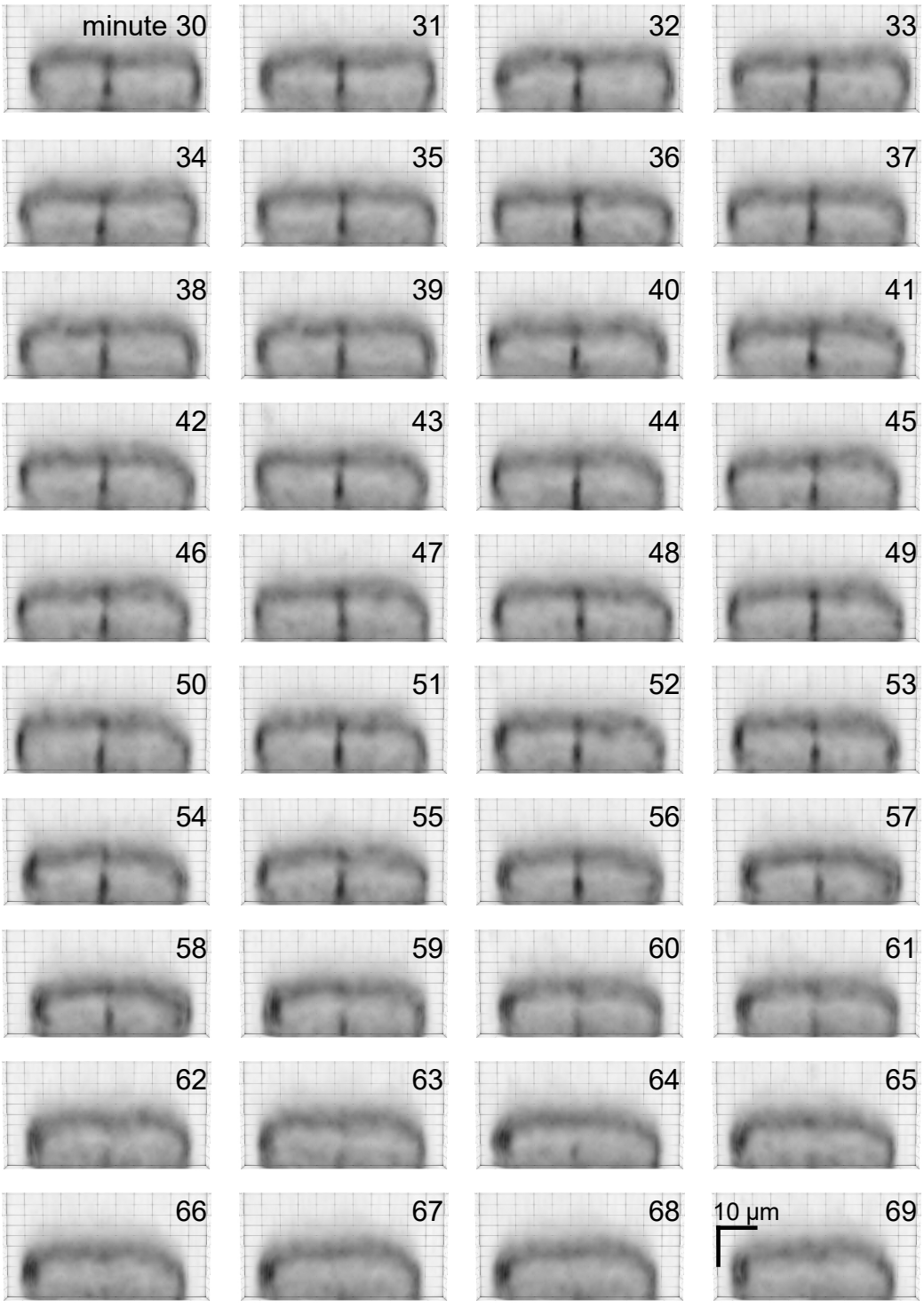


Figure 3-7: NR disassembly. U-2 OS cells with endogenous labelled Lamin A-mNeonGreen*. Sample was imaged every minute with z-stacks. Images were denoised with noise2void. A stable tubular invagination is present and within 10 minutes it thins on the top and is resorbed into the bottom nuclear envelope.*

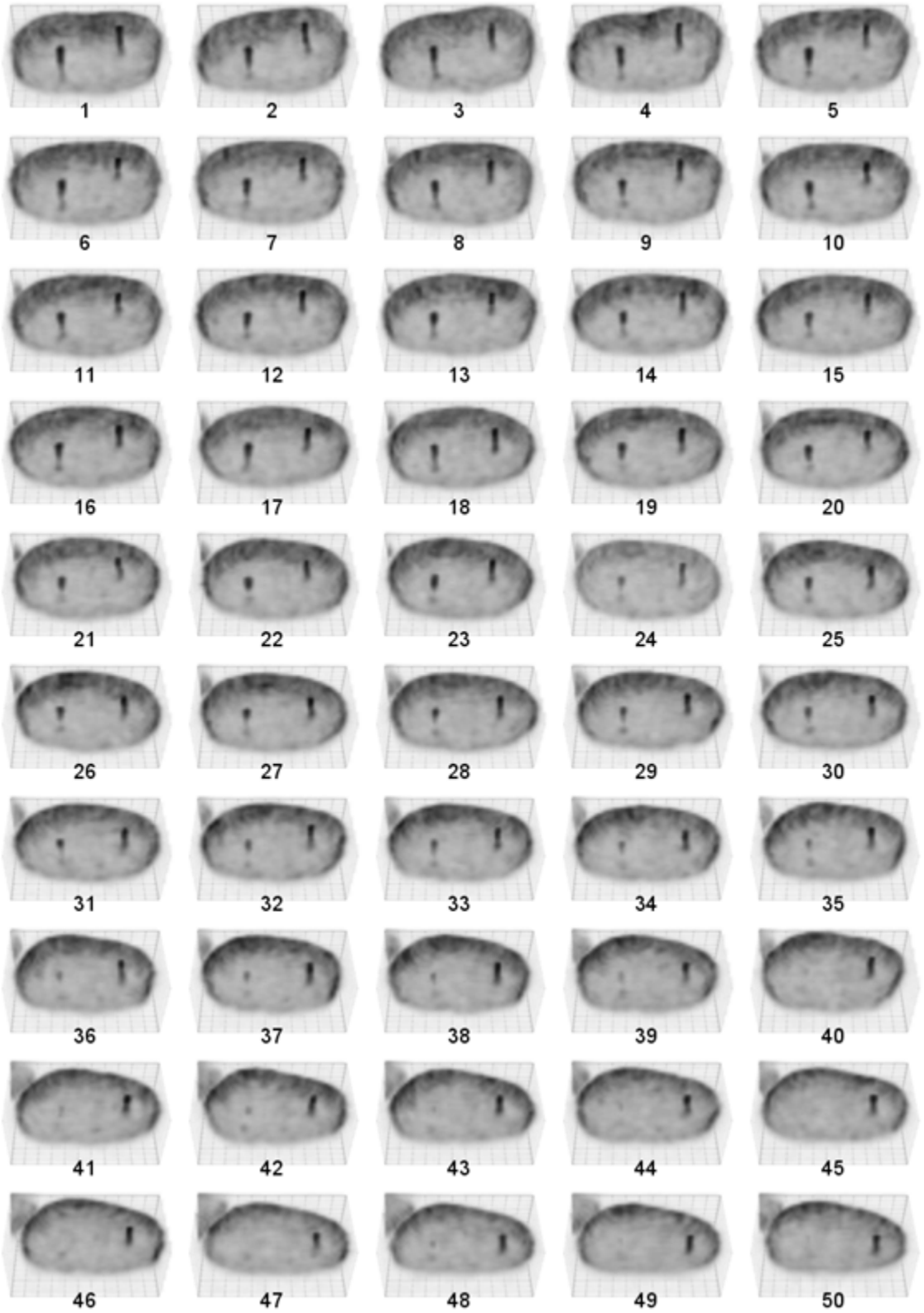


Figure 3-8: montage of a nucleus in 3D where one invagination's is disassembled while another is not. *Whole nucleus width is 16 µm.*

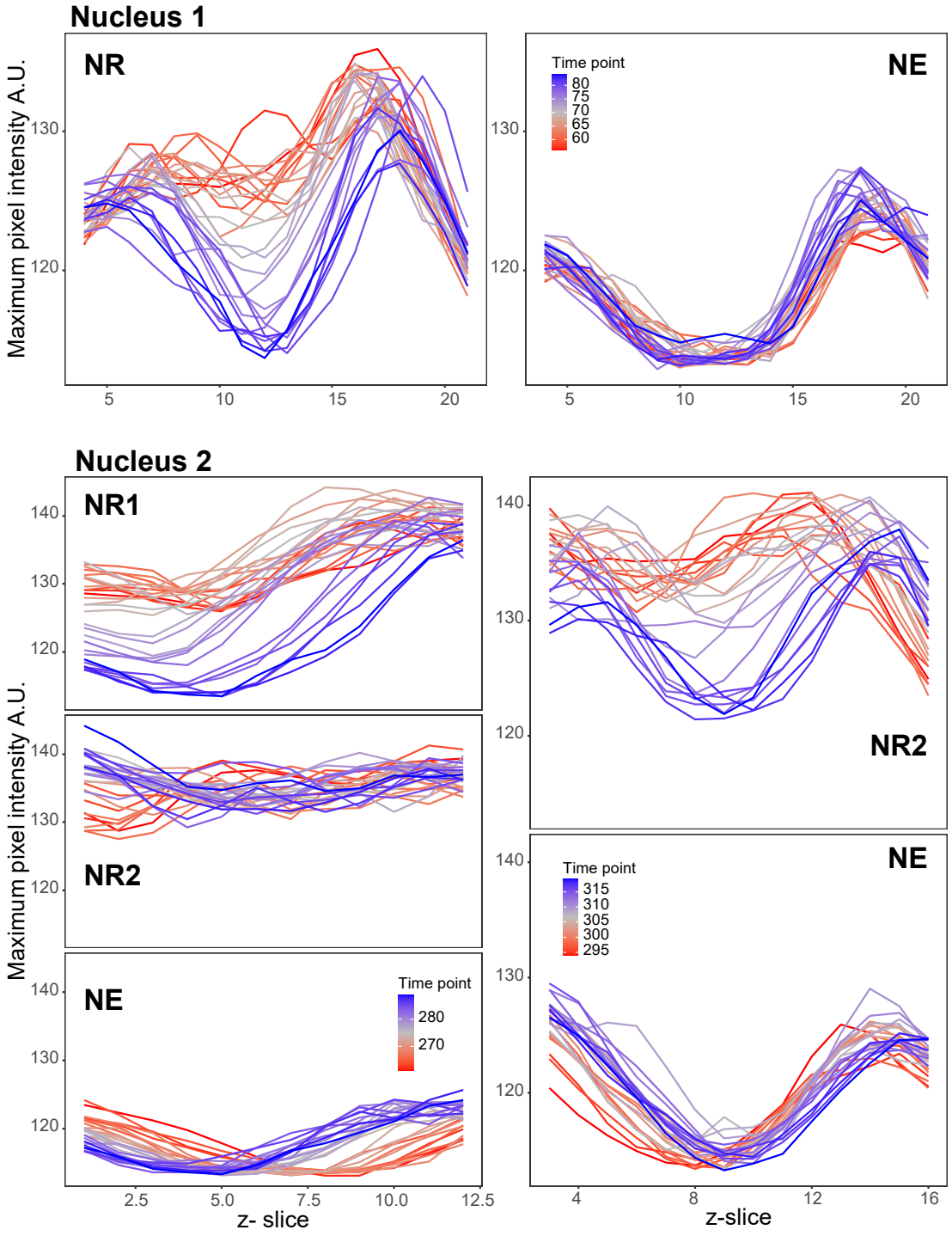


Figure 3-9: Quantification of NR disassembly. *NR disassembly in exemplar nuclei were quantified by measuring the maximum intensity in a ROI covering the NR and another one covering the nuclear envelope immediately next to the NR. The NR in nucleus 1 is disassembled over the course of 10 minutes while the surrounding nuclear envelope remains stable. Nucleus 2 has two invaginations; NR 1 is disassembled while NR2 remains but is later disassembled. In both cases the nuclear envelope remains unchanged.*

Role of membrane-curvature proteins in NR biogenesis

Since reticulons are known to be involved in the formation and maintenance of the curvature of the endoplasmic reticulum (Voeltz et al., 2006) and reticulon 4 specifically locates to regions of high membrane curvature (Kiseleva et al., 2007) we sought to investigate whether reticulon 4 is involved in the nucleoplasmic reticulum formation (**Figure 3-10** - **Figure 3-11**). Using HeLa cells co-transfected with mNeonGreen-Lamin A and Reticulon 4 – GFP we investigated whether the abundance of perinuclear Reticulon 4 increased when the cells were exposed to Saquinavir. We found no difference in its amount over a time range of 24 hours (**Figure 3-10** A). The perinuclear Reticulon 4 abundance did not change but since its distribution may have changed, we investigated whether the foci were brighter; again, in a time period of 24 hours we saw no difference in their brightness when the cells we exposed to Saquinavir (**Figure 3-10** B). When we look specifically in regions where there are forming infoldings we can see that there is indeed an increase in the reticulon 4 abundance relative to a random position of the nuclear envelope where there are no morphological changes (**Figure 3-10** C). **Figure 3-10** D is an example of two infolding that have a bright reticulon 4 foci. The green arrowheads at 5h30 and 5h45 after Saquinavir addition indicate Reticulon 4 foci in positions that later become infoldings (magenta arrowheads at 6h00 and 6h30). After the infolding is formed the Reticulon 4 abundance relative to the length of the infolding decreases (**Figure 3-10** E), although a foci remains at the base of the infolding (white arrowheads at 7h30).

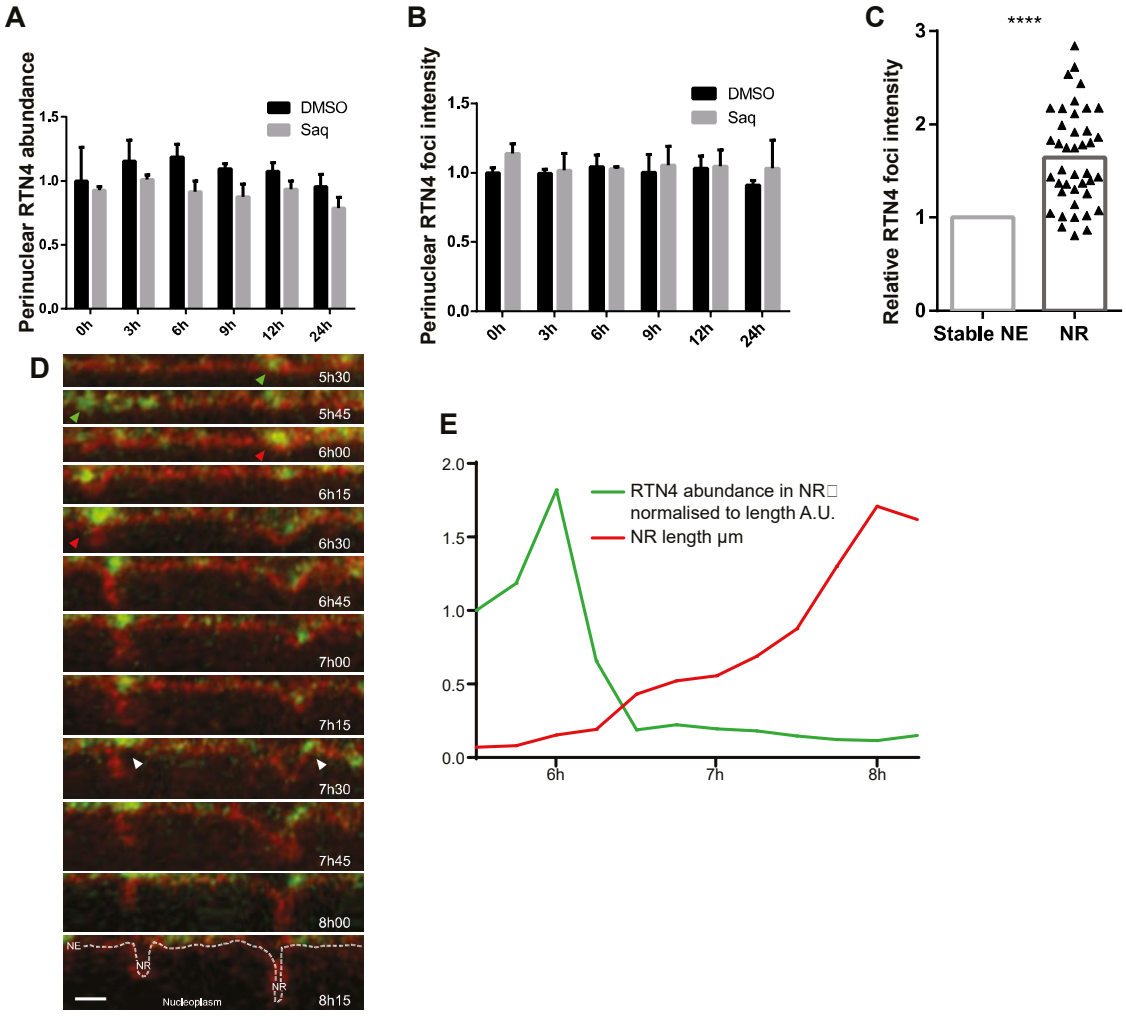


Figure 3-10: Perinuclear RTN4-GFP abundance and intensity within foci does not change when NR formation is induced with Saquinavir. *RTN4 is recruited at the sites of forming NR.* ***(A)*** *Perinuclear RTN4-GFP abundance relative to initial DMSO control. Hela cells were co-transfected with Lamin A-mNeonGreen and RTN4-tdTomato. Images were acquired in the midplane. Formation of NR was pharmacologically induced with Saquinavir at t=0. The raw integrated density was measured in a 1.5µm wide region of interest around the nuclear envelope based on the Lamin A localisation. The perinuclear abundance is the ratio of the raw integrated intensity over the mean intensity (to control for different overall levels of expression) normalised to the area of the ROI. DMSO result for 0h was set to 1 and the rest was adjusted accordingly. The mean and SD of three independent replicates is plotted, on average 67 cells per condition per replica.* ***(B)*** *Perinuclear RTN4-GFP foci intensity relative to initial DMSO control. The perinuclear foci intensity is the perinuclear abundance divided by the area of the foci. DMSO result for 0h was set to 1 and the rest was adjusted accordingly. Foci detection is based on the Maximum Entropy threshold algorithm. The mean and SD of three independent replicates is plotted, on average 67 cells per condition.* ***(C)*** *RTN4 foci intensities were measured specifically at NR forming sites and compared to random sites of stable nuclear envelope. n = 3, 41 foci; **** P < 0.0001.* ***(D)*** *HeLa cells were co-transfected with Sec61β-RFP and RTN4-GFP. Formation of NR was pharmacologically induced with Saquinavir at t=0. Z-stacks were acquired every 15 minutes. Green arrow: recruitment sites of RTN4. Red arrow: sites of developing invaginations. White arrow: presence of RTN4 at the base of the invagination. Scale bar=2µm.* ***(E)*** *Quantification of the Reticulon 4 abundance and NR length versus time.*

Figure 3-11 depicts a HeLa cell transfected with mNeonGreenLamin A and Reticulon 4 -tdTomato containing an infolding that ends as a tube traversing the nucleoplasm. In Z slices 6 to 12 a foci in the proximity of the area of the nuclear envelope that becomes an infolding can be seen.

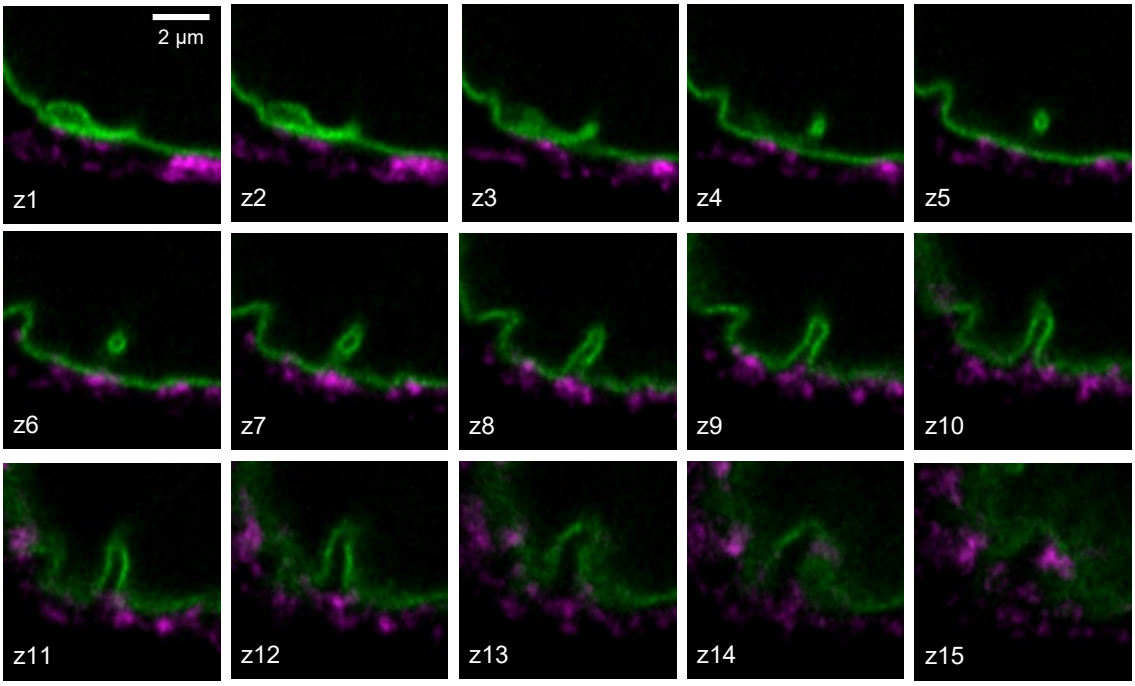


Figure 3-11: Reticulon 4 is present in the proximity of nuclear envelope infoldings and invaginations. *HeLa Cells were transfected with Lamin A mNeonGreen and Reticulon 4 tdTomato. NR was induced with Saquinavir*

Observing that Reticulon 4 is found in the proximity of curved membranes is not enough evidence to claim that it is involved either in the formation or the maintenance of the nucleoplasmic reticulum. So, we then used siRNA to knock down Reticulon 4 in Hela cells and checked whether it changed the mean number of invaginations per nucleus. In **Figure 3-12** we can see that in the presence of Saquinavir both with the reticulon 4 siRNA and a control siRNA we have an increase in the number of

invaginations relative to the cells that had no Saquinavir and that there is no significant difference between the number of invaginations in cells with the Reticulon 4 siRNA or the control siRNA although the increase relative to the no treatment condition is significant at a higher p value for the null hypothesis.

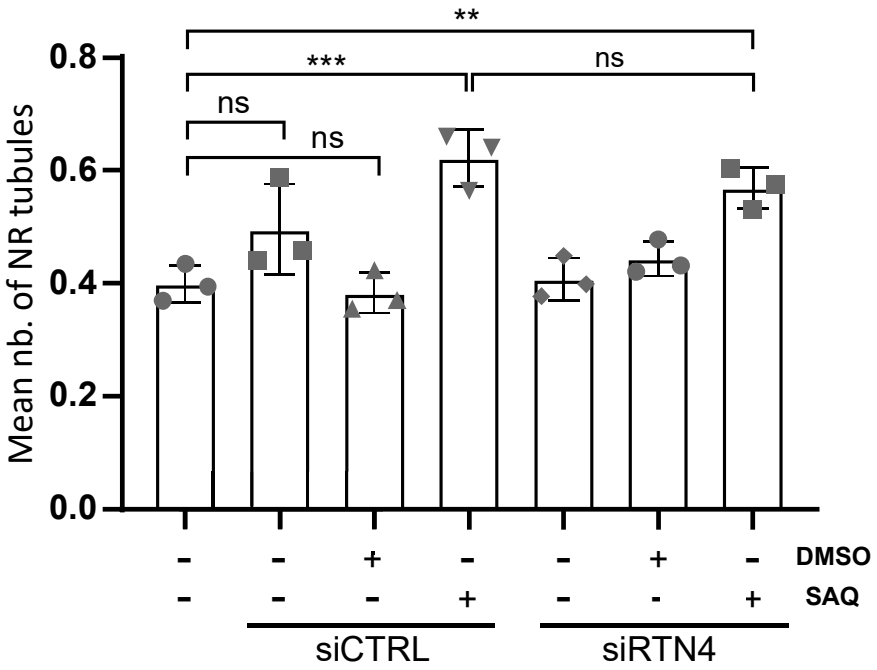


Figure 3-12: Reticulon 4 knockdown by siRNA reveals that it is not essential for NR formation. *HeLa cells expressing mNeonGreen Lamin A were transfected with siRNA targeting reticulon 4 then left for 24 hours before inducing NR formation with Saquinavir.*

3. Discussion

Here we have demonstrated that it is possible to tag both Lamin A and Lamin B1 in their endogenous locus with fluorescent proteins and this enabled us to see for the first time the assembly and disassembly of the nucleoplasmic reticulum in live cells with a high spatial and temporal resolution.

There is a very large number of mutations both in Lamin A and Lamin B that can cause laminopathies (Broers et al., 2006; Caron et al., 2007; Méndez-López and Worman, 2012; Navarro et al., 2006; Raharjo et al., 2001; Vigouroux and Capeau, 2005; Wang et al., 2016; Worman, 2011; Worman and Schirmer, 2015; Worman et al., 2010). These include progeria, lipodystrophies, muscular dystrophies, and neuropathies. Yet, adding the 26.6 kDa globular fluorescent protein mNeonGreen (Shaner et al., 2013) or mScarlet (26.4 kDa, Bindels et al., 2017) does not seem to change the way both lamins interact with the rest of the nuclear envelope though Emerin and the Lamin B receptor. In addition, one of the hypotheses of why the accumulation of pre-Lamin A leads to an increase in the abundance of nucleoplasmic reticulum is that the farnesyl group before cleavage from the pre-Lamin A by ZMPSTE-24 leads to a different lamina web that created these tubes. It would be interesting to further test that hypothesis by tagging Lamin A with fluorescent proteins of varying sizes and see whether they affect the nuclear envelope morphology (although it is only possible to tag the N-terminus of Lamin A because the C-terminus is cleaved when the farnesyl group is removed).

We assessed whether the response to Saquinavir of the newly created cell lines was different in terms of cell death and found that there is no difference meaning that having the farnesyl group only in the C-terminus or having also the mNeonGreen fluorophore in the N-terminus did not change the functioning of the Lamin. In addition to this we found that we could still induce NR formation with Saquinavir and with oestrogen and progesterone in Ishikawa cells.

Having HeLa cells with both Lamin A and Lamin B1 endogenously labelled with fluorescent proteins enabled us to measure the apparent density of the lamina in the nuclear envelope versus its invaginations and we found that the density (brightness divided by the volume) increased in the tubular invaginations. The images used for this were acquired on an LSM880 with the Airyscan super-resolution having a theoretical 120 nm resolution in X-Y and 350-nm axial resolution for z-stacks meaning that the resolution of the images is sufficient for this analysis. Note as well that this was only possible because we tagged the endogenous loci of these genes and that using immunofluorescence would have brought issues related to the potentially different accessibility of the antibodies to the antigen in the area of the nuclear envelope that has a curvature opposite to that of the tubular invaginations. In the future it would be interesting to further investigate the structure of the lamina by expansion microscopy so that the meshwork becomes discernible and to use multiple antibodies against the same lamin with known epitope targets so that one can orientate the filaments.

In the past, it has been postulated that the NR is a remnant of the way the nuclear envelope is re-assembled after cell division. We have shown that in Ishikawa

cells it is possible to assemble and disassemble these structures without mitosis and nuclear envelope reassembly. Indeed after 24 hours of hormone exposure we had an increase in the number of invaginations and after 3 hours post hormone removal the number of invaginations decreases. We used CFSE to measure the rate of cell division and found that it is about 30 hours both for cells with oestrogen plus progesterone or without meaning that the formation and dissolution of the NR had to occur without cell division. It is indeed possible that some invaginations represent vestiges of nuclear envelope reassembly, but it is certainly not the case for all of them and it implies that there is a dedicated machinery for its formation.

The advances in image denoising methods enabled the acquisition of long time courses with short intervals and 3D stacks. We used unstimulated U-2 OS cells expressing mNeonGreen Lamin A and imaged the cells at intervals of 1 or 1.5 minutes. We observed the assembly and disassembly of invagination in interphase. We found that new invaginations could be formed within minutes and that the formation was accompanied with a release of some nucleoplasmic material. At this stage we do not know why this happens. It could be caused by the incorporation of NPC in that structure or the induction of the change of curvature in the membrane that breach the nuclear envelope in the inflection point.

We also found instances of NR disassembly during interphase and documented that it could also happen within minutes. The exploration of the movies may have revealed features of this process. We observed examples where the tube disassembles by first narrowing close to the apical side, followed by an apparent break that permits

withdrawal and resorption of the severed channels into the nuclear envelope at both ends. Collection and careful analysis of additional time lapse movie data will be essential to establish whether this is a general pattern.

We also found striking examples in which a nucleus containing more than one NR channel exhibited loss of one channel with no effect on the remaining NR structures. We take this to imply that a specific disassembly mechanism can target specific NR channels, without a general loss of these structures from a nucleus: one could be disassembled while the other remains meaning that the mechanism that disassembles it can be specific enough to maintain certain tubes while others are removed. Future experiments would involve imaging the nuclei simultaneously with a fluorescent Lamin, a fluorescent component of the NPC and a lipid dye. This would reveal the order of successive events required to assemble or disassemble these structures. This will require the use of bright fluorophores and more advanced denoising techniques such as Struct Noise2Void (Broaddus et al., 2020) that is better suited for the removal of structured noise often found in short exposure images from spinning disk microscopes.

Finally, we explored the potential role of reticulon 4 in NR formation. We found no increase in its abundance or changes in its distribution when inducing NR formation with Saquinavir, but we found that it was present in the vicinity of forming invaginations. However we must remember that as Herman Hesse writes in Siddhartha “When someone seeks, then it easily happens that his eyes see only the thing that he seeks” (Hesse and Rosner, 1971), indeed not all foci were associated with NR. In addition to this, we found that knocking down with siRNA reticulon 4 had no effect on the formation

of NR meaning that either the siRNA we used was not effectively removing reticulon 4 or that when reticulon 4 is removed another protein with a similar function compensated or that simply reticulon 4 is not involved in the formation of this structure. Nevertheless, other proteins and lipids involved in the formation and maintenance of the curvature in the nuclear envelope are likely to be needed. Indeed, the lipid composition plays a key role in the membrane curvature and fusion. In fact, it has been shown that diacylglycerol is essential for nuclear envelope fusion in high-curvature areas (Chung et al., 2018). Additionally phosphoinositide are modulators of membrane morphology (Larijani et al., 2014) causing positive curvatures. Other proteins causing curvatures in the membrane might include flippases and floppases that that either flip an excess or not sufficient lipids across the membrane leaflets causing an asymmetric accumulation of lipids and invaginations. ESCRT-like proteins that assemble in concentric spirals around membrane budding could also lead to the formation of invaginations of the nuclear envelope (Peeters et al., 2022). Additionally, the depletion of Torsins-like proteins may also cause invaginations of the nuclear envelope (Rampello et al., 2020).

We now know more about the assembly and disassembly of this structure. The next chapter will explore its function.

4. Role of NR in bidirectional nucleocytoplasmic transport

"To measure is to know."

- Lord Kelvin (19th century)

1. Introduction

Even though the nuclear envelope has been observed in early electron micrographs in the mid-twentieth century and its function predicted, the role of the NR, which was also observed in early electron micrographs, has been largely ignored or hypothetical at best. The main presumption is that the NR brings deep into the nucleus the same, or similar, functions than the rest of the nuclear envelope. Although this seems reasonable there has never been any evidence supporting or refuting this claim. Two functions have been described in the literature with different degrees of

compelling evidence. They include calcium release in the nucleoplasm and movement of vesicular structures deep inside the nucleus, either inbound extracellular vesicles, or outbound nascent viral particles.

Calcium signalling is involved in virtually every cellular process and is essential for regulation of enzymatic reactions, signalling pathways and gene expression. Echevarría et al. (2003) found that the NR contains inositol triphosphate ($InsP_3$) receptors that are essential for calcium signalling and are indeed capable of regulating calcium signals in subnuclear regions. Interestingly Lui et al. (2003) also found that NR can contain $InsP_3$ receptors but not all DiOC6(3) positive invaginations were positive for $InsP_3$ receptors. Marius et al., (2006) found that ryanodine receptors also involved in calcium release were present in the NR and (Guatimosim et al., 2008) demonstrated that the inositol triphosphate and ryanodine receptors were present in cardiomyocyte NR. Echevarría et al. (2003) demonstrated that nuclear protein kinase C (PKC) translocates to the nucleus where it is involved in gene expression regulation (Martelli et al., 2006).

The Lorico group found that extracellular membrane vesicles are associated with the NR both *in vitro* and in breast cancer patient biopsies (Rappa et al., 2017). In addition, when vesicle-associated membrane protein A (VAP-A), the cytoplasmic oxysterol-binding protein–related protein 3 (ORP3), or the late endosome–associated small GTPase Rab7 were silenced by siRNA no late-endosome were found in the nuclear envelope invaginations. Furthermore, FRET demonstrated that these three proteins interact more in the nuclear envelope invaginations than in the cytoplasm (nuclear

envelope invaginations versus nuclear envelope was not compared). They show that when cells are treated with nocodazole no vesicles are found in the nuclear envelope invaginations. However, they show that when VAP-A or ORP3 are silenced with shRNA no Rab7+ late endosomes are found in the nucleoplasm of the cells meaning that that import mechanism is not specific to the NR (Santos et al., 2018). Finally, they show that the antifungal drug Itraconazole inhibits delivery of extracellular vesicles to the nucleus through the nuclear envelope and it's invaginations (Santos et al., 2021).

One of the potential functions of the NR is accelerating the bidirectional exchange of material between the nucleoplasm and cytoplasm. Schoen et al. (2017) simulated the diffusion of mRNA in a theoretical spheric nucleus with or without a single tubular invagination of different lengths and diameter. They found a significant theoretical reduction in the diffusion time in the proximity of the invagination and the global average was decreased by 10%. The aim of this chapter it to demonstrate experimentally whether there is or not nucleo-cytoplasmic exchange of material through the nucleoplasmic reticulum.

We began our investigation of a potential role for NR in nuclear import and export by first examining the relationship between NR abundance and DNA content or nuclear size, arguing that if nuclear import or export was functionally enhanced by NR, we would expect its abundance to increase with demand, in the form of larger nuclei or a greater DNA content. We then turned to the issue of import/export competence of NR by assessing the presence of two essential structural pre-requisites: a cytoplasmic core and NPC.

We then turned to a functional analysis of nuclear import and export and sought a relationship between these processes and the presence and positioning of NR channels. In order to address that question, it is essential to have a high spatio-temporal control of the import and export of material though the nuclear envelope. We used two experimental systems to achieve tightly regulated nuclear import and export: PhoCl (Zhang et al., 2017) and LEXY (Niopek et al., 2016). PhoCl is a photocleavable protein that was engineered from mMaple (McEvoy et al., 2012) such that it spontaneously cleaves when photoconverted with violet light (~ 400 nm) (Zhang et al., 2017). When PhoCl is fused to the cytoplasmic domain of a protein of the plasma membrane, such as CD2, in one terminus and a fluorescent protein with a nuclear localisation signal on the other terminus, the nascent un-converted protein delivers the fluorophore to the plasma membrane and sequesters it there. When the fusion protein at the plasma membrane is photocleaved with violet light the fluorescent protein with its nuclear localisation signal is released and promptly imported into the nucleus. LEXY, the light-inducible nuclear export system (Niopek et al., 2016), is a derivative of LINuS, the light-inducible nuclear localization signal (Niopek et al., 2014). Both systems are based on the AsLOV2 Domain (a naturally photo-switchable protein from *Avena sativa*) (Lungu et al., 2012; Strickland et al., 2012). This AsLOV2 protein photo-cages the peptide present in its C-terminus (a nuclear localisation sequence for LINuS and a nuclear export sequence for LEXY). By carefully selecting nuclear localisation and nuclear exports signals the authors engineered fusion proteins that can be imported (LINuS) or exported (LEXY) to and from the nucleus on demand and reversibly with blue light (~ 450 - 495 nm). When

these fusion proteins are combined with a fluorescent protein it is possible to follow its movement across the cell and the nuclear envelope.

We hypothesised that the NR contains functional nuclear pore complexes that enable the bidirectional exchange of material between the cytoplasm and nucleoplasm and that this facilitated transport might provide an advantage in terms of cell proliferation.

In this chapter we:

1. Investigate when NR is present in relation to the volume and DNA content of the nuclei and cell cycle (**Figure 4-1** and **Figure 4-2**).
2. Since the presence of NPC is essential for the exchange of material, we probed whether all invaginations had them (plus cytoplasmic cores) (**Figure 4-3** to **Figure 4-5**).
3. Using photoinducible systems for the import and export of material in and from the nucleoplasm we followed fluorescent proteins and demonstrated that there is indeed exchange of material at the NR (**Figure 4-6** to **Figure 4-8**).
4. Explored the relationship between single colony's parameters and NR content (**Figure 4-9** to **Figure 4-11**).

2. Results

The function of the NR has been at best hypothetical. Here we aimed to measure whether the NR is actually involved in the exchange of material across the nuclear envelope and whether it facilitates delivery and collection of material from deep within the nucleoplasm.

One way of gathering information about the function of the NR is by looking where and when it is present. For this we stained Ishikawa cells with DAPI and anti-Lamin A to visualise DNA content plus the nuclear envelope. Three-dimensional confocal microscopy was used to image un-synchronised cells (**Figure 4-1** A). Nuclei were then segmented, and their volume and DNA content was measured (**Figure 4-1** B). The DNA content was used to categorise the nuclei into G1, G2 or polyploid nuclei (G2*2) meaning nuclei that went through replication once without mitosis. The scatter plot shows a classic distribution of DNA content versus volume similar to a DNA versus side scatter (SSC) traditionally obtained by flow cytometry meaning that the measured results are plausible and correct. The NR abundance was then quantified manually for each nucleus and box plots for G1, G2 and G2*2 were made (**Figure 4-1** C). We can see that there are significantly more invaginations in G1 than in G2 and that the number of invaginations increases significantly again for the polyploid cells. This illustrates how NR can assemble and disassemble without mitosis.

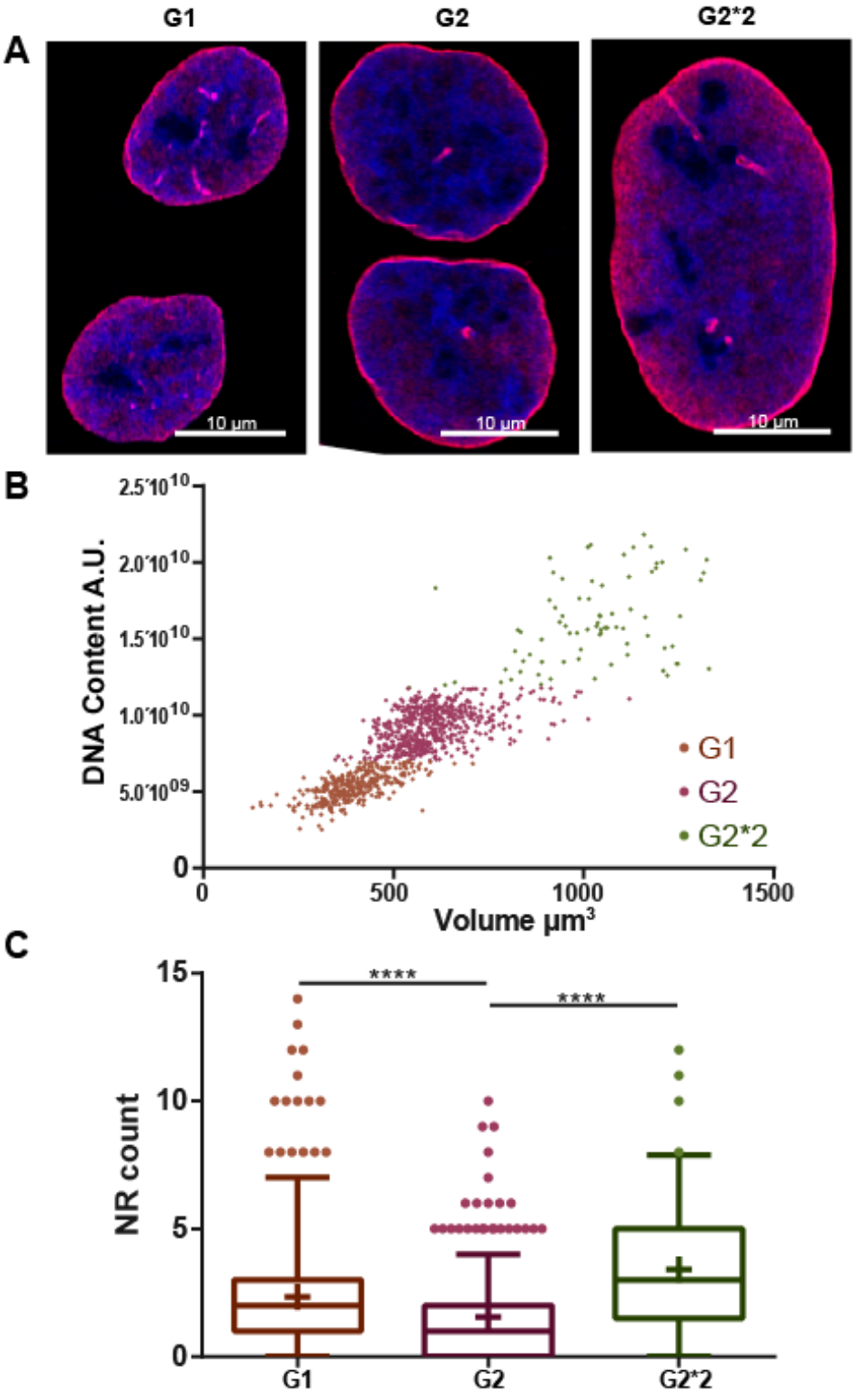


Figure 4-1: NR abundance is correlated to nuclei volume and DNA content*. (**A**) Ishikawa cells were stained for DNA (DAPI) and Lamin A (mouse anti Lamin A, anti-mouse AF594) and imaged by 3D confocal microscopy. (**B**) Nuclei were scored for volume, DNA content and NR abundance. (**C**) Based on DNA content nuclei were divided in 3 categories and plotted against NR abundance. Data from three replicates; G1 n=360, G2 n= 568, G2*2 n=81. Box is lower 1st to upper 3rd quartile with median and "+" for the mean; whiskers are 5-95 percentile, **** for P < 0.0001.*

Figure 4-2 is a further exploration of the data in **Figure 4-1**. We can see that the less DNA there is, and the smaller the nuclei are, the more invaginations there are - this is a known feature of the nuclear envelope immediately after nuclear envelope reassembly - and those invaginations quickly disassemble before entering G2. The novel observation is that the larger the nuclei are and the more DNA they have the more invaginations they contain. This could support the hypothesis that the NR provides the classic nuclear envelope functions to regions that are further away from the periphery of the nuclear envelope. The NR count versus DNA density shows that there is no correlation between these two variables.

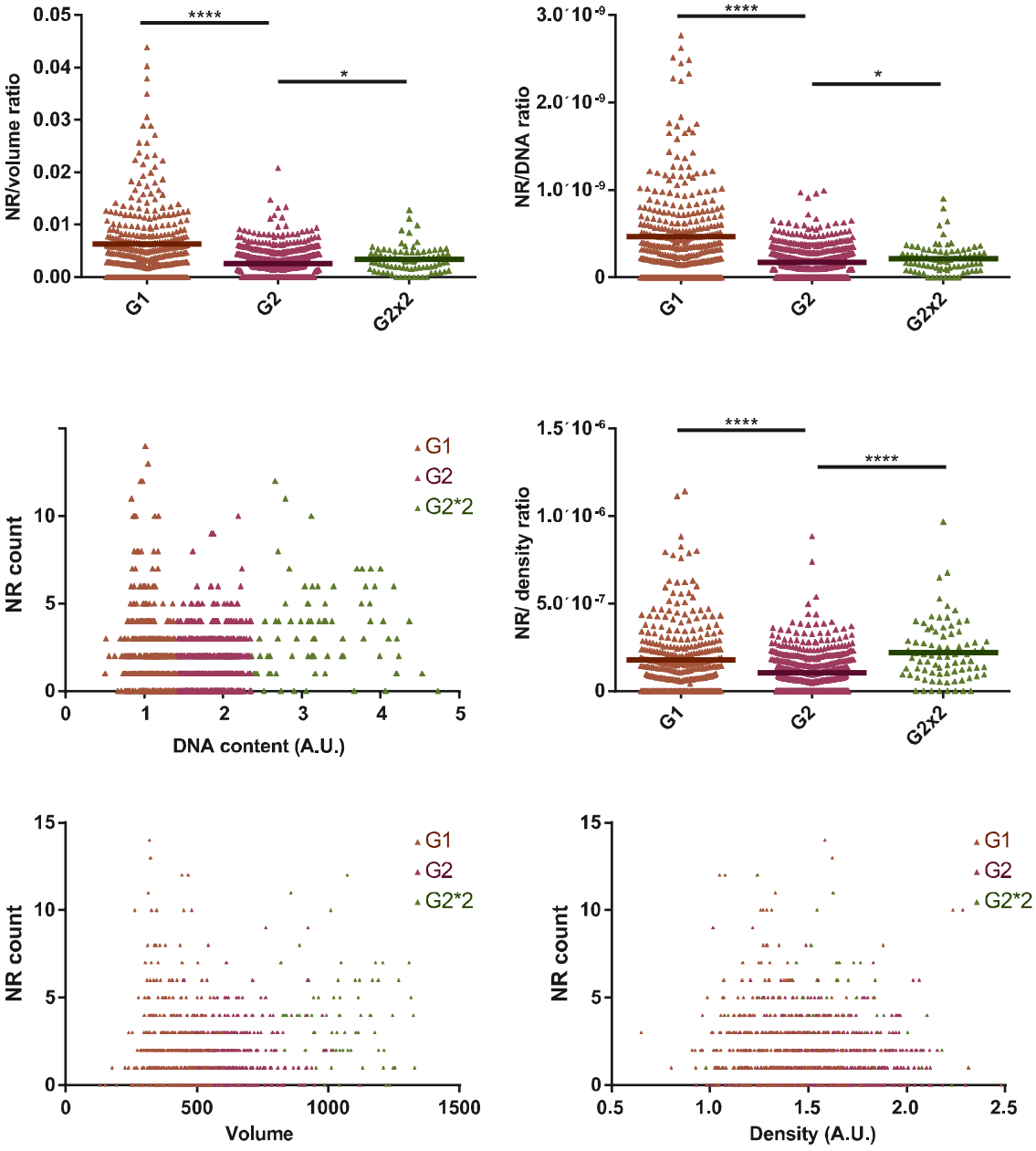


Figure 4-2: Advanced analysis of NR count vs volume and DNA density from previous figure. *NR counts are the number of tubular invaginations pre nucleus. "DNA content" is the raw integrated density per nucleus (sum of all pixel intensities - units are arbitrary). "Density" is the DNA content divided by the volume of the nuclei.*

In order to have exchange of material between the nucleoplasm and cytoplasm though the NR those invaginations need to have a cytoplasmic core that exhibits diffusional continuity with the bulk cytoplasm. **Figure 4-3** illustrates that Invaginations visible by tagging the lamina with a fluorescent label have indeed a cytoplasmic core. Here the nuclear envelope was tagged with mNeonGreen-Lamin A; the spot in the centre of the nucleoplasm is a tubular invagination crossing the whole nucleus as visible in the orthogonal projection at the position of the arrowhead. In order to visualise the cytoplasmic core of the NR cells were permeabilised alive with a 750 µg/mL saponin solution containing a secondary goat anti rabbit IgG Alexa Fluor 546 to fill the cytoplasm. This indeed reveals the presence of the cytoplasmic core of the NR and confirms its continuity with the bulk cytoplasm.

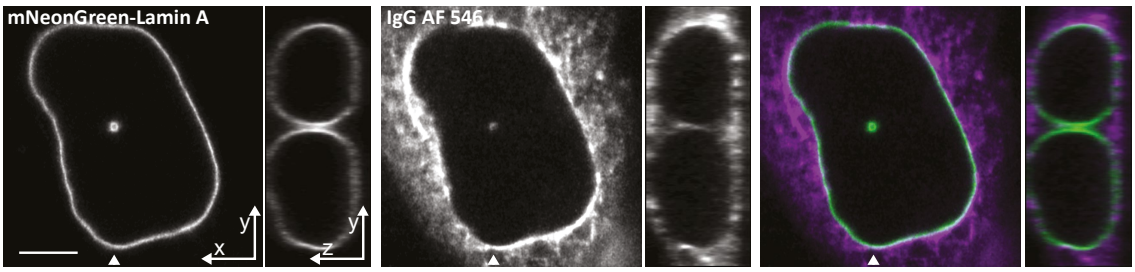


Figure 4-3: NR contains a cytoplasmic core. *Cytoplasmic loading in Ishikawa cells by IgG AF 546 to visualize the cytoplasmic core of the invagination. Arrowhead indicates position of orthogonal projection in the panels to the right. Scale bar 5 µm.*

Having a cytoplasmic core is not sufficient proof of exchange of material across the NR. Invaginations need to have nuclear pore complexes (NPC) though which material is exchanged. We then explored the abundance of NPC in the NR; for this we stained nuclei with anti-Lamin B1 - to visualise the nuclear envelope and its

invaginations -, anti-Nup 98 and Nup 153 - components of the NPCs - and anti-Nesprin 2 – component of the LINC complex sitting between the inner and the outer nuclear envelope membranes that allows us to distinguish type 1 from type 2 invaginations. We found that all these elements are present in the invaginations of the nuclear envelope (**Figure 4-4**). However, **Figure 4-5** AB illustrates that not all invaginations visible with anti-Lamin B1 contain NPC (top-right arrowhead) meaning that potentially different invaginations have different functions or that they are in a different state relative to their formation. We used Ishikawa cells and scored the invaginations visible in the anti-Lamin B1 staining into 4 levels of LINC and NPC abundance – from absent to abundant. **Figure 4-5** C is the resulting quantification (numbers indicate percentage of invaginations falling in each category). In the control of unperturbed cells 90% of the invaginations have NPC (100 -1.9 - 0.5 - 3 - 4.6) while 86.5% of the invaginations have LINC complex (100 - 4.6 - 4.3 - 3 - 1.6). Finally, 95.4% (100 – 4.6) of the invaginations have either NPC or LINC complex meaning that they are likely type 2 invaginations comprising the inner and the outer membrane. When NR formation is induced with physiological levels of oestrogen and progesterone for 24 h there is an increase in the abundance of invaginations. However, those invaginations have no or few NPC and LINC complexes (bottom left quadrants). Another 24 h later only 1.9% of the invaginations have no NPC or LINC complexes. Presumably, invaginations are formed – as they become visible with the Lamin B1 stain – then NPCs and LINC complexes are recruited.

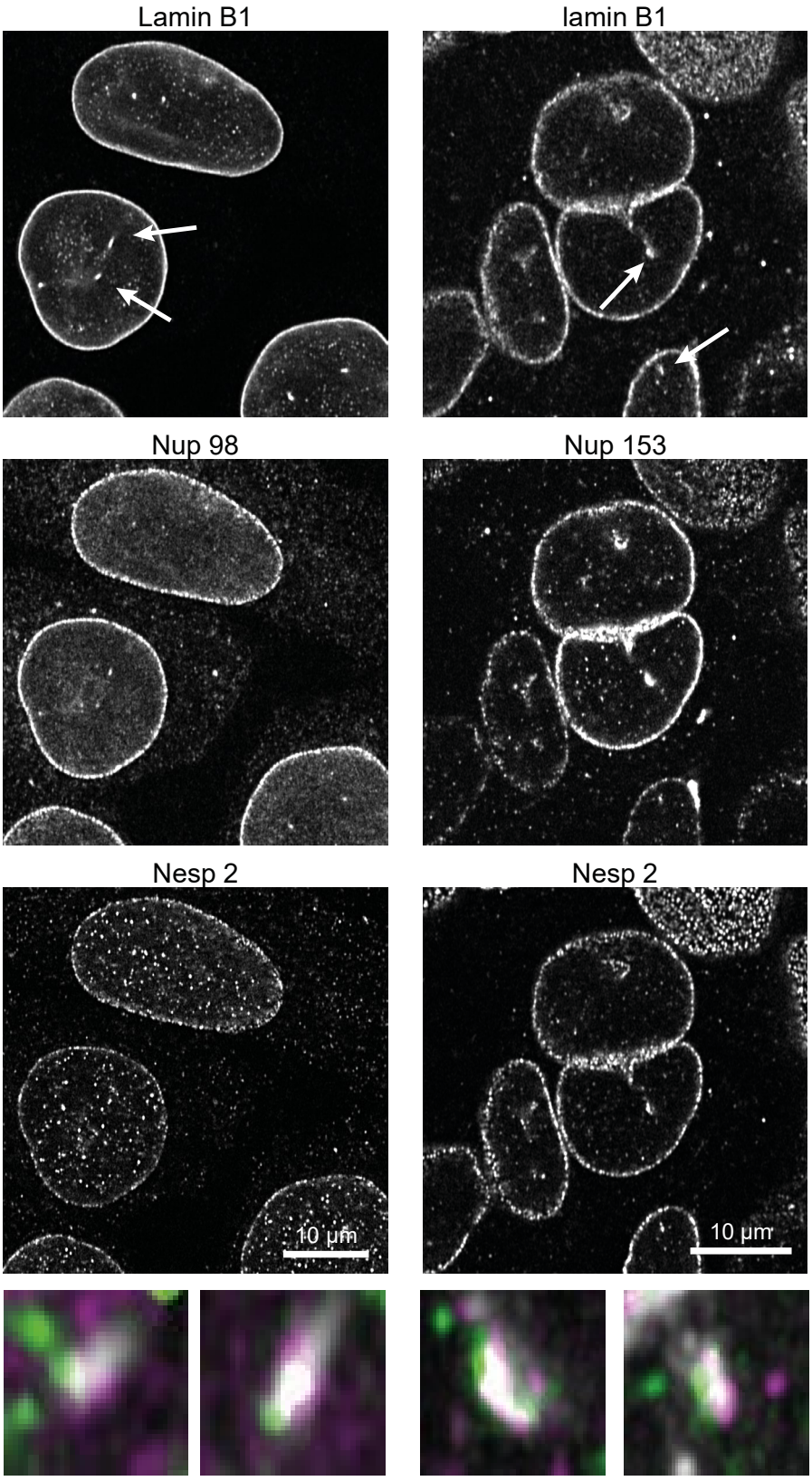


Figure 4-4: Nups and LINC are found in the nucleoplasmic reticulum. *Immunofluorescence of Ishikawa cells with anti-Lamin B1, anti-Nup 98, anti Nup 153 and anti Nesprin 2 demonstrate that these components are present in the invaginations of the nuclear envelope.*

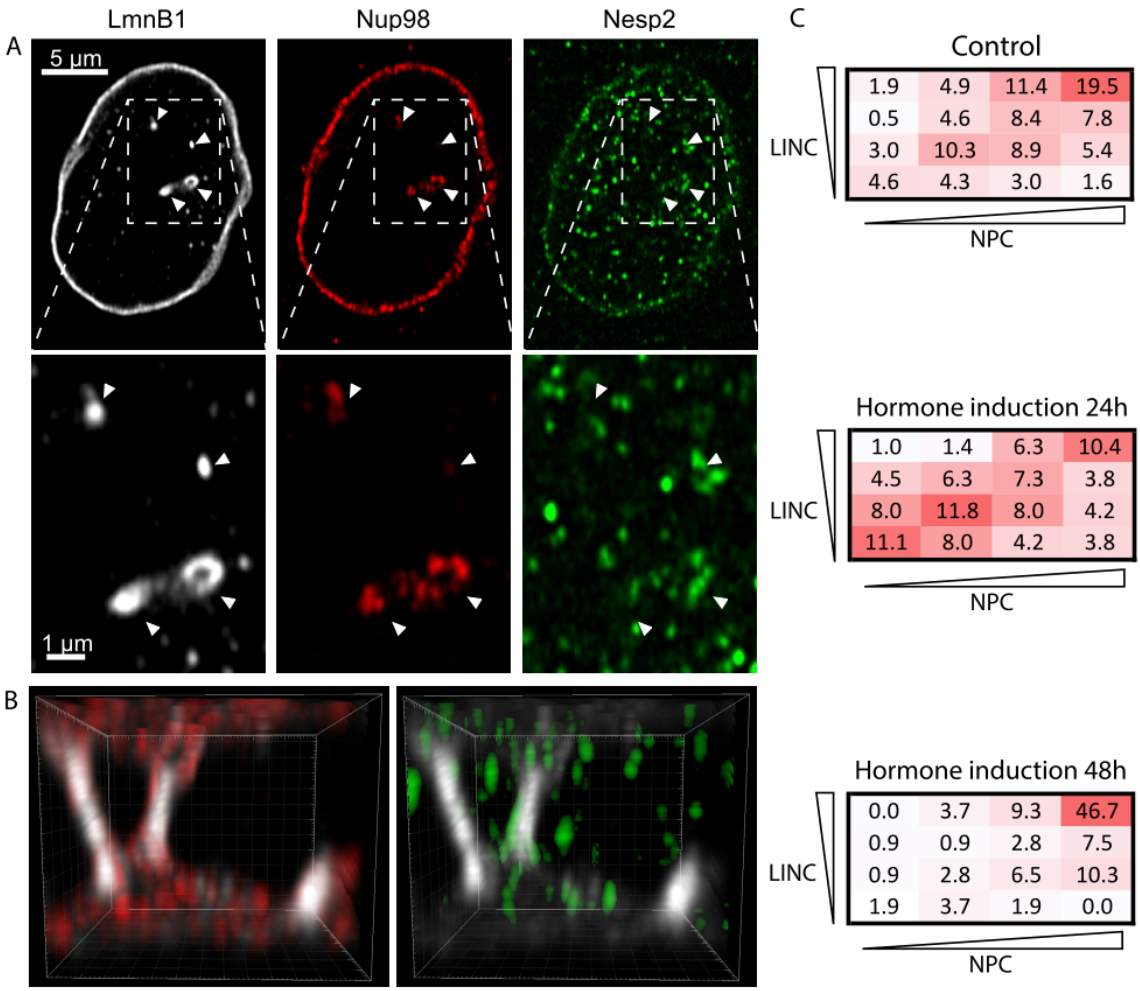


Figure 4-5: When NR formation is pharmacologically induced with oestrogen and progesterone, invaginations are first formed then NPC and LINC are recruited to the NR. (A) *Immunofluorescence of Ishikawa cells with anti-Lamin B1-Cy5, Nup98-AF594, Nesp2-AF488 showing nuclear envelope invaginations with different amounts of LINC and NPC.* ***(B)*** *3D reconstruction of a section of the nucleus shown in A.* ***(C)*** *Individual invaginations were scored for the abundance of LINC and NPC in uninduced Ishikawa cells and both at 24 and 48h after NR formation induction. Analysis from 3 replicates were pooled, n is respectively 370, 288 and 107.*

Once again, having a connected cytoplasmic core and NPC is not evidence of exchange of material across the NR. There exists a variety of tools to follow movement of protein tracers within cells, some suitable for live cell use and others based on biochemical fractionation approaches. In order to study the role of NR in nucleocytoplasmic transport, an imaging method is preferred in order to distinguish between the contribution of NR channels and the bulk nuclear envelope. One way of

visualising exchange of material across the NR in the living cell is by following a fluorophore. The inherent difficulty in this approach is synchronisation of a wave of import tracking marker proteins so that routes into the nucleus along rapid transport pathways can still be distinguished. Multiple light inducible systems for the release of a fluorophore exist. They include PhoCl – a photocleavable protein that splits when exposed to 400nm light (Zhang et al., 2017), - and LEXY - a light-inducible nuclear export system based on a fusion protein containing both NLS and NES sequences but the NES sequence is only exposed to exportins when exposed to blue light (Niopek et al., 2016).

Fusion proteins comprised of CD2-PhoCl with fluorescent proteins and a nuclear localisation signal were designed, cloned, and expressed in HCT cells (**Figure 4-6** A). The presence of CD2 in the N-terminus of this fusion protein restricts its presence to the plasma membrane plus ER and its exclusion from the nucleoplasm. When the photocleavable fragment of this fusion protein is exposed to UV light it dissociates releasing the now soluble fluorophore with the nuclear localisation signal that is imported to the nucleus. **Figure 4-6** B is the mean intensity in the nucleoplasm over time after PhoCl cleavage at 50 sec and it demonstrates that this construct indeed permits cargo release from the cytoplasm followed by import into the nucleoplasm. **Figure 4-6** C is an example cell post photo-release and the intensity profile across the nucleus is plotted. It shows that, as expected, there is a gradient of intensity at the proximity of the nuclear envelope and there is also a gradient of intensity around the NR. **Figure 4-6** D shows another example where this time the invagination is horizontal and imaged in its midplane; after photo-release of tdTomato from the plasma membrane it is

imported to the nucleus and a gradient of concentration is visible around the nuclear envelope (t90) and around the NR (t280).

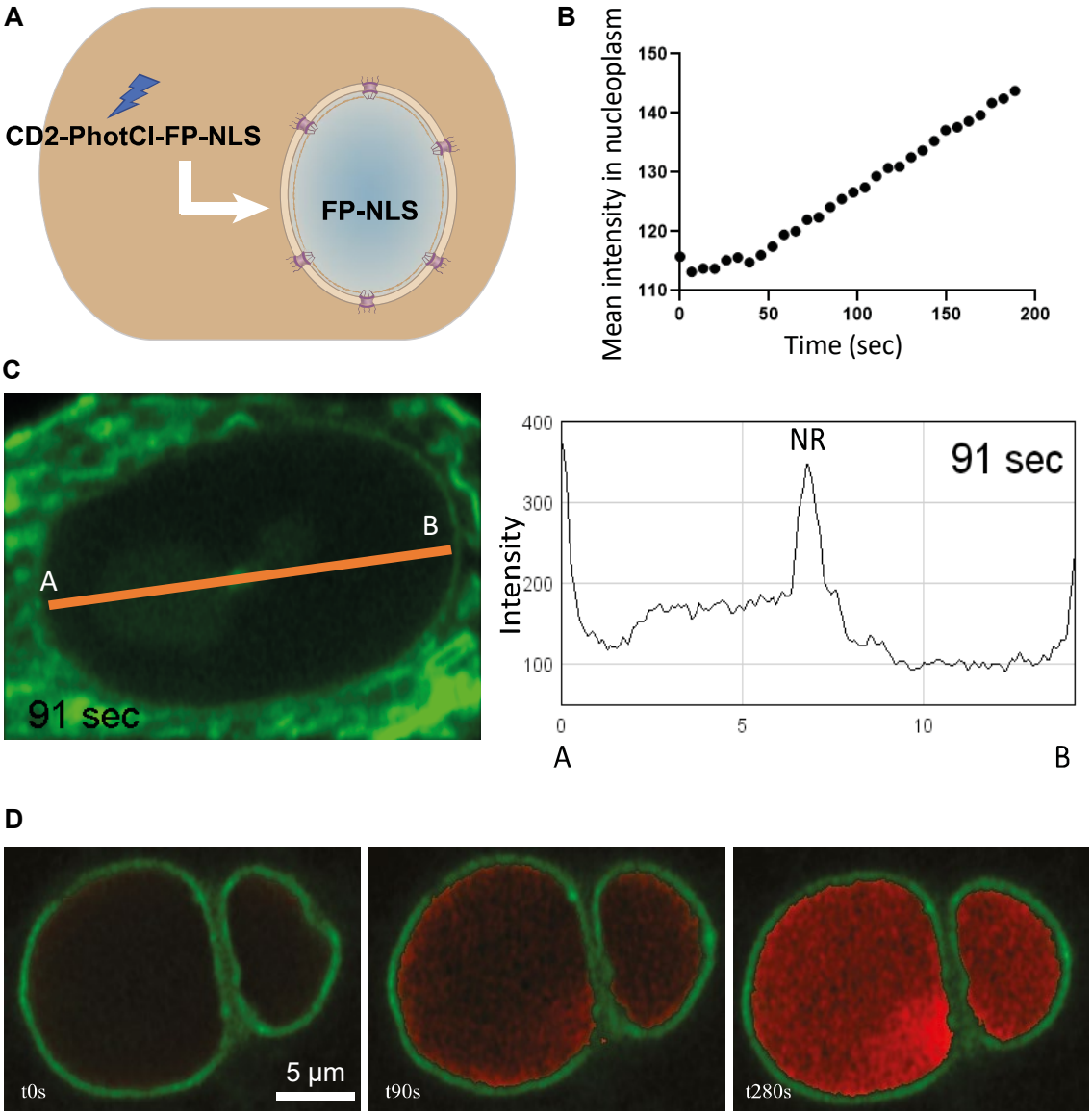


Figure 4-6: Synchronous release of a cargo targeted to the nucleus can be achieved by photocleaving the fusion protein CD2-Photocleaveable protein-FP-NLS with UV light in HCT cells *(**A**). Immediately after cleavage the FP is released and imported into the nucleus. Plot is mean intensity in the nucleoplasm over time post cleavage (**B**). (**C**) Sample cell with CD2-PhoCl-mNeonGreen-NLS; line indicates the position of the intensity profile at 91 seconds post cleavage. and allows the visualisation of a gradient of concentration around the nuclear envelope and the NR in conjunction to Lamin A-mNeonGreen. For better visualisation, tdTomato outside of the nucleus has been masked based on the Lamin A ring (**D**).*

The LEXY system allows export of material from the nucleoplasm to the cytoplasm. We used that system to measure the material exported across the nuclear envelope and NR (**Figure 4-7**). Panel A is the mean intensity over time in the nucleoplasm and in the core of the NR. At time point 12, blue light is used to release the photocaged NES and export the fusion protein including the fluorescent protein to the cytoplasm. Interestingly the intensity in the core of the NR was lower to that of the nucleoplasm before export and higher after export. Panel B is the mean intensity in concentric across the nuclear envelope over time. This shows a gradient of concentration around the nuclear envelope both before and after photo-uncaging of the nuclear export signal. Panel C is the mean intensity over time in concentric rings around the NR. Complying with panel A, it shows a gradient of concentration both before and after export. Panel D are the corresponding images for key time points: at t0 most of the signal is in the nucleoplasm. After the export is initiated at t25 the concentration in the nucleoplasm and cytoplasm are equal. At this stage, the mean intensity in the core of the NR and the nucleoplasm are also equal (panel A). At T80 most of the material has been exported from the nucleoplasm and is now in the cytoplasm. Arrows indicate the position of the NR as visible in the Lamin A mNeonGreen image. A dimmer area in the position of the NR is visible at t0 and a brighter one is visible at t80. This is consistent with the idea that material is exported though the NR and that the core of the NR is continuous with the cytoplasm such as it had a lower mean intensity that in the nucleoplasm but higher than in the bulk of the cytoplasm due to its proximity to the nucleoplasm.

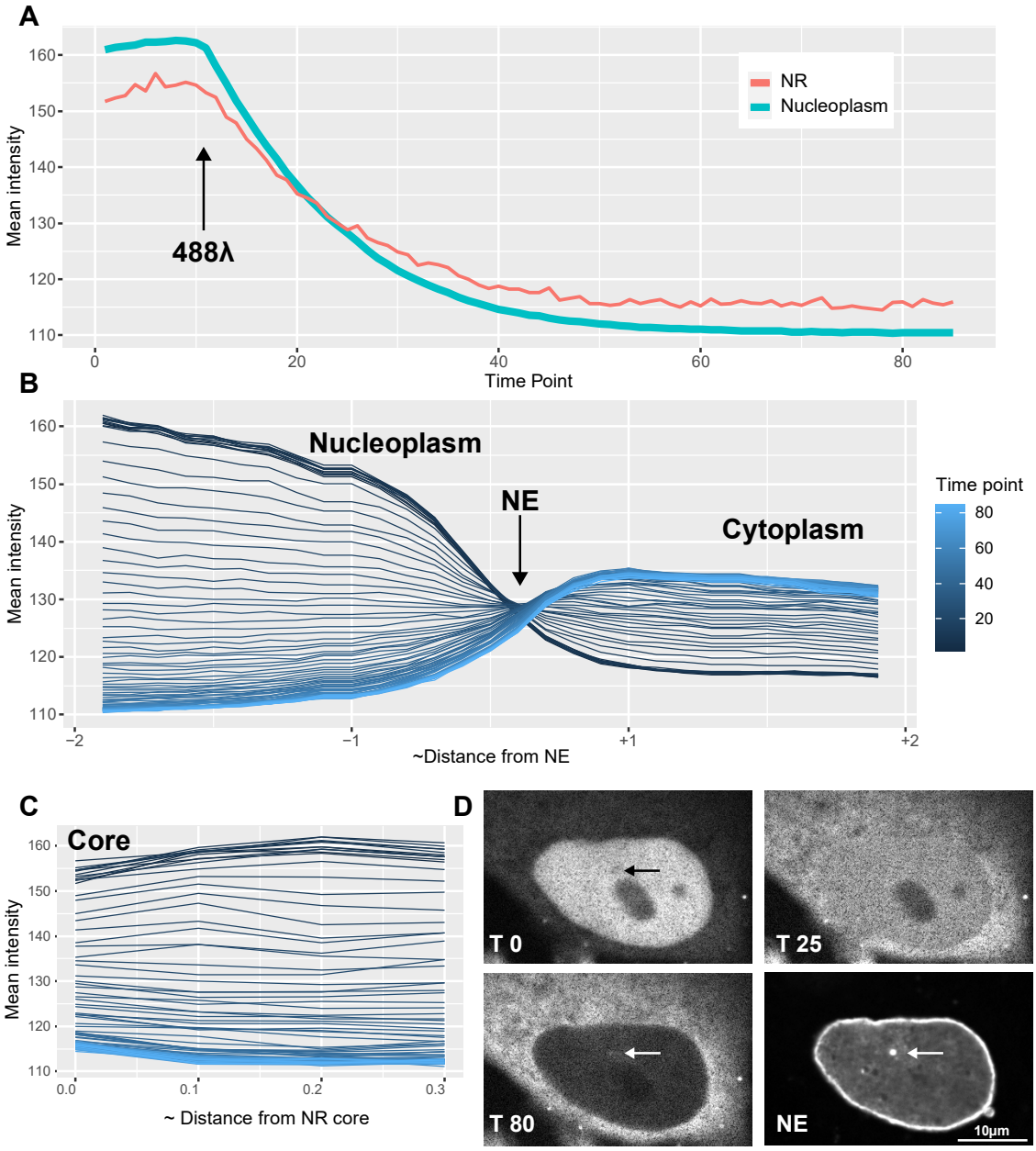


Figure 4-7: The LEXY system allows export of material from cytoplasm to nucleoplasm. (A) *Mean intensity over time in the nucleoplasm and core of the NR. At t12 the photocaged NES is released and the protein is exported from the nucleoplasm.* ***(B)*** *Intensity across the nucleus over time. The darker shades of blue are the first time points. The horizontal axis is the distance from the nuclear envelope.* ***(C)*** *Mean intensity in concentric rings radiating from the NR core over time.* ***(D)*** *Corresponding cell with LEXY depicted at key time points.*

We have shown that there is a gradient of concentration around the nuclear envelope both inward and outward as depicted by the S-shaped curves (**Figure 4-7** B). A reasonable control for the S-shaped curved would be to plot the same graphs but for a non-soluble fluorescent-tagged marker protein such as H4-mCherry. The purpose being to assess whether this S-shape is due to the continuous dynamic exchange of material around the nuclear envelope or whether it is due to the geometry of the nucleus and the point spread function. Cells were transfected with histone H4-mCherry then imaged and processed in the same way as the LEXY samples (**Figure 4-8** A). Top panels are intensity profiles of individual cells transfected with H4-mCherry (cells 1 to 3) while bottom row of panels are cells transfected with LEXY-mCherry (cells 4 to 6). Blue lines are the intensity profiles for Hoechst, green line for Lamin A mNeonGreen and red lines for mCherry fusion proteins. Profiles for Hoechst have as expected a low intensity in the cytoplasm, a peak due to the condensed heterochromatin then a lower plateau. The profile for the Lamin A mNeonGreen signal is similar to that of Hoechst, with a peak due to the presence of the lamina at the periphery of the nuclear envelope. Finally, both mCherry-H4 and LEXY-mCherry have S-shaped curves. For proper comparison mCherry curves for both fusion proteins were plotted on the same graph with the minima and maxima normalised (**Figure 4-8** B). The profile for non-soluble H4-mCherry is steeper than for the soluble LEXY-mCherry. The difference in the gradients being most likely due to the steady export-import at the nuclear envelope.

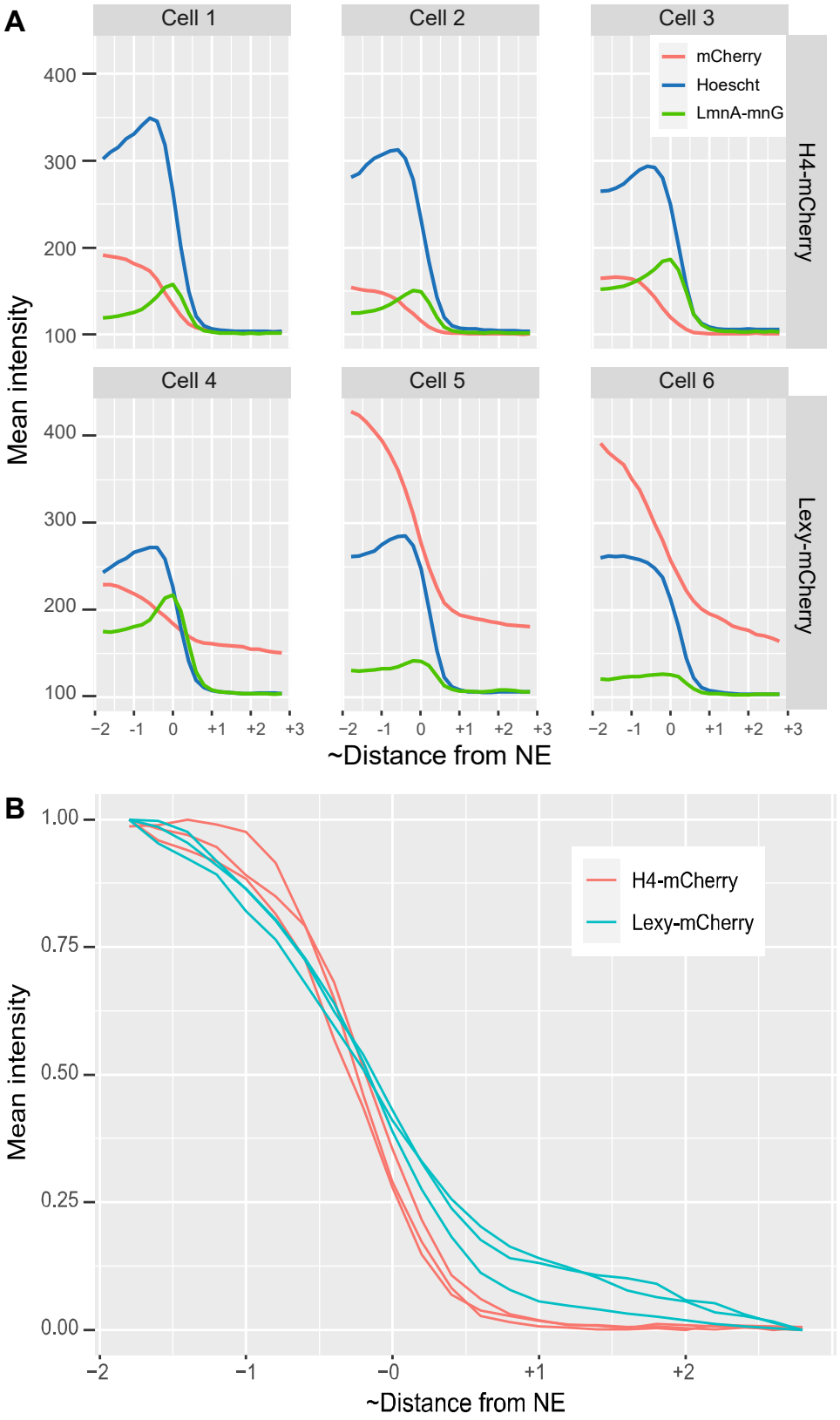


Figure 4-8: H4-mCherry intensity profile is steeper than LEXY mCherry across the nuclear envelope. (A) *intensity profiles for individual cells. Blue line for Hoechst, green for Lamin A mNeonGreen, red for H4-mCherry or LEXY-mCherry.* ***(B)*** *H4-mCherry and LEXY-mCherry profiles with maxima and minima normalized to 1 and 0, respectively.*

A natural follow up question would be whether having cells with nuclei containing invaginations provides any advantage in terms of cell proliferation for example. To answer that question, U-2 OS cells expressing mNeonGreen Lamin A were single sorted by flow cytometry into 96 well plates then left to grow for 10 days. Then they were imaged on a spinning disk and the resulting images were segmented and the number of invaginations per cell measured. Three replicates having 160 colonies and totalling 84,452 cells were analysed. The first observation is that colonies can have very different sizes (**Figure 4-9**). The analysis of the number of cells per colony versus the average number of invaginations per cell for each colony reveals that colonies with fewer cells have a higher average NR count (**Figure 4-10**, top left). In accordance with previous results (**Figure 4-1**), when colonies have cells with larger nuclei or a larger DNA content, they also have a higher average NR count (**Figure 4-10**, top right, bottom left). There is also an increase in the number of invaginations with an increase in nuclear circularity, although this is somewhat expected because larger nuclei tend to have higher circularities (**Figure 4-10**, middle left, **Figure 4-11**). An interesting observation is that colonies that have brighter nuclear envelopes have more invaginations (**Figure 4-10**, middle right) although the brightness of the nuclear envelope is correlated to the DNA content and nuclear area and nuclear circularity (**Figure 4-11**). The colonies that have the most space in between cells have most invaginations as well (**Figure 4-10**, bottom right).

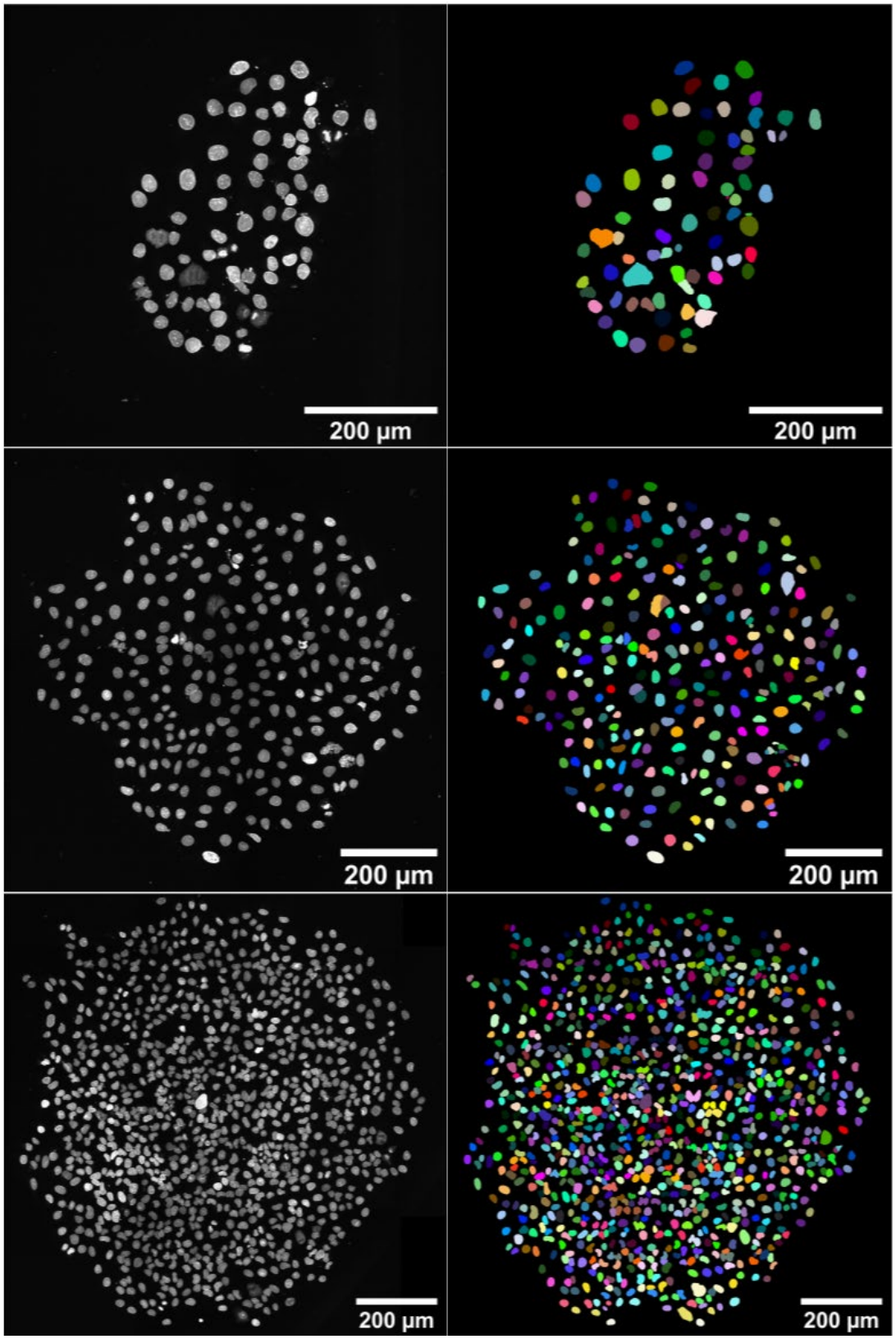


Figure 4-9: Colonies resulting from single cells can have very different resulting sizes. *U-2 OS cells were seeded as single cells then imaged after 10 days. The images on the right are the resulting segmentations from Cellpose; each nucleus displayed with a different colour.*

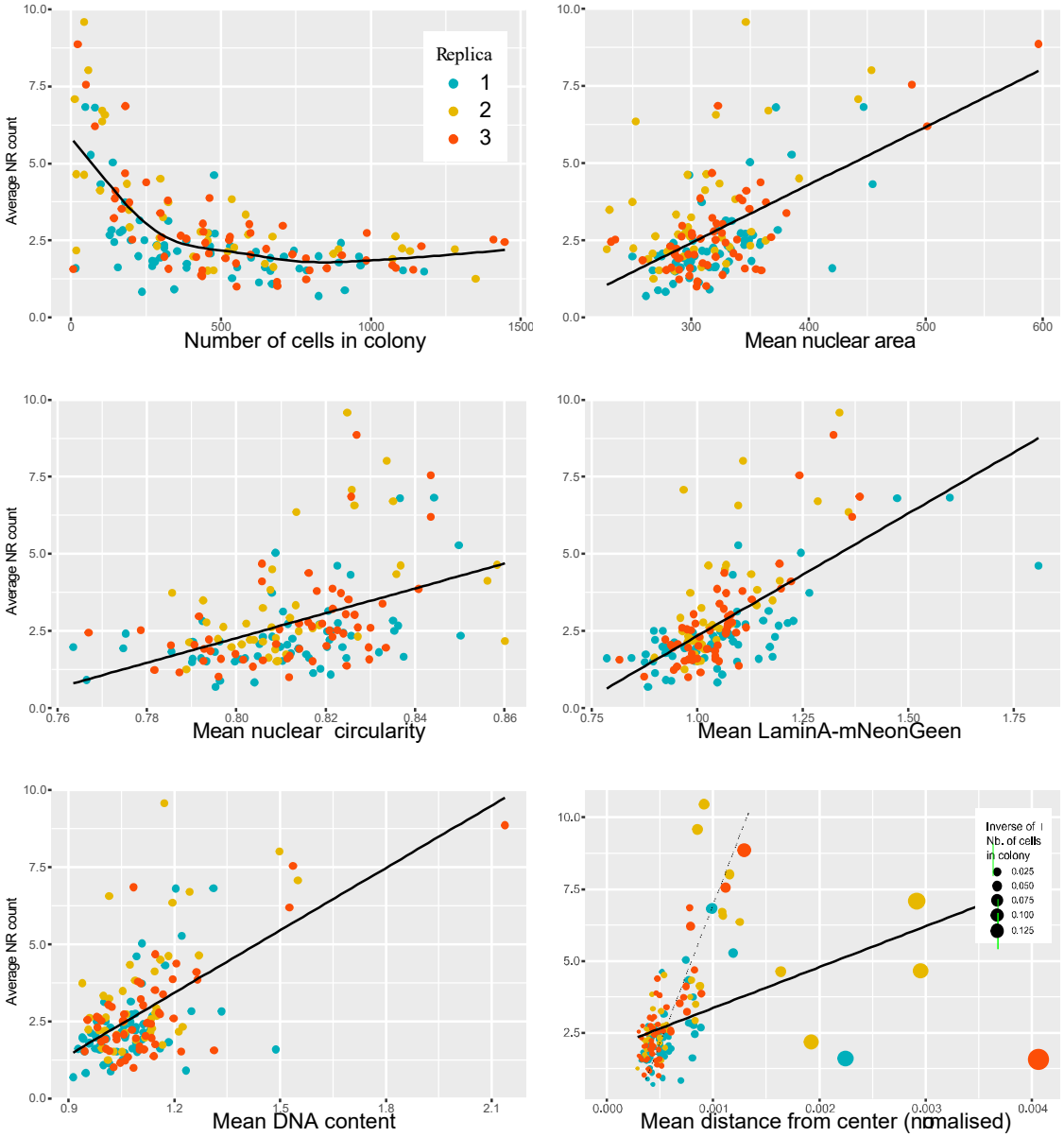


Figure 4-10: Analysis of the U-2 OS colonies resulting from single cells. *Cells were sorted in 96 well plates then left to expand for 10 days before being imaged. Resulting images were then segmented and the number of invaginations for each cell was counted and morphological features such as the area or the circularity were computed. Larger colonies have fewer invaginations of the nuclear envelope.*

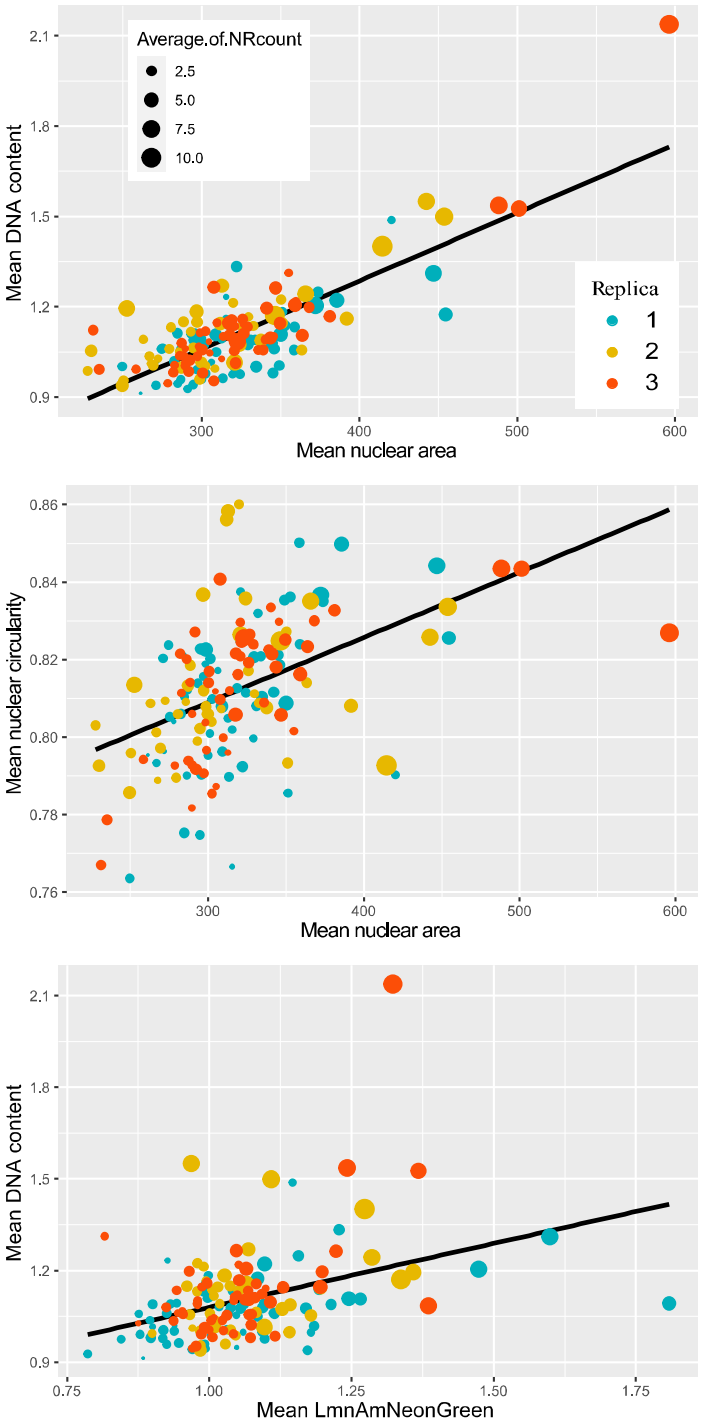


Figure 4-11: Further analysis of data in Figure 4-10 revealing the relationship between nuclear area versus DNA content, nuclear area versus nuclear circularity and mean Lamin A mNeonGreen brightness and DNA content.

3. Discussion

The function of the NR has been elusive. Here we sought to establish whether the NR has a role in the exchange of material deep within the nucleus. For this, we used 3D confocal microscopy in live and fixed cells, expressing fusion proteins or by immunofluorescence. We have shown that the NR has a cytoplasmic core and, in Ishikawa cells, 24 to 48 hours post pharmacological induction, nuclear pore complexes and LINC complexes are recruited to the newly formed invaginations. We have also demonstrated that we can photo-induce the import or export of material to or from the nucleoplasm and that there is a continuous exchange of material thought the NR.

In order to gain insight into the function of the nucleoplasmic reticulum is it useful to assess when and under what conditions the NR is present. For that we grew Ishikawa cells and stained their nuclear envelope and DNA so that the NR abundance could be quantified, and the volume of the cells measured. We found that nuclei in early G1 tend to have multiple invaginations of the nuclear envelope while there are fewer in G2 and if the nucleus becomes polyploid (and the largest volume) then the number increases again. This indicated - again - that it is possible to assemble and disassemble the invaginations of the nuclear envelope without going through mitosis and nuclear envelope re-assembly. Having more invaginations when nuclei are the largest or have more DNA may indicate that one of the potential functions of the NR is to increase the exchange of material when certain nuclear regions are away from the nuclear envelope.

This could be to provide a substrate for the genomic lamina associated domains or to allow exchange of material such as transcription factors.

In order to have exchange of material through the invaginations of the nuclear envelope it is essential that these invaginations have a cytoplasmic core continuous with the rest of the cytoplasm and contain nuclear pore complexes. We found that indeed the NR can contain visible cytoplasmic cores when stained with a protein that is excluded from the nucleoplasm and that these invaginations contain nuclear pore complexes. Interestingly, we also found that when inducing NR formation with hormones in Ishikawa cells, there is first formation of the NR visible with the lamin staining then LINC and NPCs are recruited to the structure.

We found that when releasing material from the plasma membrane using PhoCl and a fluorescent protein with nuclear localisation signals from the cytoplasm it is imported to the nucleus. Visible gradients of concentration were detected around the nuclear envelope and around the tubular invaginations. The difficulties with the use of PhoCl resides in the fact that as PhoCl is a derivative of the photoconvertible fluorescent protein mMaple and it is green before exposure to UV light then it becomes red and finally it photocleaves with a half-life of ~ 900 seconds. This implies that PhoCl is visible in both the green and red channels, thus increasing the difficulty of its use. In addition, the long photocleavage half-life makes the flow of material though the nuclear envelope diffuse in time. We attempted to mitigate these issues with the use of split fluorescent proteins. The idea behind the biomolecular fluorescence complementation (Miller et al., 2015) is to create two fusion proteins each containing half fluorescent protein. When

the two halves are in contact, they reconstitute the whole fluorescent protein and become fluorescent. Our plan was to have half FP bound to PhoCl and the other half to a nucleoporin in the nuclear pore complex. If the bio-complementation were successful, this would have revealed undoubtedly the NPCs through which the protein was imported into the nucleus. However, unfortunately the bio-complementation between CD2-PhoCl-Ct_mLumin-NLS on one hand and Nt_mLumin bound to Nup62 (central FG Nup), Nup93 (linker Nup between basket and transmembrane ring) or Nup98 (central Nup) on the other hand was not successful (plasmid construction was successful – no fluorescence was detected). Split mVenus was also trialled with no success. This may be because the import machinery is stronger than the non-covalent binding between the two halves, or because the NPC half was not accessible to the other one. Since this may have not worked due to not creating covalent bonds in the re-united split fluorescent proteins, we tried to use the FRB-FKBP system where in presence of Rapamycin those two proteins form a covalent bond (Banaszynski et al., 2005). We used CD2-PhoCl-sfGFP-FKBP-NLS on one hand and H2B-mCherry-FRB-HA, mCherry-FRB-Nup62, mCherry-FRB-Nup93, Nup93-mCherry-FRB or mCherry-FRB-Nup98 on the other hand with no success.

An alternative to the system using a photocleavable protein is the use of LEXY that allows us to synchronously induce the export of a nucleoplasmic fluorescent fusion protein. This allowed us to export nucleoplasmic material very quickly and measure its abundance over time in concentric rings around the nuclear envelope both inwards or outwards. We found that there are gradients of concentration, as expected, around the nuclear envelope, but also in and around the invaginations of the nuclear envelope. In

order to ensure that those gradients of concentration were *bona fide* due to the exchange of material and not because of the geometry of the nucleus, the PSF, the axial resolution, the diffraction of light, or refractive index differences, we also measured those intensity profiles for Hoechst, Lamin A mNeonGreen and H4-mCherry. We found that there are also apparent gradients of concentration however, the steepest gradient is the one for the LEXY-mCherry fusion protein meaning that the observed gradients of concentration are legitimate and that there is indeed exchange of material through the NR. It is worth noting that engineering of the pKa of both LINuS or LEXY could make these proteins accumulate into the nucleoli thus enabling the visualisation of specific import or export to or from the nucleoli.

A derivative function of the NR, though its increased exchange of material may be gene expression regulation. The invaginations allow delivery of transcription factors to genomic regions that would be otherwise away from the nuclear envelope so that they can be regulated faster. In addition, the invaginations provide a substrate for the lamina associated domains. The van Steensel lab created a system that fluorescently labels Lamina Associated domains using Dam-Lamin B1 and a modified DpnI enzyme that binds to methylated DNA without cleaving it (named ^{m6}A-Tracer) and they found that LADs are modestly mobile during interphase but after mitosis there is a reshuffle of the LADs and they are stochastically repositioned in the nucleus around the nuclear envelope and the nucleoli (Kind et al., 2013). Possibly, if a constitutive LAD find itself away from the nuclear envelope it either maintains invaginations post nuclear envelope re assembly or new invaginations are formed so that every constitutive LAD has an available lamina. This would extend the NE spatial organising function to its

invaginations. If constitutive LADs frequently are found in the periphery of the nucleoli and this leads to invaginations in those positions this may account for the high association between the NR and nucleoli.

NR formation is both preceded by, and succeded by, gene expresion changes. In the following chapter we used next generation sequencing (NGS) to map those changes and gain insights into the commun alteration when NR induction is done with Saquinavir or oestrogen plus progesterone.

5. Global transcriptome analysis of NR induction

"Knowledge has a beginning but no end."

Geeta S. Lyengar, 1998

1. Introduction

We previously investigated how and when the NR is assembled and its role in the exchange of material across the nuclear envelope. The last facet in this study is the transcriptome analysis under conditions of NR induction. The transcriptome is the pool of RNA present in a cell at a given time. This is composed primarily by coding RNA or mRNA, but it also includes non-coding RNA such as microRNA. Each cell has a unique transcriptome that reflects its current state of gene expression. The transcriptome bridges the genome to the proteome and changes in NR abundance and formation can affect gene expression and thus the proteome. In order to find the unique changes

caused by NR induction we explored the intersection of the transcriptome changes between pharmacologically (physiological levels of oestrogen and progesterone in Ishikawa cells) or pathologically (Saquinavir) induced NR formation; this eliminates from the candidate list the genes that ware changed by the presence of either of these inducers but are not consequences of the NR formation. This reduces the probability of looking at unique changes in response to the individual stimulus that are not related to NR.

The rationale behind the investigation of transcriptome changes during NR induction is that changes in nuclear envelope morphology - such as invaginations reaching the central regions of the nucleoplasm - may change gene expression due to the availability of new potential lamina associated domains or the availability of a particular element that would otherwise be limited to the nuclear periphery. This could include particular ions, or compositional features that have local effects on gene expression. Transcription factors sequestration or delivery of a precursor or a transcriptions factor or an enhancer to a particular site may also be involved in those gene expression changes. Finally, the selective ability of a mRNA to be efficiently moved outside of the nucleus though the NR and have its initial non-sense mediated decay test for adequacy made in NR rather than in the bulk cytoplasm may change the kinetics of production, particularly if there are splice forms that give premature termination in translation.

Two main methods are used to measure the abundance of mRNA in cells. (i) Microarrays are collection of selected DNA probes that bind to fluorescently labelled

targets. For transcriptome analysis, mRNA is extracted and purified then it is reverse transcribed and fluorescently labelled. This labelled cDNA is then hybridised to the microarray; the excess and unbound probes are removed and finally the resulting microarray is imaged and the fluorescence for each probe is quantified. The main limitation for this method is that it is possible to probe only for known targets. (ii) RNA sequencing, on the other hand, does not rely on a set of defined targets. For Illumina sequencers, the reverse transcribed RNA is amplified with fluorescently labelled nucleotides containing terminator caps so that only one nucleotide is added at a time. The nucleotide is read by detecting the fluorescence then both the cap and the label are removed, and the process is repeated. This results in reads that are then aligned with the human reference genome so that it is possible to quantify the absolute levels of each corresponding RNA.

We hypothesised that the analysis of changes in gene expression when NR formation is induced with Saquinavir, or physiological levels of oestrogen and progesterone would enable us to identify the genes that are required for NR formation or that change because of NR formation.

In this chapter we:

1. Identify the RNA species that were significantly changed when NR formation is induced with Saquinavir or oestrogen plus progesterone in Ishikawa cells (**Figure 5-1** and **Table 5-1**).

2. Analyse whether certain chromosomes are specifically targeted (**Figure 5-4** and **Figure 5-5**).
3. Found a set of genes and pathways that are activated and repressed when NR formation is induced (**Table 5-2**).
4. Study the miRNAs that are changed under the previously described conditions (**Table 5-3** and **Figure 5-6**).
5. Explore the links between lipid metabolism and NR abundance (**Figure 5-7** and **Figure 5-8**).

2. Results

In order to identify genes that may be responsible of the formation of the nucleoplasmic reticulum or genes that may be expressed differently as a result of the formation of the NR, we induced its formation with Saquinavir or physiological levels of oestrogen plus progesterone for 6 hours and then extracted mRNA and sequenced it using the Illumina technology. We found that 4998 genes were significantly (p-value adjusted < 0.02) changed when NR formation was induced with Saquinavir (about half in each direction) while it was only 61 for the cells treated with hormones (45 downregulated and 16 upregulated) (**Figure 5-1**).

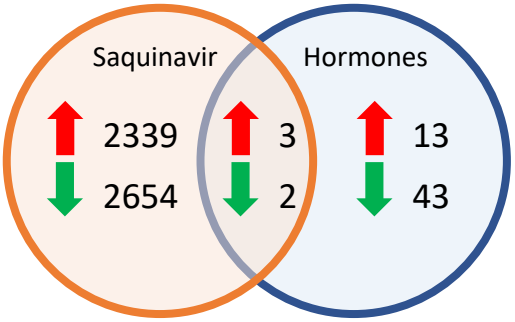


Figure 5-1: Number of genes with p-adj<0.02 when NR formation is induced with either Saquinavir or Hormones

Although its utility is debated, it is traditional to validate the key results of RNA-Seq by qPCR. As expected, the gene expression changes found by RNA-Seq are similar to those found by qPCR (**Figure 5-2**). This confirms that our RNA-Seq results are likely to be valid.

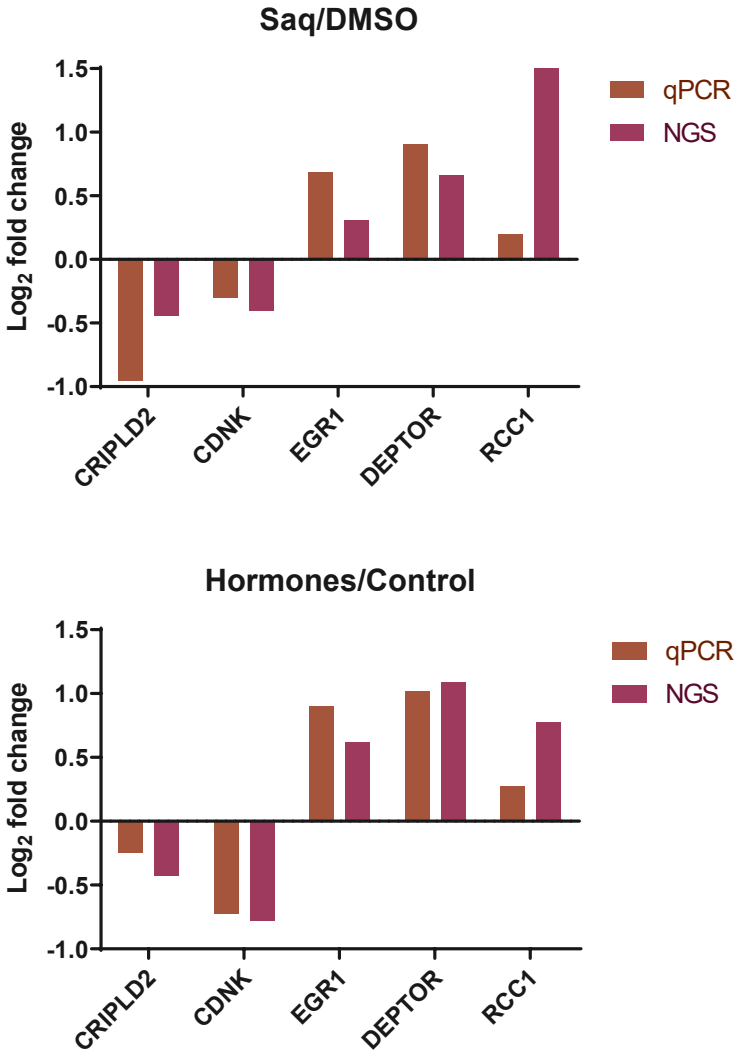


Figure 5-2: qPCR validation of the RNA-Seq experiments. *Log2 fold change of genes that were significantly changed in both Saquinavir, and Hormone treated cells measured by RNA-Seq and qPCR.*

Five genes were found to be significantly changed in the same direction in both conditions. They are summarised in **Table 5-1**. The expression of both CDKN1C and CRISPLD2 were reduced in the Saquinavir, and hormone treated cells. The expression of EGR1, DEPTOR, and RCC1 were increased.

The Cyclin dependent kinase inhibitor 1C is a protein encoded by the CDKN1C gene (in chromosome 11) and regulates multiple key aspects of cancer, through its protein kinase inhibitor activity (Kavanagh and Joseph, 2011). It is involved in cell growth control by cell cycle arrest. Both pro and anti-apoptotic functions were found. It promotes cell differentiation and reduces cell motility and invasion and thus inhibits cancer progression. CDKN1C protein is absent in several cancers. CDKN1C is primarily found in the nucleoplasm and secondarily in the cytosol (Thul et al., 2017).

The Cysteine-rich secretory protein LCCL domain-containing 2 is encoded by the CRISPLD2 gene (in chromosome 16). Its main function has been described for its implication in the orofacial cleft (Duncan et al., 2017) although this has been found to be the case in Chinese populations but not in European population. This protein also has anti-inflammatory properties and is involved in cell expansion and migration in lung fibroblasts and epithelial cells (Zhang et al., 2016). This protein is found in the nucleoplasm plus nucleoli, and is also predicted to be secreted out of the cell (Thul et al., 2017).

The Early growth response 1 protein is encoded by the EGR1 gene (in chromosome 5). This is a transcription regulator that activates differentiation and mitogenesis. Its expression is reduced in cancers (Pontén et al., 2008; Uhlén et al., 2017)

and it is believed to be a tumour suppressor protein (Li et al., 2019). EGR1 is primarily found in the nucleoplasm (Thul et al., 2017) but also in the cytoplasm of cancer cells.

The DEP domain containing MTOR interacting protein is encoded by the DEPTOR gene (in chromosome 8). Its main function is to negatively regulate mTORC1 and mTORC2 and hence reduce protein synthesis (Kim et al., 2002), regulate cell proliferation and motility (Hay and Sonenberg, 2004). DEPTOR is found in the nucleoplasm and mitochondria (Thul et al., 2017).

The Regulator of Chromosome Condensation 1 is encoded by the RCC1 gene (in chromosome 1). This protein is responsible for the generation of the RanGTP gradients for the necessary docking of the nuclear envelope to the nucleosome after mitosis (Nemergut et al., 2001). RCC1 is found in the nucleoplasm and nuclear envelope (Thul et al., 2017).

Table 5-1: Genes that were significantly changed in Saquinavir and Hormones treatment and have the same directionality.

			Saquinavir		Hormones	
	symbol	**name**	**log2 FoldChange**	**padj**	**log2 FoldChange**	**padj**
Decreased	CDKN1C	Cyclin dependent kinase inhibitor 1C	-0.408	0.005	-0.778	0.016
	CRISPLD2	Cysteine rich secretory protein LCCL domain containing 2	-0.447	1.428×10^{-09}	-0.426	0.001
Increased	EGR1	Early growth response 1	0.311	4.690×10^{-15}	0.619	2.165×10^{-15}
	DEPTOR	DEP domain containing MTOR interacting protein	0.664	0.01	1.091	0.005
	RCC1	Regulator of chromosome condensation 1	1.679	6.610×10^{-150}	0.778	9.815×10^{-6}

Since it has been described that multiple cancers have increased NR abundance we explored the levels of expression of these genes in multiple healthy and cancerous tissues. We used the publicly available consensus dataset for RNA expression in tissues from the Human Protein Atlas (Uhlén et al., 2015, 2017). This consists of the normalised RNA levels for 55 distinct tissues and was obtained from the combination of the Genotype-Tissue Expression Project (Lonsdale et al., 2013) and from the Human Proteome Atlas project (Uhlén et al., 2015) by RNA sequencing. The Cancer Genome Atlas provided the data for the cancer tissues. All three datasets were generated by RNA sequencing and are expressed as normalized protein-coding transcripts per million. **Figure 5-3** recapitulates this data. Colon and rectum adenocarcinomas, lung adenocarcinoma, lung squamous cell carcinoma, skin cutaneous melanoma, kidney chromophobe, kidney renal clear and cell carcinoma and kidney renal papillary cell carcinoma were available in the Cancer Genome Atlas dataset but were excluded because they correspond to multiple tissue subtypes that were represented by a single healthy reference in the healthy consensus dataset.

We found that the expression of CDKN1C and EGR1 is decreased in all cancers present in **Figure 5-3**. CRISPLD2's expression is also decreased in all cancers except in pancreatic cancer. DEPTOR appears to be also decreased in most cancers (except endometrial and testis cancer) although the range of the reduction is smaller than for the previous two genes. RCC1 is decreased in all cancers except cervical, endometrial, and bladder urothelial carcinoma. This shows that the observed changes in our Saquinavir and hormone treated samples and the changes in the cancers versus healthy tissues are decoupled meaning that the relationship between the apparent NR

abundance changes that certain cancers may have are independent from the expression of our five gene hits. PCNA (polymerase delta auxiliary protein) and VIM (vimentin) were added to the graph because they are both tumour markers that are increased and decreased respectively in cancer. PCNA is a protein that facilitates the DNA replication required for rapidly dividing cancerous cells and it's increased expression is a tumorigenic marker (Stoimenov and Helleday, 2009). VIM is a protein used as marker whose expression is reduced in cancer. This demonstrates that our healthy versus cancer comparison is valid.

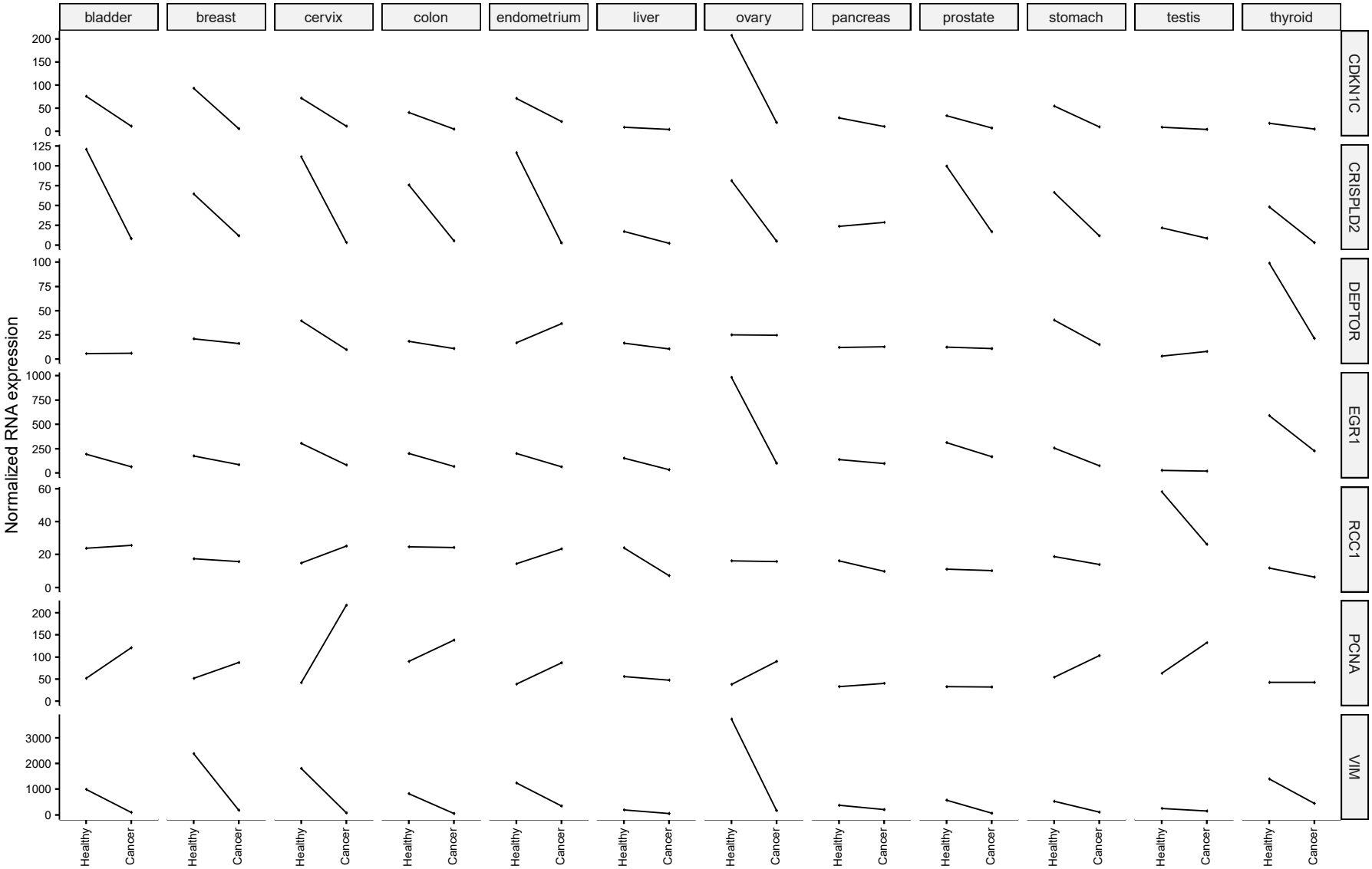


Figure 5-3: RNA expression changes in cancer versus healthy tissue. Cancer figure is an average of 134 to 1075 (median 373) samples. The Healthy figure is the normalised expression level from a consensus dataset. Data from the Human Protein Atlas (Uhlén et al., 2015, 2017)

This RNA-Seq analysis provided us with a list of genes that were significantly changed under Saquinavir or Hormone treatment. A legitimate question would be whether certain chromosomes were specifically targeted. To address this, the number of genes that were significantly up or downregulated in the Saquinavir treated cells were counted and plotted in **Figure 5-4 A**. It appears that the larger chromosomes have more genes that are significantly changed however when normalising the number of changed genes by the number of genes for each chromosome there is no difference between the chromosomes (**Figure 5-4 B**). **Figure 5-5** is the same analysis but for the hormone treated cells; chromosome 11 may be more changed than the rest but since there were only 61 significantly changed genes, the numbers are too small to draw definite conclusions.

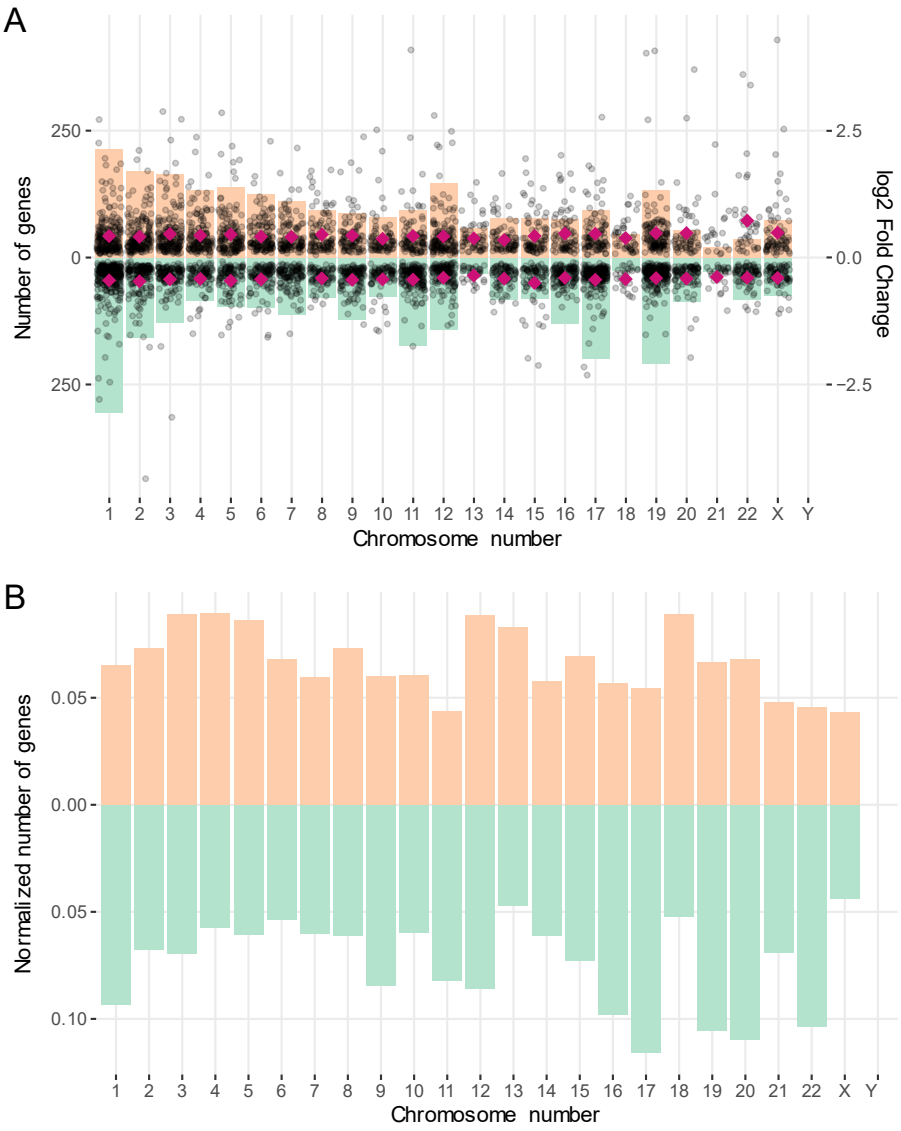


Figure 5-4: No specific chromosome is significantly changed by Saquinavir in Ishikawa cells. ***(A)*** *Number of genes significantly changed per chromosome and the log2 fold change for each one of them (magenta lozenges is the mean change).* ***(B)*** *is the number of genes changed per chromosome normalised to total number of genes in the chromosome.*

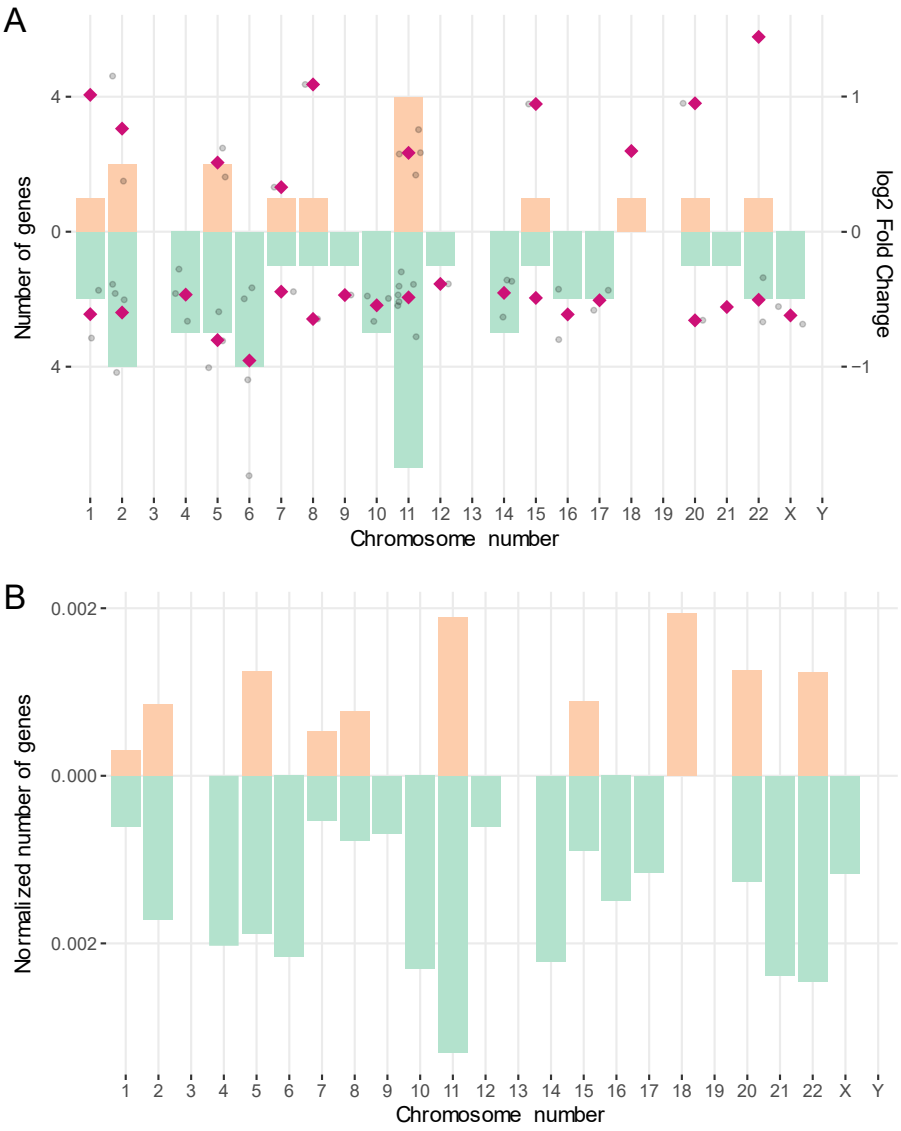


Figure 5-5: No specific chromosome is significantly changed by Oestrogen and Progesterone in Ishikawa cells. (A) *Number of genes significantly changed per chromosome and the log2 fold change for each one of them (magenta lozenges is the mean change).* ***(B)*** *is the number of genes changed per chromosome normalised to total number of genes in the chromosome.*

The analysis of the RNA-Seq provided us with a list of genes that were significantly changed across conditions. Instead of looking at the individual changes in gene expression, changes in gene sets or pathways can be measured. We found that there were 11 and 13 pathways whose activity was decreased in Saquinavir, and

Hormone treated cells respectively while there were 490 and 19 pathways decreased in Saquinavir and hormones respectively (***Table 5-2***). There were no pathways in common between the Saquinavir or Hormone treated cells. Nevertheless, it is interesting to note that half of the pathways decreased in the hormone treated cells relate to lipid metabolism, including cholesterol synthesis. On the other hand, the pathways increased related to cell motility and its regulation.

Table 5-2: Number of pathways significantly changed in Ishikawa cells treated with Saquinavir or oestrogen plus progesterone.

Pathways	Saquinavir	Hormones	In common
Increased	11	13	0
Decreased	490	19	0

The nature of the RNA-Seq experiment we did also allowed us to find the micro RNAs that were also significantly changed. The number of miRNAs changed in each condition is summarised in **Figure 5-6**. And the ones that are in common between both conditions are described in **Table 5-3**.

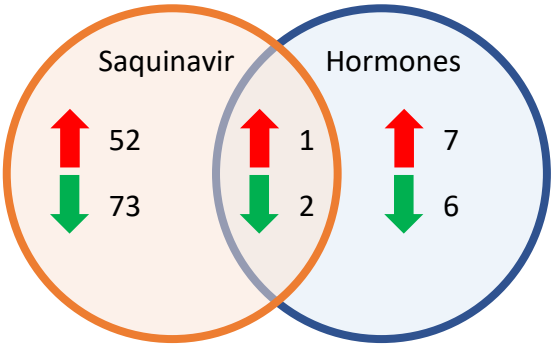


Figure 5-6: Venn diagram of miRNA expression changes in Saquinavir and Hormones treatment.

Table 5-3: miRNAs significantly changed in Saquinavir and Hormones treatment.

	Hormones			Saquinavir		
miRNA	baseMean	log2 FoldChange	padj	baseMean	log2 FoldChange	padj
MIR125B1	173.0584	0.6131	0.0001	111.6868	0.46	0.0026
MIR551A	76.3262	-1.0329	0.0052	47.3213	-0.6968	0.0136
MIR29C	135.1634	-1.2801	0.0117	76.8073	-1.066	0.0004

Links between lipid metabolism and NR formation

Amongst the pathways that whose activity were reduced in the hormone treated cells, half were related to lipid metabolism. Since we know that newly synthesised lipids are required for NR formation (Drozdz et al., 2017; Lagace and Ridgway, 2005; Pytowski et al., 2019) this was unexpected. We hypothesised that if the "traditional" pathways are decreased but we still need newly synthesised lipids then there must be something in the non-canonical pathways that occur when certain enzymes do not function as normal. We explored the NR abundance in cells from patients that have mutations in Phosphate Cytidylyltransferase 1A, Choline, (PCYT1A) also known biochemically as CTP:phosphocholine cytidylyltransferase α (CCTα). We found that certain mutations lead to an increase in the NR abundance while others do not (**Figure 5-7**). Indeed, skin fibroblasts harbouring the mutation PCYT1A p.A99V or p.S323Afs*38 had more invaginations of the nuclear envelope than the control cells. Meanwhile, cells harbouring p.V142M plus p.E280de or p.E280del and p.S333Lfs*164 showed no significant increase of NR abundance relative to the control.

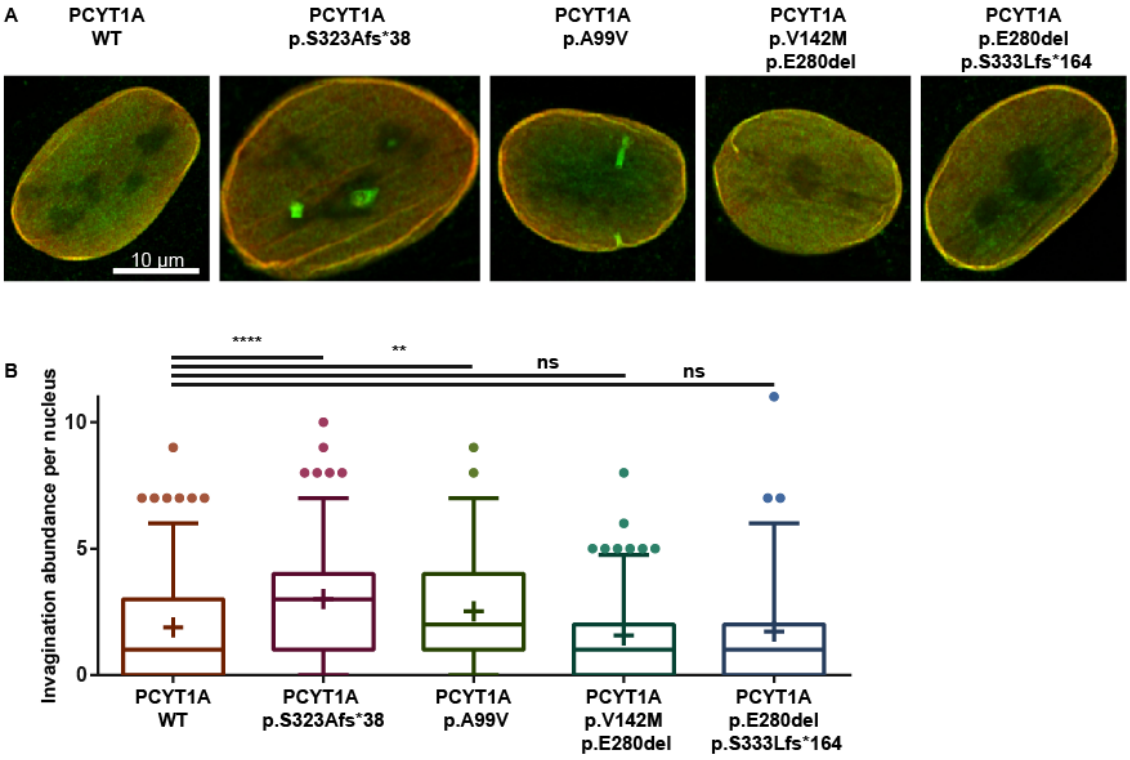


Figure 5-7: NR abundance increased in patients with some mutations in the PCYT1A gene. (A) *Skin fibroblasts were stained with anti-Lamin A and anti-Lamin B1.* ***(B)*** *NR abundance was scored based on the lamin A images. Data from three replicates, n is respectively 189, 164, 158, 164, 162. Box is lower 1st to upper 3rd quartile with median and "+" for the mean; whiskers are 5-95 percentile, **** for P < 0.0001, ** for P < 0.01, ns for non-significant.*

We then imaged those cells by Transmission Electron Microscopy (TEM) and found that NR from cells carrying the mutations that increased NR abundance could have a structure consisting of two nuclear envelopes (i.e. four bilayer membranes) while this was not observed in the WT cells (**Figure 5-8**).

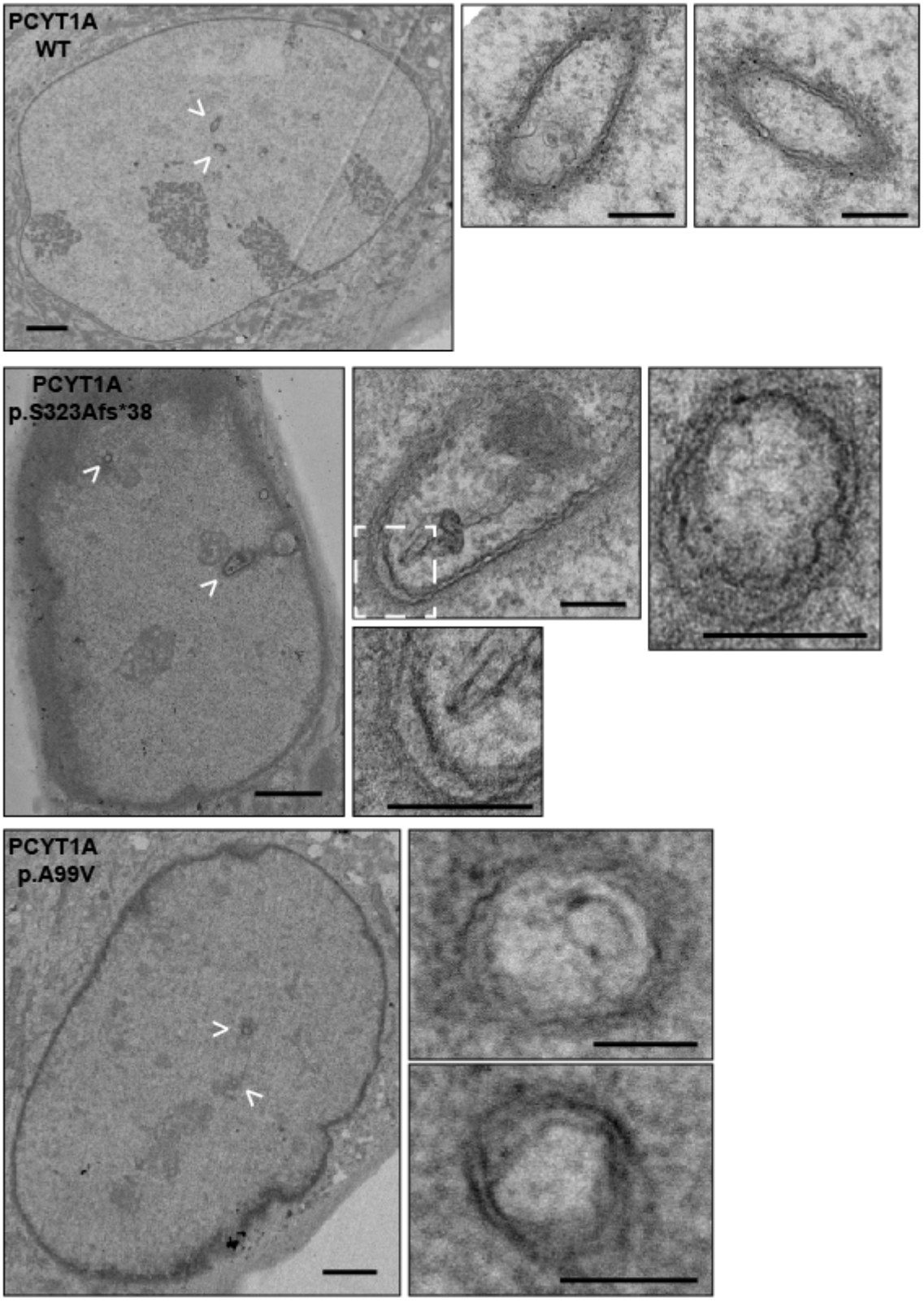


***Figure 5-8: Electron microscopy of PCYT1A mutant cells**. The NR in cells carrying the mutated PCYT1A can have quadruple membraned-NR.*

We previously demonstrated that newly synthesised lipids are incorporated into newly formed nuclear envelope invaginations (Drozdz et al., 2017; Pytowski et al., 2019). Indeed, cells pulsed with deuterated choline for 12 h while NR formation is induced with hormones (in Ishikawa cells) or Saquinavir (in HeLa cells), revealed by NanoSIMS (Nanoscale secondary ion mass spectrometry) analysis that deuterated elements are enriched in the NR. NanoSIMS is a method that allows to create composition maps for a sample. This uses an ion-beam to erode a sample which creates secondary ions that are sent to an ion mass spectrometer. Pulsed deuterated choline was used as a precursor to the lipid synthesis so that all newly synthesised choline-containing lipids would also be deuterated (**Figure 5-11, Figure 5-12**). In other experiments reported in these papers, the labelled precursor was pulsed deuterated stearate, such that the fatty-acyl moiety of nascent phospholipids became labelled. Similar results were obtained with this alternative labelling approach. A $^{2}H/^{1}H$ ratio map is then created that reveals where the ^{2}H is incorporated. A backscattered electron microscopy image is used to identify the regions of the sample that have invaginations of the nuclear envelope (**Figure 5-9** A) then that region is processed with the NanoSIMS and creates the said $^{2}H/^{1}H$ ratio maps (**Figure 5-9** B, D; **Figure 5-10** B,D). The three-dimensional analysis of the $^{2}H/^{1}H$ ratio maps revealed that the forming invagination has a higher $^{2}H/^{1}H$ ratio that the stable nuclear envelope with the highest ratios at the tip of the invagination (In Ishikawa cells: **Figure 5-9** C, in Hela cells: **Figure 5-10** C,D) and in regions with high membrane curvature (HeLa cells: **Figure 5-10** A, B).

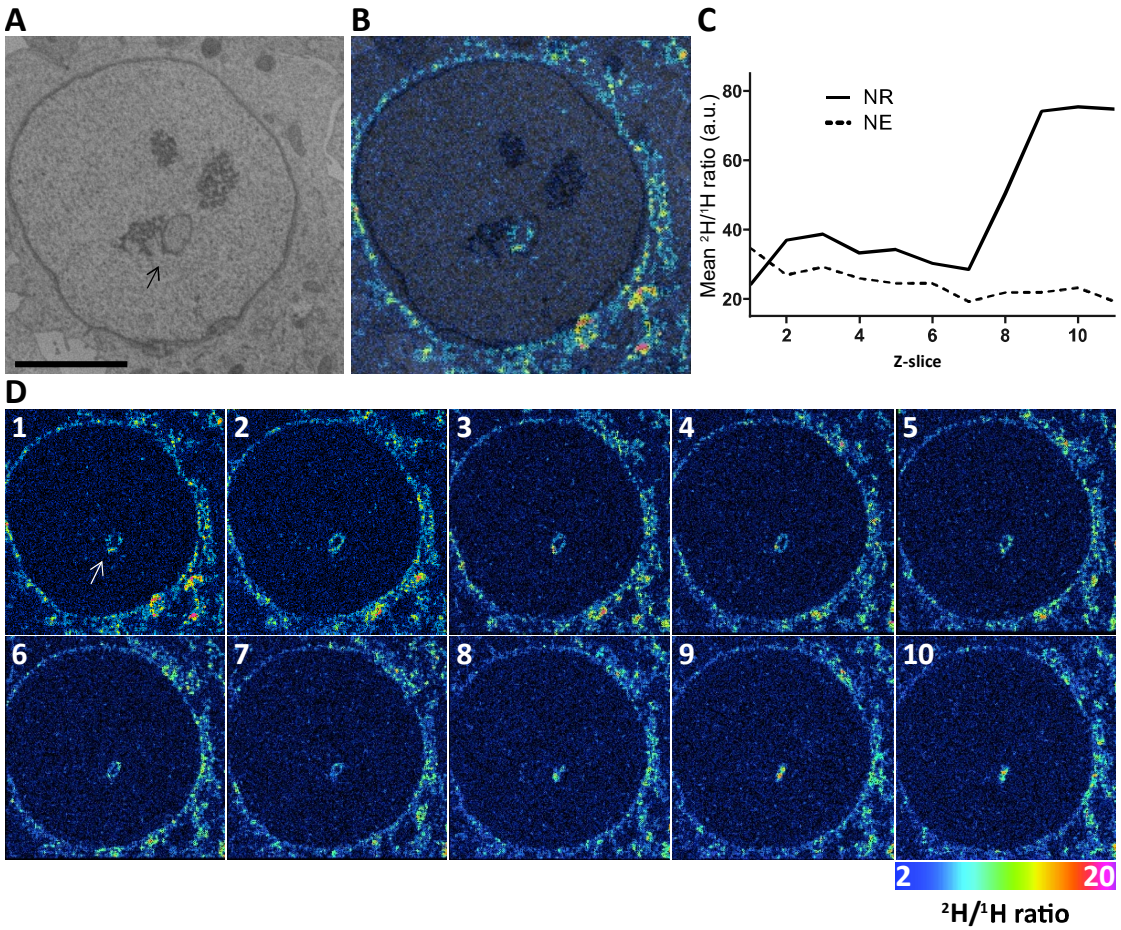


Figure 5-9: NanoSIMS analysis of Ishikawa cells with NR formation induced with hormones and pulse chased with deuterated choline for 12 hours. ***(A)*** *backscattered electron microscopy image revealing the position of the nuclear envelope and an invagination.* ***(B)*** *corresponding $^{2}H/^{1}H$ ratio map.* ***(C)*** *Quantification of the $^{2}H/^{1}H$ ratio in the nuclear envelope and NR.* ***(D)*** *Single planes of the $^{2}H/^{1}H$ ratio map. Figure from Pytowski et al., 2019.*

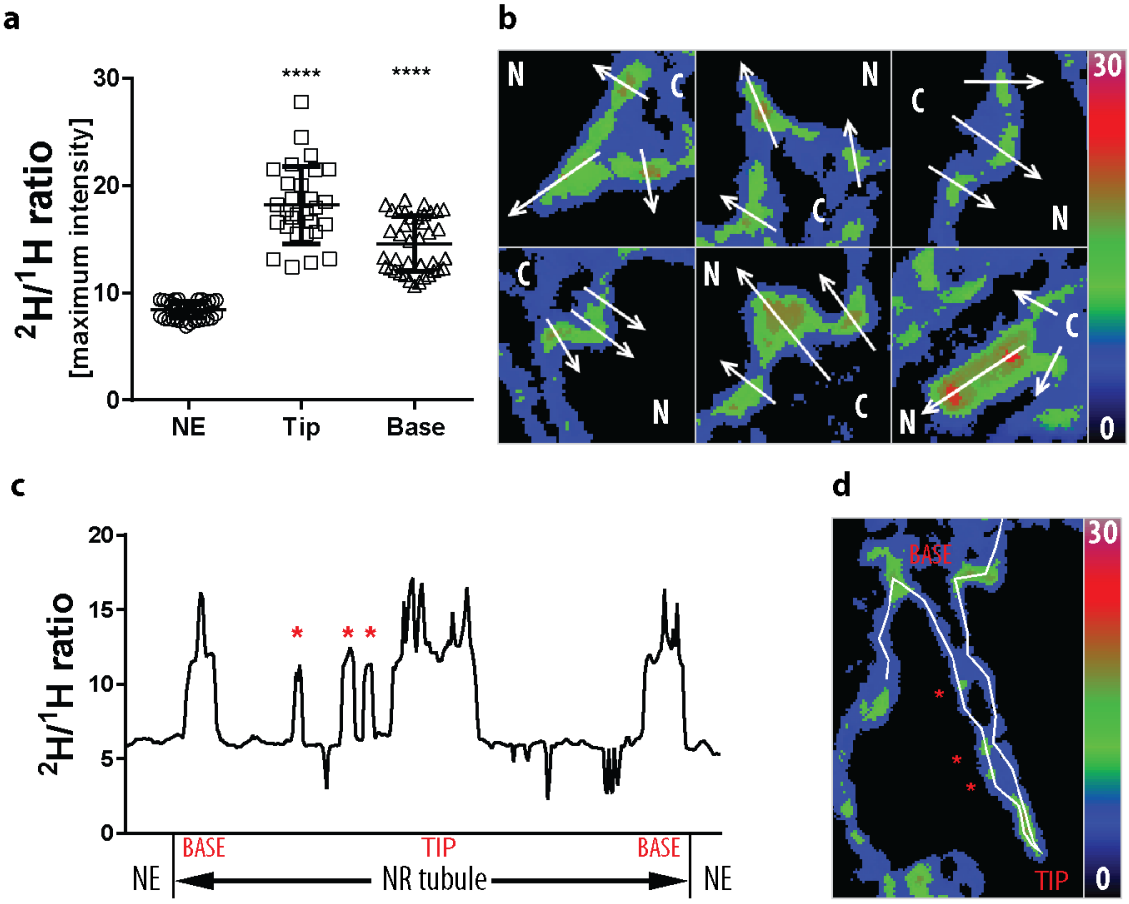


Figure 5-10: NanoSIMS analysis of HeLa cells with NR formation induced with Saquinavir and pulse chased with deuterated choline for 12 hours. (A) *Quantification of the $^2H/^1H$ ratios in areas of high membrane curvature in* ***(B)****. **(C)** Quantification of the $^2H/^1H$ ratios in an invagination of the nuclear envelope* ***(D)****. Figure from Drozdz et al., 2017.*

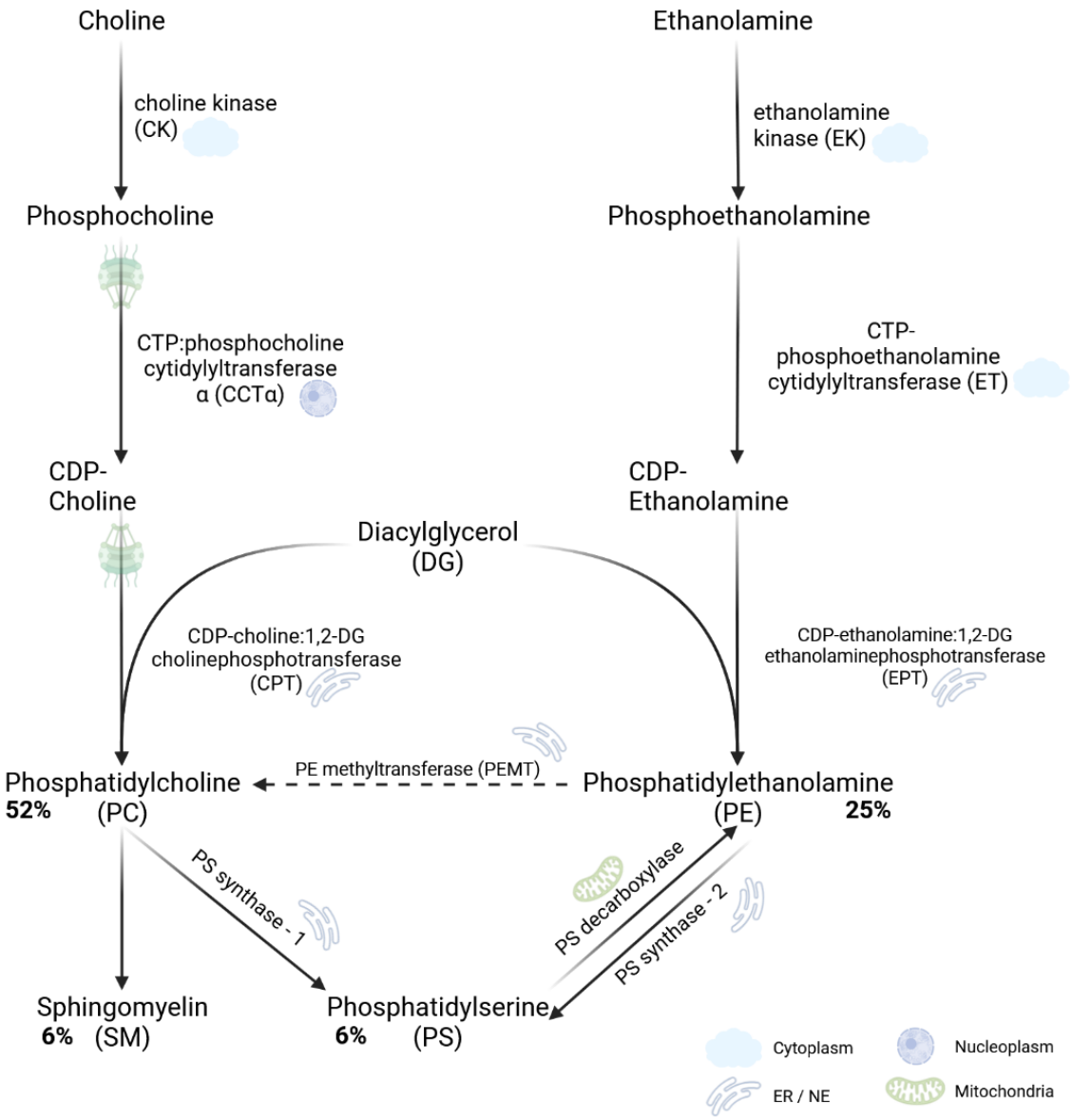


Figure 5-11: Synthesis pathway for Phosphatidylcholine, Phosphatidylethanolamine, Phosphatidylserine and Sphingomyelin in mammalian cells. *Percentages indicate approximate lipid content in the nuclear envelope (measured in cells from rat liver). Pictograms indicate the subcellular location for the enzyme. (Vance, 2015)*

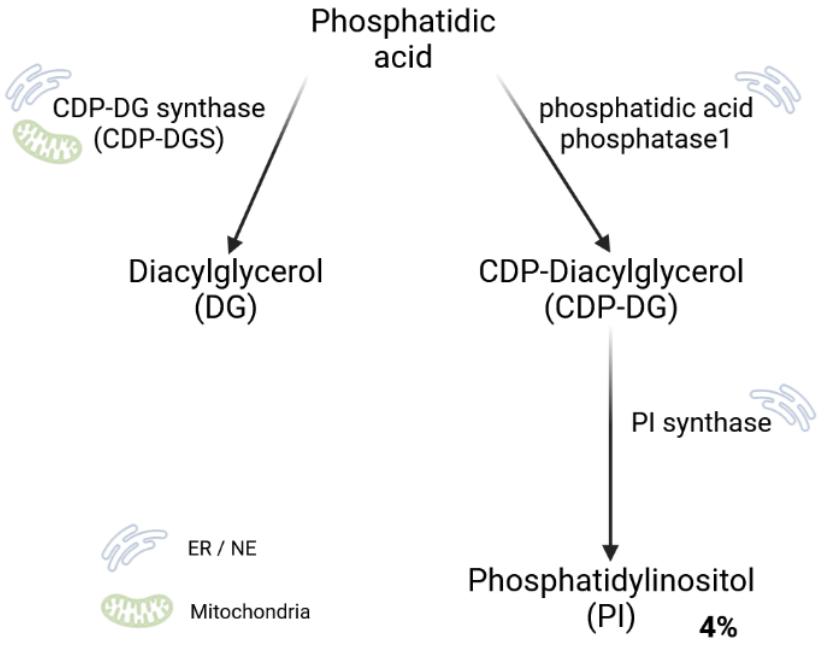


Figure 5-12: Synthesis pathway for Diacylglycerol, and Phosphatidylinositol in mammalian cells. *Percentages indicate approximate lipid content in the nuclear envelope (measured in cells from rat liver). Pictograms indicate the subcellular location for the enzyme. (Vance, 2015)*

3. Discussion

Gene expression changes when NR formation is induced can give us information about the required or resulting changes. We induced NR formation by both physiological and pathological means in human endometrial cells (Ishikawa cells). The intersection of the RNAs – and their corresponding genes and pathways, and miRNAs – provided us with a list of 5 genes and 3 miRNAs that might be essential for NR formation or are a direct consequence of its formation. In this list are confounded (i) the gene expression changes required for NR formation (or turnover) and its underlying mechanism for NR biogenesis and regulation; (ii) gene expression changes that result from NR induction (or turnover) and its functional roles.

Chromosomes are organised within the nucleus in distinct, but fluid, territories. Chromosomes and their sub-domain locations depends on gene expression activity - active regions of euchromatin being at the periphery of the nucleus near the nuclear envelope. Certain genomic sequences are associated with the lamina (Lamina Associated Domains - LADs), others are associated with nucleoli (by the Nucleolar organizer region - NORs). Additional spatial organisation emerges from self-interaction of chromosome regions forming topologically associated domains (TADs). Those peripheral domains that require proximity to the nuclear envelope may also be associated to the nucleoplasmic reticulum when it is present in the central nucleoplasm. This is why we then investigated whether certain chromosomes were specifically targeted and found that no single chromosome was changed with either treatment.

Additionally, the intersection of the Venn Diagram was not large enough to address whether a specific genomic region was targeted in that case. We also found that the abundance of our hits is not mirrored in the most common cancers suggesting that the NR abundance and whether the tissue is healthy or cancerous may be decoupled.

We identified several pathways that were significantly changed in either condition but not in both. Unexpectedly, in the hormones treated cells, pathways related to lipid synthesis had significantly reduced gene expression. This was a surprise because we know that lipid synthesis is required for new NR formation (Goulbourne et al., 2011; Drozdz et al., 2017; Pytowski et al., 2019). This may mean that non canonical pathways are used for the NR formation. This is further suggested by the fact that skin fibroblasts from patients with different mutations in CCTα have different levels of NR abundance and a different morphology. Indeed, skin fibroblasts from patients harbouring p.V142M plus p.E280de or p.E280del and p.S333Lfs*164 have a *near complete absence* of PCYT1A and had no significant increase of NR relative to the control. Conversely, skin fibroblasts harbouring the mutation PCYT1A p.A99V or p.S323Afs*38 had more invaginations of the nuclear envelope than the control cells; the PCYT1A p.A99V mutation leads to a 15 to 30 % decrease in CCTα expression and a 2-fold reduction of phosphatidyl choline synthesis due to the perturbation of the catalytic domain of the enzyme (Cornell et al., 2019; Hoover-Fong et al., 2014; Jurgens, 2017). To summarise, when PCYT1A is absent there is no NR abundance increase while it does increase when a mutated form of PCYT1A is present in the cells. This implies that two distinct scavenger pathways come into action depending on whether PCYT1A is present or not and only the one with PCYT1A leads to more NR. This might be the case because

different pathways may produce different lipids from within different compartments of the cell and thus have different effects on nuclear envelope morphology. Indeed it has been shown that PCYT1A is enriched in the tips of the invaginations of the nuclear envelope where newly synthesised phosphatidyl choline is accumulated (as revealed by the NanoSIMS experiments (Drozdz et al., 2017; Pytowski et al., 2019), meaning that absence of PYCT1A from the nuclear envelope is likely to reduce NR abundance. Interestingly, we observed by electron microscopy that skin fibroblasts with PCYT1A p.A99V or PCYT1A p.S323Afs*38 had invaginations with a double nuclear envelope (i.e. a quadruple bilayer): this layout would still provide structural support to the nuclear envelope and genome with its lamina associated domain and it would allow delivery of diffusible ions such as calcium for gene expression regulation. However, exchange of larger material such as proteins that need to pass thought the nuclear pores complexes is likely to be compromised by the additional double bilayer. The phenotype that we see in the CCTa deficient cells may be the accumulation of planar membranes (with cylindrical PC) produced from conical Phosphatidylethanolamine (PE) by PE methyltransferase (PEMT). This would also lead to the accumulation of the membrane curvature inducing lipid diacylglycerol.

It is also interesting to mention that PEMT is activated by oestrogen (Resseguie et al., 2007) and that increased PEMT expression may reduce the synthesis of phosphatidylcholine by the CDP-choline pathway (Cui et al., 1995). This is then an example of membrane shape regulation by the balance of fluxes though different lipid synthetic pathways and may explain the increased NR abundance in endometrial cells when exposed to this hormone.

It remains to be investigated whether the changes in gene expression are related to the delivery of a diffusible molecule into a particular chromosome domain territory. If this were the case, then there would be a positional correlation between the genes that we find commonly deregulated in the presence of more NR. If such is the case, then it is likely that we will find that there is a morphological similarity in the location on chromatin of the elements that are co-regulated. Based on our analysis of the gene expression changes and their chromosome position we found that no chromosome, in its entirety, was specifically changed. However, chromosome positioning and territories are fluid within the nucleus, meaning that a Fluorescence In Situ Hybridization (FISH) analysis might be more appropriate to assess whether our 5 gene hits are in the vicinity of the nuclear envelope or the NR. Finally, the NGS analysis is blind to post-translational modifications meaning that if the NR affects or is affected by these then those changes are absent from our analysis. Mass spectrometry could be used to measure protein abundances and identify post-translational modifications in both saquinavir, and hormone treated samples.

6. Perspective and future directions

“I fully realize that I have not succeeded in answering all of your questions.

Indeed, I feel I have not answered any of them completely. The answers I have found only serve to raise a whole new set of questions, which only lead to more problems, some of which we weren’t even aware were problems.

To sum it all up… in some ways I feel we are confused as ever, but I believe we are confused on a higher level, and about more important things.”

Inspired from Earl C. Kelley, The Workshop Way of Learning (Kelley, 1951),

possibly modified by Peyman Milanfar, (2021)

The nucleoplasmic reticulum has been an elusive structure for over 50 years. This structure has been found in countless tissues and organisms under various conditions, both in health and disease. Evidence has piled up to show that this structure is assembled by a highly regulated mechanisms that requires newly synthesised proteins and lipids in interphase.

It was thought that the NR was observed only *in vitro* as an artefact or that it was simply a remnant of nuclear envelope reassembly with no real function. We have demonstrated that the NR is in fact a highly regulated structure that is in indeed found *in vitro* and in virtually every cell line, both in 2D and 3D cultures plus it is found in tissue sections from humans and other eukaryotes. We have demonstrated that we can detect NR with immunofluorescences tagging various components of the nuclear envelope or ER, or over-expression/endogenous expression of various fusion proteins with fluorescent proteins. We demonstrated that the formation of the NR can be induced in various ways, both physiologically and pathologically. We also demonstrated that the NR enables exchange of material deep within the nucleoplasm.

The aims of the thesis were to (i) further understand how and when the nucleoplasmic reticulum is assembled; (ii) identify how it is structured and if/how it differs from the nuclear envelope; (iii) evaluate its function in terms of exchange or material between the cytoplasm and nucleoplasm; (iv) Elucidate what are the gene expression changes that occur when the nucleoplasmic reticulum formation is induced.

(i) We imaged for the first time the assembly of new LmnA-mNeonGreen invaginations of the nuclear envelope in live cells with an unprecedented spatio-

temporal resolution. This was enabled by the combination of highly sensitive cameras and denoising methods. In the future, multi-channel imaging including other components of the nuclear envelope such as NPCs, lipids, or curvature-inducing proteins will enable to address in what order those components are assembled.

(ii) We, and others, identified a number of components that are found in the nucleoplasmic reticulum. However, proteins specifically enriched in the invaginations of the nuclear envelope remain to be identified. BioID may be used for this purpose (see section iv). Alternatively two main projects may lead to the identification of NR enriched proteins: (a) OpenCell, a project aiming to tag endogenously all human proteins by CRISPR and image them by 3D live imaging in HEK293T cells (Cho et al., 2022); (b) The Human Protein Atlas that has the same aims but utilises antibodies with 2D microscopy (Thul et al., 2017). The analysis of those dataset may reveal NR-specific proteins.

The structure of the lamina may also differ between the bulk nuclear envelope and its invaginations due to the difference in their degree of curvature and orientations. The use of expansion microscopy combined to super resolution microscopy may provide insights into the organisation of the lamina in the nucleoplasmic reticulum.

(iii) We identified the associations between nuclear volume/DNA content with NR abundance. However, we found that when DNA content increases so does the volume. This means that we cannot know whether the increase in NR abundance is due to the increase in volume or the increase in DNA content (or both). Recently a set of compounds that increases or decreases nuclear size was identified (Tollis et al., 2022). The use of such compounds may allow to decouple the nuclear volume from DNA

content and elucidate whether the changes in NR content are due to one or the other. The association of the NR with nucleoli indicates that the distribution is not random. This implies that it has a function. One such function may be the exchange of material a though the NR and we have demonstrated that is it indeed the case. Other functions may include the sequestration of transcription factors by the lamina (Dauer and Worman, 2009; Choi and Worman, 2014; Serebryannyy and Misteli, 2017).

(iv) We identified a number of genes that are changed when NR formation is induced, however, other research avenues could include the further exploration of links between candidates from RNA-Seq and NR formation using activation or repression of target genes using CRISPR with dCas9-VPR or dCas9-KRAB. In this system an enzymatically inactive ('dead') Cas9 is targeted to genes of interest with an RNA guide complementary to the target sequence. The target sequence for gene activation is before the transcription start site (TSS); there the dead Cas9 fused to activation domain (such as VPR – VP64, p65, Rta) binds and promotes transcription. For gene repression the dead Cas9 is targeted downstream of the transcription start site and is fused to repressors (transcriptional repressor peptide KRAB) that reduces gene transcription. Both systems would allow to measure changes in NR abundance with either activation or repression of the selected genes and would allow us to infer whether those genes were necessary for NR formation or not. Other tests may include the activation and repression of genes involved in lipid synthesis so that the enzymes - and the lipids synthesised by them - necessary for NR formation can be identified. Alternatively, different lipid stains (Filipin III, Bromine-Sudan Black, etc.) may reveal a difference in the composition of the membrane of the NR versus the rest of the nuclear envelope. If not,

the incubation of the cells with excess of various lipids may also reveal which ones change the nuclear envelope morphology and NR abundance. The NanoSIMS experiments revealed that newly synthesised lipids pulse-labelled using deuterated choline or stearate are selectively incorporated in the newly formed invaginations, with particular enrichment at the tip of blind-ended channels and at the base in regions of high negative curvature. This distribution has potential implications for the biogenesis and stabilisation of NR structures. This analysis has concentrated on the phosphatidylcholine component of the phospholipid bilayer because of its high abundance, but other methods including NMR or 3D OrbiSIMS supporting label-free metabolic imaging may also reveal the differences in composition between the NR and the rest of the nuclear envelope. Indeed studies have shown that NMR can be used to analyse the lipid composition of the nuclear envelopes (Dazzoni et al., 2020). Cryo-OrbiSIMS enables three-dimensional label-free metabolic imaging (Passarelli et al., 2017); although it currently lacks the resolution needed to gain new information from the nuclear envelope, its use in combination with sample expansion (Damstra et al., 2022) (lipid-retaining expansion remains to be developed) may further our understanding of the contribution of different lipids on nuclear envelope membrane curvatures.

Various strategies have been used to manipulate lipids or lipid metabolism in live samples. The activation and repression of genes coding for lipid-synthesizing enzymes or lipid-consuming enzymes can be used to alter lipid pathways (either by RNA delivery, transient over-expressions, or CRISPR). However, this strategy lacks the spatio-temporal resolution required to study live biological membranes. This is due to the lack of

subcellular alteration control; additionally, the slow response may be mitigated by internal cellular homeostasis. To address those limitations other lipid manipulation strategies can be used. This includes the direct delivery of fully-matured enzymes that either consume or synthesise lipids. For example, this strategy was employed to consume diacylglycerol by micro-injecting diacylglycerol kinase or PIP_2 5-phosphatase Syn1 and it revealed that diacylglycerol is necessary for the formation of ER tubes in mammalian cells (Domart et al., 2012) and in sea urchin eggs (Wang et al., 2013). Both these publications (and others) also demonstrate that the addition of exogenous lipids can alter the membranes. Indeed, the delivery of 1,2 diacylglycerol by liposomes enriched with that lipid can rescue the effects of induced diacylglycerol catabolism in terms of ER morphology. With similar methods Ulloa et al. (2019) demonstrated that phosphatidylethanolamine can also be used to reverse the effect of reduced diacylglycerol (albeit less efficiently than with the direct liposome delivery of diacylglycerol).

The manipulation of lipid concentrations by genetic activation or repression of synthetic or catabolic pathways is slow and not localised to any specific compartment; the exogenous delivery of enzymes or lipids is fast but again not localised. The FRB – FKBP dimerization system enables fast and localised interventions. In this system, rapamycin, or an analogue (rapalogue) is used to dimerise FRB to FKBP. This allows to create fusion proteins than can be localised to specific cellular compartments. Indeed this has been used for example to recruit a 5-phosphatase to the plasma membrane and convert PtdIns(4,5)P_2 into PtdIns(4)P (Varnai et al., 2006) or to simply deplete it (Hammond et al., 2012). In the first case they found that the conversion inhibited

calcium signalling at the plasma membrane and in the second case they measured the depletion effect on others PtdIns and found that it prevents correct localisation of proteins that dimerise with PtdIns. Other groups recruited the PtdIns3P-specific 3-phosphatase myotubularin to the endosomal membranes and found that when PtdIns3P was absent endosomal maturation was prevented (Fili et al., 2006). When the phosphoinositide 4-phosphatase Sac 1 was recruited to the Golgi apparatus, the reduction in PtdIns4P reduced the Golgi trafficking (Szentpetery et al., 2010). When a diacylglycerol kinase was targeted to the Golgi apparatus it depleted diacylglycerol and prevented nuclear envelope reassembly after mitosis plus it led to the reduction of tubular ER abundance (while multi-lamellar sheets abundance increased) (Chung et al., 2018); interestingly the addition of diacylglycerol could mitigate the effect of the diacylglycerol kinase. In summary the FRB – FKBP rapalog system could enable us to locally manipulate lipids in the nuclear envelope. For example, one could engineer a FKBP - LmnA or Emerin – FKBP and target lipid synthesising or consuming enzymes to the inner nuclear envelope (nucleoplasmic or luminal face respectively) and measure the effect of NE morphology including NR prominence in the presence or absence or rapalogue.

We described how the candidates from RNA-Seq could be further studied. Another avenue to understand the role of NR in gene expression regulation could be the identification of genes or proteins in the proximity of the NR. Currently there are no methods that allow this. If there were proteins that were identified as being highly enriched in the NR it would be possible to do DamID or BioID with the methylase or the biotin ligase bound to that *still-to-be-identified* protein. Previous efforts in the lab to

identify specific NR marker proteins by isolating monoclonal antibodies from mice immunised with TX-114 membrane fractions of surface-stripped sheared nuclei were of limited success. Although excellent antibodies specific for fully processed mature lamin B1 were generated (e.g. 8D1), no NR-specific marker proteins were identified. In the absence of marker proteins to specify localisation of a methylase or biotin ligase fusion protein, it is necessary to fall back upon methods that permit spatial restriction of activation. However, there are at this stage no photo-activable DamID or BioID. Methods have been developed for the light-dependant crosslinking of protein-protein (Fancy and Kodadek, 1999) or DNA-protein (Matsumoto and Hanawalt, 2000; Shigdel et al., 2008). These methods could, in principle, provide high spatial control of the sites of protein-DNA interaction that would permit downstream isolation of DNA associated with selected sub-volumes of the nucleus. This would provide a high spatial control of the proteins or DNA that one can purify and then identify, but this would be a very challenging enterprise that will require single cells 'omics with advanced automated light microscopy combining automatic identification of the invaginations of the nuclear envelope, then their photo-treatment and finally the biochemical treatment of the samples.

Another line of evidence has begun to emerge indicating that it is possible to select cells with low or high NR abundance and create subsequent populations that maintains the initial NR abundance. Further selection of cells with low or high NR abundance further scores that phenotype. These selection of cells and subsequent monoclonal population are done under the same conditions for both the high and low NR abundance cell lines (same media, same incubator, same environment, same

handling). This indicates that only internal factors are sufficient to lead to these differences. Additionally, if the distribution of NR were random then there would be a stochastic regression to the mean and all populations would have comparable NR abundances post selection. The corollary is that something internal and hereditary to the cells controls the NR abundance. The identification of this internal regulator could be potentially done by exploring the differences between those colonies. The differences could reside in the lipid composition of the nuclear envelope or the gene organisation for example. Chromosome paints could be used to find differences in genome organisation, and lipids could be studied as described above.

From the earliest EM observations (Bourgeois et al., 1979), the NR has indeed been a very enigmatic structure (and even its existence *in vivo* has been questioned) and we hope that this thesis has further our appreciation of this structure. I have sought to bring together morphological and functional observations of NR to offer a framework for future experiments.

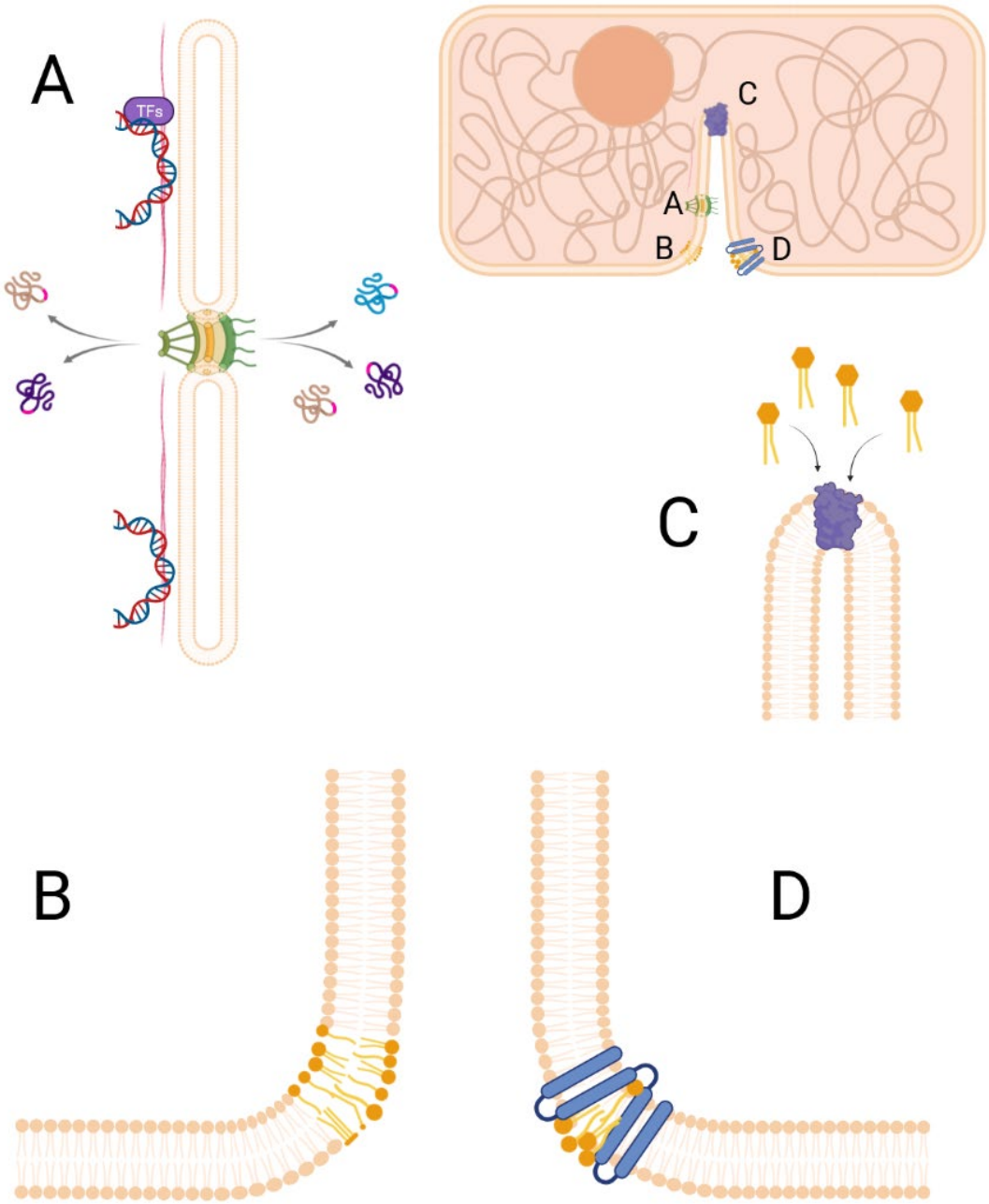


Figure 6-1: Graphical summary illustrating structure-function. ***(A)*** *Bidirectional transport across the nucleoplasmic reticulum, lamina-associated domains, transcription factors sequestration.* ***(B)*** *Curvature of the membranes may be induced by lipids that are synthesised and incorporated in the NR* ***(C)****.* ***(D)*** *proteins may also induce membrane curvature. In panels B, C, D only the inner nuclear membrane is illustrated. Diagram created in BioRender.*

7. References

Aebi, U., Cohn, J.B., Buhle, L., and Gerace, L. (1986). The nuclear lamina is a meshwork of intermediate type filaments. Nature *323*, 560–564. .

Agrawal, A., and Lele, T.P. (2019). Mechanics of nuclear membranes. J. Cell Sci. *132*. https://doi.org/10.1242/jcs.229245.

Ahn, J., Jo, I., Kang, S., Hong, S., Kim, S., Jeong, S., Kim, Y.-H., Park, B.-J., and Ha, N.-C. (2019). Structural basis for lamin assembly at the molecular level. Nat. Commun. *10*, 3757. https://doi.org/10.1038/s41467-019-11684-x.

Alberts, B. (2015). Molecular biology of the cell (New York, NY: Garland Science, Taylor and Francis Group).

Avedanian, L., Jacques, D., and Bkaily, G. (2011). Presence of tubular and reticular structures in the nucleus of human vascular smooth muscle cells. J. Mol. Cell. Cardiol. *50*, 175–186. https://doi.org/10.1016/j.yjmcc.2010.10.005.

Banaszynski, L.A., Liu, C.W., and Wandless, T.J. (2005). Characterization of the FKBP·Rapamycin·FRB Ternary Complex. J. Am. Chem. Soc. *127*, 4715–4721. https://doi.org/10.1021/ja043277y.

Beaudouin, J., Gerlich, D., Daigle, N., Eils, R., and Ellenberg, J. (2002). Nuclear Envelope Breakdown Proceeds by Microtubule-Induced Tearing of the Lamina. Cell *108*, 83–96. https://doi.org/10.1016/S0092-8674(01)00627-4.

Bengtsson, L., and Wilson, K.L. (2004). Multiple and surprising new functions for emerin, a nuclear membrane protein. Curr. Opin. Cell Biol. *16*, 73–79. https://doi.org/10.1016/j.ceb.2003.11.012.

Benson, D.A., Cavanaugh, M., Clark, K., Karsch-Mizrachi, I., Lipman, D.J., Ostell, J., and Sayers, E.W. (2012). GenBank. Nucleic Acids Res. *41*, D36–D42. https://doi.org/10.1093/nar/gks1195.

Berrios, M. (1998). Nuclear Structure and Function, Volume 53 - 1st Edition.

Bezin, S., Fossier, P., and Cancela, J.-M. (2008). Nucleoplasmic reticulum is not essential in nuclear calcium signalling mediated by cyclic ADPribose in primary neurons. Pflüg. Arch. - Eur. J. Physiol. *456*, 581–586. https://doi.org/10.1007/s00424-007-0435-8.

Bindels, D.S., Haarbosch, L., van Weeren, L., Postma, M., Wiese, K.E., Mastop, M., Aumonier, S., Gotthard, G., Royant, A., Hink, M.A., et al. (2017). mScarlet: a bright monomeric red fluorescent protein for cellular imaging. Nat Meth *14*, 53–56. .

Boubriak, I.I., Malhas, A.N., Drozdz, M.M., Pytowski, L., and Vaux, D.J. (2017). Stress-induced release of Oct-1 from the nuclear envelope is mediated by JNK phosphorylation of lamin B1. PLOS ONE *12*, e0177990. https://doi.org/10.1371/journal.pone.0177990.

Bourgeois, C.A., Hemon, D., and Bouteille, M. (1979). Structural relationship between the nucleolus and the nuclear envelope. J. Ultrastruct. Res. *68*, 328–340. http://dx.doi.org/10.1016/S0022-5320(79)90165-5.

Briand, N., and Collas, P. (2020). Lamina-associated domains: peripheral matters and internal affairs. Genome Biol. *21*, 85. https://doi.org/10.1186/s13059-020-02003-5.

Broaddus, C., Krull, A., Weigert, M., Schmidt, U., and Myers, G. (2020). Removing Structured Noise with Self-Supervised Blind-Spot Networks. In 2020 IEEE 17th International Symposium on Biomedical Imaging (ISBI), pp. 159–163.

Broers, J.L.V., Ramaekers, F.C.S., Bonne, G., Ben Yaou, R., and Hutchison, C.J. (2006). Nuclear lamins: Laminopathies and their role in premature ageing. Physiol. Rev. *86*, 967–1008. https://doi.org/10.1152/physrev.00047.2005.

Burke, B., and Stewart, C.L. (2013). The nuclear lamins: flexibility in function. Nat. Rev. Mol. Cell Biol. *14*, 13–24. https://doi.org/10.1038/nrm3488.

Bussolati, G. (2008). Proper detection of the nuclear shape: ways and significance. Rom J Morphol Embryol *49*, 435–439. .

Callan, H.G., and Tomlin, S.G. (1950). Experimental studies on amphibian oocyte nuclei. I. Investigation of the structure of the nuclear membrane by means of the electron microscope. Proc. R. Soc. Lond. B Biol. Sci. *137*, 367–378. https://doi.org/10.1098/rspb.1950.0047.

Caron, M., Auclair, M., Donadille, B., Béréziat, V., Guerci, B., Laville, M., Narbonne, H., Bodemer, C., Lascols, O., Capeau, J., et al. (2007). Human lipodystrophies linked to mutations in A-type lamins and to HIV protease inhibitor therapy are both associated with prelamin A accumulation, oxidative stress and premature cellular senescence. Cell Death Differ. *14*, 1759–1767. https://doi.org/10.1038/sj.cdd.4402197.

Carr, A. (2000). HIV protease inhibitor-related lipodystrophy syndrome. Clin. Infect. Dis. Off. Publ. Infect. Dis. Soc. Am. *30 Suppl 2*. https://doi.org/10.1086/313854.

von Chamier, L., Laine, R.F., Jukkala, J., Spahn, C., Krentzel, D., Nehme, E., Lerche, M., Hernández-Pérez, S., Mattila, P.K., Karinou, E., et al. (2021). Democratising deep learning for microscopy with ZeroCostDL4Mic. Nat. Commun. *12*, 2276. https://doi.org/10.1038/s41467-021-22518-0.

Cho, N.H., Cheveralls, K.C., Brunner, A.-D., Kim, K., Michaelis, A.C., Raghavan, P., Kobayashi, H., Savy, L., Li, J.Y., Canaj, H., et al. (2022). OpenCell: Endogenous tagging for the cartography of human cellular organization. Science *375*, eabi6983. https://doi.org/10.1126/science.abi6983.

Choi, J.C., and Worman, H.J. (2014). Nuclear envelope regulation of signaling cascades. Adv. Exp. Med. Biol. *773*, 187–206. https://doi.org/10.1007/978-1-4899-8032-8_9.

Chow, K.-H., Factor, R.E., and Ullman, K.S. (2012). The nuclear envelope environment and its cancer connections. Nat. Rev. Cancer *12*, 196–209. https://doi.org/10.1038/nrc3219.

Chung, G.H.C., Domart, M.-C., Peddie, C., Mantell, J., Mclaverty, K., Arabiotorre, A., Hodgson, L., Byrne, R.D., Verkade, P., Arkill, K., et al. (2018). Acute depletion of diacylglycerol from the cis-Golgi affects localized nuclear envelope morphology during mitosis. J. Lipid Res. *59*, 1402–1413. https://doi.org/10.1194/jlr.M083899.

Chung, G.H.C., Domart, M.-C., Peddie, C., Mclaverty, K., Arabiotorre, A., Hodgson, L., Verkade, P., Arkill, K., Collinson, L.M., and Larijani, B. Acute Depletion of Diacylglycerol from the Cis-Golgi Affects Localised Nuclear Envelope Morphology During Mitosis. 38. .

Clubb, B.H., and Locke, M. (1998). 3T3 cells have nuclear invaginations containing F-actin. Tissue Cell *30*, 684–691. https://doi.org/10.1016/S0040-8166(98)80087-6.

Coffinier, C., Hudon, S.E., Farber, E.A., Chang, S.Y., Hrycyna, C.A., Young, S.G., and Fong, L.G. (2007). HIV protease inhibitors block the zinc metalloproteinase ZMPSTE24 and lead to an accumulation of prelamin A in cells. Proc. Natl. Acad. Sci. *104*, 13432–13437. https://doi.org/10.1073/pnas.0704212104.

Cohen, S.N., Chang, A.C., and Hsu, L. (1972). Nonchromosomal antibiotic resistance in bacteria: genetic transformation of Escherichia coli by R-factor DNA. Proc. Natl. Acad. Sci. U. S. A. *69*, 2110–2114. .

Collings, D.A., Carter, C.N., Rink, J.C., Scott, A.C., Wyatt, S.E., and Allen, N.S. (2000). Plant Nuclei Can Contain Extensive Grooves and Invaginations. Plant Cell *12*, 2425–2439. https://doi.org/10.1105/tpc.12.12.2425.

Cooke, I.R., and Deserno, M. (2006). Coupling between Lipid Shape and Membrane Curvature. Biophys. J. *91*, 487–495. https://doi.org/10.1529/biophysj.105.078683.

Cooke, I.R., and Deserno, M. Coupling between Lipid Shape and Membrane Curvature. Biophys. J. 9. .

Cornell, R.B., Taneva, S.G., Dennis, M.K., Tse, R., Dhillon, R.K., and Lee, J. (2019). Disease-linked mutations in the phosphatidylcholine regulatory enzyme CCTα impair enzymatic activity and fold stability. J. Biol. Chem. *294*, 1490–1501. https://doi.org/10.1074/jbc.RA118.006457.

Corrigan, D.P. (2005). Prelamin A endoproteolytic processing in vitro by recombinant Zmpste24. Biochem J *387*, 129–138. .

Crisp, M. (2006). Coupling of the nucleus and cytoplasm: role of the LINC complex. J Cell Biol *172*, 41–53. .

Cui, Z., Houweling, M., and Vance, D.E. Expression of phosphatidylethanolamine N-methyltransferase-2 in McArdle-RH7777 hepatoma cells inhibits the CDP-choline pathway for phosphatidyicholine biosynthesis via decreased gene expression -of CTP:phosphocholine cytidylyltransferase. 7. .

Damstra, H.G., Mohar, B., Eddison, M., Akhmanova, A., Kapitein, L.C., and Tillberg, P.W. (2022). Visualizing cellular and tissue ultrastructure using Ten-fold Robust Expansion Microscopy (TREx). ELife *11*, e73775. https://doi.org/10.7554/eLife.73775.

Dauer, W.T., and Worman, H.J. (2009). The Nuclear Envelope as a Signaling Node in Development and Disease. Dev. Cell *17*, 626–638. https://doi.org/10.1016/j.devcel.2009.10.016.

Dazzoni, R., Grélard, A., Morvan, E., Bouter, A., Applebee, C.J., Loquet, A., Larijani, B., and Dufourc, E.J. (2020). The unprecedented membrane deformation of the human nuclear envelope, in a magnetic field, indicates formation of nuclear membrane invaginations. Sci. Rep. *10*, 5147. https://doi.org/10.1038/s41598-020-61746-0.

D'Eletto, M., Oliverio, S., and Di Sano, F. (2020). Reticulon Homology Domain-Containing Proteins and ER-Phagy. Front. Cell Dev. Biol. *8*, 90. https://doi.org/10.3389/fcell.2020.00090.

Dickey, A., and Faller, R. (2008). Examining the contributions of lipid shape and headgroup charge on bilayer behavior. Biophys. J. *95*, 2636–2646. https://doi.org/10.1529/biophysj.107.128074.

Dittmer, T.A., and Misteli, T. (2011). The lamin protein family. Genome Biol. *12*, 222. https://doi.org/10.1186/gb-2011-12-5-222.

Dockery, P., Ismail, R.M., Li, T.C., Warren, M.A., and Cooke, I.D. (1997). The effect of a single dose of mifepristone (RU486) on the fine structure of the human endometrium during the early luteal phase. Hum. Reprod. Oxf. Engl. *12*, 1778–1784. .

Domart, M.-C., Hobday, T.M.C., Peddie, C.J., Chung, G.H.C., Wang, A., Yeh, K., Jethwa, N., Zhang, Q., Wakelam, M.J.O., Woscholski, R., et al. (2012). Acute Manipulation of Diacylglycerol Reveals Roles in Nuclear Envelope Assembly & Endoplasmic Reticulum Morphology. PLoS ONE *7*, e51150. https://doi.org/10.1371/journal.pone.0051150.

Drozdz, M.M., Jiang, H., Pytowski, L., Grovenor, C., and Vaux, D.J. (2017). Formation of a nucleoplasmic reticulum requires de novo assembly of nascent phospholipids and shows preferential incorporation of nascent lamins. Sci. Rep. *7*, 7454. https://doi.org/10.1038/s41598-017-07614-w.

Duncan, K.M., Mukherjee, K., Cornell, R.A., and Liao, E.C. (2017). Zebrafish models of orofacial clefts. Dev. Dyn. *246*, 897–914. https://doi.org/10.1002/dvdy.24566.

Echevarría, W., Leite, M.F., Guerra, M.T., Zipfel, W.R., and Nathanson, M.H. (2003). Regulation of calcium signals in the nucleus by a nucleoplasmic reticulum. Nat. Cell Biol. *5*, 440–446. https://doi.org/10.1038/ncb980.

Ernest I. Kohorn, Susan I. Rice, Susan Hemperly, and Mildred Gordon (1972). The relation of the structure of progestational steroids to nucleolar differentiation in human endometrium. J. Clin. Endocrinol. Metab. *34*, 257–264. https://doi.org/doi:10.1210/jcem-34-2-257.

Fancy, D.A., and Kodadek, T. (1999). Chemistry for the analysis of protein–protein interactions: Rapid and efficient cross-linking triggered by long wavelength light. Proc. Natl. Acad. Sci. *96*, 6020–6024. https://doi.org/10.1073/pnas.96.11.6020.

Feria-Velasco, A., Aznar-Ramos, R., and González-Angulo, A. (1972). Ultrastructural changes found in the endometrium of women using megestrol acetate for contraception. Contraception *5*, 187–201. http://dx.doi.org/10.1016/0010-7824(72)90045-5.

Fili, N., Calleja, V., Woscholski, R., Parker, P.J., and Larijani, B. (2006). Compartmental signal modulation: Endosomal phosphatidylinositol 3-phosphate controls endosome morphology and selective cargo sorting. Proc. Natl. Acad. Sci. U. S. A. *103*, 15473–15478. https://doi.org/10.1073/pnas.0607040103.

Fischer, A.H. (2014). The Diagnostic Pathology of the Nuclear Envelope in Human Cancers. In Cancer Biology and the Nuclear Envelope, (Springer, New York, NY), pp. 49–75.

Franke, W.W., Scheer, U., Krohne, G., and Jarasch, E.D. (1981). The nuclear envelope and the architecture of the nuclear periphery. J. Cell Biol. *91*, 39s–50s. https://doi.org/10.1083/jcb.91.3.39s.

Fricker, M., Hollinshead, M., White, N., and Vaux, D. (1997). Interphase Nuclei of Many Mammalian Cell Types Contain Deep, Dynamic, Tubular Membrane-bound Invaginations of the Nuclear Envelope. J. Cell Biol. *136*, 531–544. .

Gehrig, K., and Ridgway, N.D. (2011). CTP:phosphocholine cytidylyltransferase α (CCTα) and lamins alter nuclear membrane structure without affecting phosphatidylcholine synthesis. Biochim. Biophys. Acta BBA - Mol. Cell Biol. Lipids *1811*, 377–385. https://doi.org/10.1016/j.bbalip.2011.04.001.

Gehrig, K., Cornell, R.B., and Ridgway, N.D. (2008). Expansion of the Nucleoplasmic Reticulum Requires the Coordinated Activity of Lamins and CTP:Phosphocholine Cytidylyltransferase α. Mol. Biol. Cell *19*, 237–247. https://doi.org/10.1091/mbc.E07-02-0179.

Gerace, L., and Huber, M.D. (2012). Nuclear lamina at the crossroads of the cytoplasm and nucleus. J. Struct. Biol. *177*, 24–31. http://dx.doi.org/10.1016/j.jsb.2011.11.007.

Giełwanowska, I., Pastorczyk, M., Lisowska, M., Węgrzyn, M., and Górecki, R.J. (2014). Cold stress effects on organelle ultrastructure in polar Caryophyllaceae species. Pol. Polar Res. *35*. https://doi.org/10.2478/popore-2014-0029.

Goryaynov, A., Ma, J., and Yang, W. (2012). Single-molecule studies of nucleocytoplasmic transport: from one dimension to three dimensions. Integr. Biol. *4*, 10–21. https://doi.org/10.1039/C1IB00041A.

Goulbourne, C.N., and Vaux, D.J. (2010). HIV protease inhibitors inhibit FACE1/ZMPSTE24: a mechanism for acquired lipodystrophy in patients on highly active antiretroviral therapy? Biochem. Soc. Trans. *38*, 292–296. https://doi.org/10.1042/BST0380292.

Goulbourne, C.N., Malhas, A.N., and Vaux, D.J. (2011). The induction of a nucleoplasmic reticulum by prelamin A accumulation requires CTP:phosphocholine cytidylyltransferase-α. J. Cell Sci. *124*, 4253–4266. https://doi.org/10.1242/jcs.091009.

Graham, T.R., and Kozlov, M.M. (2013). Interplay of proteins and lipids in generating membrane curvature. 11. .

Gruenbaum, Y., Wilson, K.L., Harel, A., Goldberg, M., and Cohen, M. (2000). Review: nuclear lamins--structural proteins with fundamental functions. J. Struct. Biol. *129*, 313–323. https://doi.org/10.1006/jsbi.2000.4216.

Guatimosim, S., Amaya, M.J., Guerra, M.T., Aguiar, C.J., Goes, A.M., Gómez-Viquez, N.L., Rodrigues, M.A., Gomes, D.A., Martins-Cruz, J., Lederer, W.J., et al. (2008). Nuclear Ca2+ regulates cardiomyocyte function. Cell Calcium *44*, 230–242. https://doi.org/10.1016/j.ceca.2007.11.016.

Guffanti, E., Kittur, N., Brodt, Z.N., Polotsky, A.J., Kuokkanen, S.M., Heller, D.S., Young, S.L., Santoro, N., and Meier, U.T. (2008). Nuclear pore complex proteins mark the implantation window in human endometrium. J. Cell Sci. *121*, 2037–2045. https://doi.org/10.1242/jcs.030437.

Haase, R., Royer, L.A., Steinbach, P., Schmidt, D., Dibrov, A., Schmidt, U., Weigert, M., Maghelli, N., Tomancak, P., Jug, F., et al. (2020a). CLIJ: GPU-accelerated image processing for everyone. Nat. Methods *17*, 5–6. https://doi.org/10.1038/s41592-019-0650-1.

Haase, R., Jain, A., Rigaud, S., Vorkel, D., Rajasekhar, P., Suckert, T., Lambert, T.J., Nunez-Iglesias, J., Poole, D.P., Tomancak, P., et al. (2020b). Interactive design of GPU-accelerated Image Data Flow Graphs and cross-platform deployment using multi-lingual code generation.

Haczkiewicz, K., Rozenblut-Kościsty, B., and Ogielska, M. (2017). Prespermatogenesis and early spermatogenesis in frogs. Zoology *122*, 63–79. https://doi.org/10.1016/j.zool.2017.01.003.

Hammond, G.R.V., Fischer, M.J., Anderson, K.E., Holdich, J., Koteci, A., Balla, T., and Irvine, R.F. (2012). PI4P And PI(4,5)P2 Are Essential But Independent Lipid Determinants Of Membrane Identity. Science *337*, 727–730. https://doi.org/10.1126/science.1222483.

Hampoelz, B., Andres-Pons, A., Kastritis, P., and Beck, M. (2019). Structure and Assembly of the Nuclear Pore Complex. Annu. Rev. Biophys. *48*, 515–536. https://doi.org/10.1146/annurev-biophys-052118-115308.

Hay, N., and Sonenberg, N. (2004). Upstream and downstream of mTOR. Genes Dev. *18*, 1926–1945. https://doi.org/10.1101/gad.1212704.

Hebbar, S., Mesngon, M.T., Guillotte, A.M., Desai, B., Ayala, R., and Smith, D.S. (2008). Lis1 and Ndel1 influence the timing of nuclear envelope breakdown in neural stem cells. J. Cell Biol. *182*, 1063–1071. https://doi.org/10.1083/jcb.200803071.

Hegele, R.A., Cao, H., Liu, D.M., Costain, G.A., Charlton-Menys, V., Wilson Rodger, N., and Durrington, P.N. (2006). Sequencing of the reannotated LMNB2 gene reveals novel mutations in patients with acquired partial lipodystrophy. Am. J. Hum. Genet. *79*, 383–389. https://doi.org/10.1086/505885.

Hesse, H., and Rosner, H. (1971). Siddhartha (Toronto; New York: Bantam Books).

Hirama, T., Lu, S.M., Kay, J.G., Maekawa, M., Kozlov, M.M., Grinstein, S., and Fairn, G.D. (2017). Membrane curvature induced by proximity of anionic phospholipids can initiate endocytosis. Nat. Commun. *8*, 1393. https://doi.org/10.1038/s41467-017-01554-9.

Hoover-Fong, J., Sobreira, N., Jurgens, J., Modaff, P., Blout, C., Moser, A., Kim, O.-H., Cho, T.-J., Cho, S.Y., Kim, S.J., et al. (2014). Mutations in PCYT1A, Encoding a Key Regulator of Phosphatidylcholine Metabolism, Cause Spondylometaphyseal Dysplasia with Cone-Rod Dystrophy. Am. J. Hum. Genet. *94*, 105–112. https://doi.org/10.1016/j.ajhg.2013.11.018.

Hutchison, C.J. (2014). B-type lamins in health and disease. Semin. Cell Dev. Biol. *29*, 158–163. https://doi.org/10.1016/j.semcdb.2013.12.012.

de Jesus, A.J., Kastelowitz, N., and Yin, H. (2014). Changes in lipid density induce membrane curvature. 8. .

Jorgens, D.M., Inman, J.L., Wojcik, M., Robertson, C., Palsdottir, H., Tsai, W.-T., Huang, H., Bruni-Cardoso, A., López, C.S., Bissell, M.J., et al. (2017). Deep nuclear invaginations are linked to cytoskeletal filaments – integrated bioimaging of epithelial cells in 3D culture. J. Cell Sci. *130*, 177–189. https://doi.org/10.1242/jcs.190967.

Jurgens, J. (2017). EXPLAINING RARE MENDELIAN PHENOTYPES: EXOME SEQUENCING AND FUNCTIONAL ANALYSIS OF SPONDYLOMETAPHYSEAL DYSPLASIA WITH CONE-ROD DYSTROPHY. Thesis. Johns Hopkins University.

Kabachinski, G., and Schwartz, T.U. (2015). The nuclear pore complex – structure and function at a glance. J. Cell Sci. *128*, 423–429. https://doi.org/10.1242/jcs.083246.

Kavanagh, E., and Joseph, B. (2011). The hallmarks of CDKN1C (p57, KIP2) in cancer. Biochim. Biophys. Acta BBA - Rev. Cancer *1816*, 50–56. https://doi.org/10.1016/j.bbcan.2011.03.002.

Kelley, E.C. (1951). The Workshop Way of Learning (Harper).

Kim, D.-H., Sarbassov, D.D., Ali, S.M., King, J.E., Latek, R.R., Erdjument-Bromage, H., Tempst, P., and Sabatini, D.M. (2002). mTOR Interacts with Raptor to Form a Nutrient-Sensitive Complex that Signals to the Cell Growth Machinery. Cell *110*, 163–175. https://doi.org/10.1016/S0092-8674(02)00808-5.

Kind, J., Pagie, L., Ortabozkoyun, H., Boyle, S., de Vries, S.S., Janssen, H., Amendola, M., Nolen, L.D., Bickmore, W.A., and van Steensel, B. (2013). Single-Cell Dynamics of Genome-Nuclear Lamina Interactions. Cell *153*, 178–192. https://doi.org/10.1016/j.cell.2013.02.028.

Kinsella, M.D., Hinrichs, B., Cohen, C., and Siddiqui, M.T. (2013). Highlighting nuclear membrane staining in thyroid neoplasms with emerin: Review and diagnostic utility. Diagn. Cytopathol. *41*, 497–504. https://doi.org/10.1002/dc.22870.

Kiseleva, E., Morozova, K.N., Voeltz, G.K., Allen, T.D., and Goldberg, M.W. (2007). Reticulon 4a/NogoA locates to regions of high membrane curvature and may have a role in nuclear envelope growth. J. Struct. Biol. *160*, 224–235. https://doi.org/10.1016/j.jsb.2007.08.005.

Kitten, G.T., and Nigg, E.A. (1991). The CaaX motif is required for isoprenylation, carboxyl methylation, and nuclear membrane association of lamin B2. J. Cell Biol. *113*, 13–23. https://doi.org/10.1083/jcb.113.1.13.

Kittur, N., Zapantis, G., Aubuchon, M., Santoro, N., Bazett-Jones, D.P., and Meier, U.T. (2007). The Nucleolar Channel System of Human Endometrium Is Related to Endoplasmic Reticulum and R-Rings. Mol. Biol. Cell *18*, 2296–2304. https://doi.org/10.1091/mbc.E07-02-0154.

Kohorn, E.I., Rice, S.I., Hemperly, S., and Gordon, M. (1972). The Relation of the Structure of Progestational Steroids to Nucleolar Differentiation in Human Endometrium. J. Clin. Endocrinol. Metab. *34*, 257–264. https://doi.org/10.1210/jcem-34-2-257.

Korfali, N., Florens, L., and Schirmer, E.C. (2016). Isolation, Proteomic Analysis, and Microscopy Confirmation of the Liver Nuclear Envelope Proteome. In The Nuclear Envelope, (Humana Press, New York, NY), pp. 3–44.

Krull, A., Buchholz, T.-O., and Jug, F. (2019). Noise2Void - Learning Denoising from Single Noisy Images. ArXiv181110980 Cs.

Lagace, T.A., and Ridgway, N.D. (2005). The Rate-limiting Enzyme in Phosphatidylcholine Synthesis Regulates Proliferation of the Nucleoplasmic Reticulum. Mol. Biol. Cell *16*, 1120–1130. https://doi.org/10.1091/mbc.E04-10-0874.

Lamble, S., Batty, E., Attar, M., Buck, D., Bowden, R., Lunter, G., Crook, D., El-Fahmawi, B., and Piazza, P. (2013). Improved workflows for high throughput library preparation using the transposome-based nextera system. BMC Biotechnol. *13*, 104. https://doi.org/10.1186/1472-6750-13-104.

Larijani, B., Hamati, F., Kundu, A., Chung, G.C., Domart, M.-C., Collinson, L., and Poccia, D.L. (2014). Principle of duality in phospholipids: regulators of membrane morphology and dynamics. Biochem. Soc. Trans. *42*, 1335–1342. https://doi.org/10.1042/BST20140224.

Larijani, B., Pytowski, L., and Vaux, D.J. (2022). The enigma of phosphoinositides and their derivatives: Their role in regulation of subcellular compartment morphology. Biochim. Biophys. Acta BBA - Biomembr. *1864*, 183780. https://doi.org/10.1016/j.bbamem.2021.183780.

Lee, R.K.Y., Lui, P.P.Y., Ngan, E.K.S., Lui, J.C.K., Suen, Y.K., Chan, F., and Kong, S.K. (2006). The nuclear tubular invaginations are dynamic structures inside the nucleus of HeLa cellsThis paper is one of a selection of papers published in this Special Issue, entitled The Nucleus: A Cell Within A Cell. Can. J. Physiol. Pharmacol. *84*, 477–486. https://doi.org/10.1139/y05-110.

Legartová, S., Stixová, L., Laur, O., Kozubek, S., Sehnalová, P., and Bártová, E. (2014). Nuclear Structures Surrounding Internal Lamin Invaginations. J. Cell. Biochem. *115*, 476–487. https://doi.org/10.1002/jcb.24681.

Lehtinen, J., Munkberg, J., Hasselgren, J., Laine, S., Karras, T., Aittala, M., and Aila, T. (2018). Noise2Noise: Learning Image Restoration without Clean Data. ArXiv180304189 Cs Stat.

Li, T., Liu, M., and Pei, D. (2019). Friend or foe, the role of EGR-1 in cancer. Med. Oncol. *37*, 7. https://doi.org/10.1007/s12032-019-1333-6.

Liu, L., Luo, Q., Sun, J., and Song, G. (2016). Nucleus and nucleus-cytoskeleton connections in 3D cell migration. Exp. Cell Res. *348*, 56–65. https://doi.org/10.1016/j.yexcr.2016.09.001.

Lonsdale, J., Thomas, J., Salvatore, M., Phillips, R., Lo, E., Shad, S., Hasz, R., Walters, G., Garcia, F., Young, N., et al. (2013). The Genotype-Tissue Expression (GTEx) project. Nat. Genet. *45*, 580–585. https://doi.org/10.1038/ng.2653.

Love, M.I., Huber, W., and Anders, S. (2014). Moderated estimation of fold change and dispersion for RNA-seq data with DESeq2. Genome Biol. *15*. https://doi.org/10.1186/s13059-014-0550-8.

Lui, P.P.Y., Chan, F.L., Suen, Y.K., Kwok, T.T., and Kong, S.K. (2003). The nucleus of HeLa cells contains tubular structures for Ca2+ signaling with the involvement of mitochondria. Biochem. Biophys. Res. Commun. *308*, 826–833. https://doi.org/10.1016/S0006-291X(03)01469-4.

Lungu, O.I., Hallett, R.A., Choi, E.J., Aiken, M.J., Hahn, K.M., and Kuhlman, B. (2012). Designing Photoswitchable Peptides Using the AsLOV2 Domain. Chem. Biol. *19*, 507–517. https://doi.org/10.1016/j.chembiol.2012.02.006.

Luo, W., Friedman, M., Shedden, K., Hankenson, K., and Woolf, P. (2009). GAGE: generally applicable gene set enrichment for pathway analysis. BMC Bioinformatics *10*, 161. .

Lyengar, G.S. (1998). Yoga: A Gem for Women (Allied Publishers Pvt).

Malhas, A., Goulbourne, C., and Vaux, D.J. (2011). The nucleoplasmic reticulum: form and function. Trends Cell Biol. *21*, 362–373. https://doi.org/10.1016/j.tcb.2011.03.008.

Malhas, A.N., Lee, C.F., and Vaux, D.J. (2009). Lamin B1 controls oxidative stress responses via Oct-1. J. Cell Biol. *184*, 45–55. https://doi.org/10.1083/jcb.200804155.

Marius, P., Guerra, M.T., Nathanson, M.H., Ehrlich, B.E., and Leite, M.F. (2006). Calcium release from ryanodine receptors in the nucleoplasmic reticulum. Cell Calcium *39*, 65–73. https://doi.org/10.1016/j.ceca.2005.09.010.

Martelli, A.M., Evangelisti, C., Nyakern, M., and Manzoli, F.A. (2006). Nuclear protein kinase C. Biochim. Biophys. Acta *1761*, 542–551. https://doi.org/10.1016/j.bbalip.2006.02.009.

Matsumoto, A., and Hanawalt, P.C. (2000). Histone H3 and heat shock protein GRP78 are selectively cross-linked to DNA by photoactivated gilvocarcin V in human fibroblasts. Cancer Res. *60*, 3921–3926. .

Mauger, J.-P. (2012). Role of the nuclear envelope in calcium signalling. Biol. Cell *104*, 70–83. https://doi.org/10.1111/boc.201100103.

Mavlyutov, T.A., Yang, H., Epstein, M.L., Ruoho, A.E., Yang, J., and Guo, L.-W. (2017). APEX2-enhanced electron microscopy distinguishes sigma-1 receptor localization in the nucleoplasmic reticulum. Oncotarget *8*, 51317–51330. https://doi.org/10.18632/oncotarget.17906.

McEvoy, A.L., Hoi, H., Bates, M., Platonova, E., Cranfill, P.J., Baird, M.A., Davidson, M.W., Ewers, H., Liphardt, J., and Campbell, R.E. (2012). mMaple: A Photoconvertible Fluorescent Protein for Use in Multiple Imaging Modalities. PLOS ONE *7*, e51314. https://doi.org/10.1371/journal.pone.0051314.

Méndez-López, I., and Worman, H.J. (2012). Inner nuclear membrane proteins: Impact on human disease. Chromosoma *121*, 153–167. https://doi.org/10.1007/s00412-012-0360-2.

Miller, K.E., Kim, Y., Huh, W.-K., and Park, H.-O. (2015). Bimolecular fluorescence complementation (BiFC) analysis: advances and recent applications for genome-wide interaction studies. J. Mol. Biol. *427*, 2039–2055. https://doi.org/10.1016/j.jmb.2015.03.005.

Navarro, C.L., Cau, P., and Lévy, N. (2006). Molecular bases of progeroid syndromes. Hum. Mol. Genet. *15*, R151–R161. https://doi.org/10.1093/hmg/ddl214.

Nejat, E.J., Szmyga, M.J., Zapantis, G., and Meier, U.T. (2014). Progesterone Threshold Determines Nucleolar Channel System Formation in Human Endometrium. Reprod. Sci. *21*, 915–920. https://doi.org/10.1177/1933719113519177.

Nemergut, M.E., Mizzen, C.A., Stukenberg, T., Allis, C.D., and Macara, I.G. (2001). Chromatin Docking and Exchange Activity Enhancement of RCC1 by Histones H2A and H2B. Science https://doi.org/10.1126/science.292.5521.1540.

Niopek, D., Benzinger, D., Roensch, J., Draebing, T., Wehler, P., Eils, R., and Di Ventura, B. (2014). Engineering light-inducible nuclear localization signals for precise spatiotemporal control of protein dynamics in living cells. Nat. Commun. *5*, 4404. https://doi.org/10.1038/ncomms5404.

Niopek, D., Wehler, P., Roensch, J., Eils, R., and Di Ventura, B. (2016). Optogenetic control of nuclear protein export. Nat. Commun. *7*, 10624. https://doi.org/10.1038/ncomms10624.

Nishida, M., Kasahara, K., Kaneko, M., Iwasaki, H., and Hayashi, K. (1985). Establishment of a new human endometrial adenocarcinoma cell line, Ishikawa cells, containing estrogen and progesterone receptors. Acta Obstet. Gynaecol. Jpn. *37*, 1103–1111. .

Ohsaki, Y., Kawai, T., Yoshikawa, Y., Cheng, J., Jokitalo, E., and Fujimoto, T. (2016). PML isoform II plays a critical role in nuclear lipid droplet formation. J. Cell Biol. *212*, 29–38. https://doi.org/10.1083/jcb.201507122.

Olins, A.L., Rhodes, G., Welch, D.B.M., Zwerger, M., and Olins, D.E. (2010). Lamin B receptor. Nucleus *1*, 53–70. https://doi.org/10.4161/nucl.1.1.10515.

P. Milanfar (2021).

Padiath, Q.S. (2006). Lamin B1 duplications cause autosomal dominant leukodystrophy. Nat. Genet *38*, 1114–1123. .

Passarelli, M.K., Pirkl, A., Moellers, R., Grinfeld, D., Kollmer, F., Havelund, R., Newman, C.F., Marshall, P.S., Arlinghaus, H., Alexander, M.R., et al. (2017). The 3D OrbiSIMS—

label-free metabolic imaging with subcellular lateral resolution and high mass-resolving power. Nat. Methods *14*, 1175–1183. https://doi.org/10.1038/nmeth.4504.

Peddie, C.J., Blight, K., Wilson, E., Melia, C., Marrison, J., Carzaniga, R., Domart, M.-C., O'Toole, P., Larijani, B., and Collinson, L.M. (2014). Correlative and integrated light and electron microscopy of in-resin GFP fluorescence, used to localise diacylglycerol in mammalian cells. Ultramicroscopy *143*, 3–14. https://doi.org/10.1016/j.ultramic.2014.02.001.

Peeters, B.W.A., Piët, A.C.A., and Fornerod, M. (2022). Generating Membrane Curvature at the Nuclear Pore: A Lipid Point of View. Cells *11*, 469. https://doi.org/10.3390/cells11030469.

Plačkić, J., Preissl, S., Nikonova, Y., Pluteanu, F., Hein, L., and Kockskämper, J. (2016). Enhanced nucleoplasmic Ca2+ signaling in ventricular myocytes from young hypertensive rats. J. Mol. Cell. Cardiol. *101*, 58–68. https://doi.org/10.1016/j.yjmcc.2016.11.001.

Pontén, F., Jirström, K., and Uhlen, M. (2008). The Human Protein Atlas—a tool for pathology. J. Pathol. *216*, 387–393. https://doi.org/10.1002/path.2440.

Popken, J., Graf, A., Krebs, S., Blum, H., Schmid, V.J., Strauss, A., Guengoer, T., Zakhartchenko, V., Wolf, E., and Cremer, T. (2015). Remodeling of the Nuclear Envelope and Lamina during Bovine Preimplantation Development and Its Functional Implications. PLOS ONE *10*, e0124619. https://doi.org/10.1371/journal.pone.0124619.

Popken, J., SCHMID, V.J., STRAUSS, A., GUENGOER, T., WOLF, E., and ZAKHARTCHENKO, V. (2016). Stage-dependent remodeling of the nuclear envelope and lamina during rabbit early embryonic development. J. Reprod. Dev. *62*, 127–135. https://doi.org/10.1262/jrd.2015-100.

Pryse-Davies, J., Ryder, T.A., and Lynn MacKenzie, M. (1979). In vivo production of the nucleolar channel system in post menopausal endometrium. Cell Tissue Res. *203*, 493–498. https://doi.org/10.1007/bf00233277.

Pytowski, Drozdz, Jiang, Hernandez, Kumar, Knott, and Vaux (2019). Nucleoplasmic Reticulum Formation in Human Endometrial Cells is Steroid Hormone Responsive and Recruits Nascent Components. Int. J. Mol. Sci. *20*, 5839. https://doi.org/10.3390/ijms20235839.

Raharjo, W.H., Enarson, P., Sullivan, T., Stewart, C.L., and Burke, B. (2001). Nuclear envelope defects associated with LMNA mutations cause dilated cardiomyopathy and Emery-Dreifuss muscular dystrophy. J Cell Sci *114*, 4447–4457. .

Rampello, A.J., Prophet, S.M., and Schlieker, C. (2020). The Role of Torsin AAA+ Proteins in Preserving Nuclear Envelope Integrity and Safeguarding Against Disease. Biomolecules *10*, 468. https://doi.org/10.3390/biom10030468.

Ran, F.A., Hsu, P.D., Lin, C.-Y., Gootenberg, J.S., Konermann, S., Trevino, A.E., Scott, D.A., Inoue, A., Matoba, S., Zhang, Y., et al. (2013). Double Nicking by RNA-Guided CRISPR Cas9 for Enhanced Genome Editing Specificity. Cell *154*, 1380–1389. https://doi.org/10.1016/j.cell.2013.08.021.

Rappa, G., Santos, M.F., Green, T.M., Karbanová, J., Hassler, J., Bai, Y., Barsky, S.H., Corbeil, D., and Lorico, A. (2017). Nuclear transport of cancer extracellular vesicle-derived biomaterials through nuclear envelope invagination-associated late endosomes. Oncotarget *8*, 14443–14461. https://doi.org/10.18632/oncotarget.14804.

Resseguie, M., Song, J., Niculescu, M.D., da Costa, K.-A., Randall, T.A., and Zeisel, S.H. (2007). Phosphatidylethanolamine N-methyltransferase (PEMT) gene expression is induced by estrogen in human and mouse primary hepatocytes. FASEB J. Off. Publ. Fed. Am. Soc. Exp. Biol. *21*, 2622–2632. https://doi.org/10.1096/fj.07-8227com.

Rybak, E.A., Szmyga, M., Zapantis, G., Rausch, M., Beshay, V.E., Polotsky, A.J., Coutifaris, C., Carr, B.R., Santoro, N., and Meier, U.T. (2011). The nucleolar channel system reliably marks the midluteal endometrium regardless of fertility status: a fresh look at an old organelle. Fertil. Steril. *95*, 1385-9.e1. https://doi.org/10.1016/j.fertnstert.2010.10.030.

Salina, D., Bodoor, K., Eckley, D.M., Schroer, T.A., Rattner, J.B., and Burke, B. (2002). Cytoplasmic Dynein as a Facilitator of Nuclear Envelope Breakdown. Cell *108*, 97–107. https://doi.org/10.1016/S0092-8674(01)00628-6.

Saltel, F., Giese, A., Azzi, L., Elatmani, H., Costet, P., Ezzoukhry, Z., Dugot-Senant, N., Miquerol, L., Boussadia, O., and Wodrich, H. (2017). Unr defines a novel class of nucleoplasmic reticulum involved in mRNA translation. J Cell Sci *130*, 1796–1808. .

Santos, M.F., Rappa, G., Karbanová, J., Kurth, T., Corbeil, D., and Lorico, A. (2018). VAMP-associated protein-A and oxysterol-binding protein–related protein 3 promote the entry of late endosomes into the nucleoplasmic reticulum. J. Biol. Chem. *293*, 13834–13848. https://doi.org/10.1074/jbc.RA118.003725.

Santos, M.F., Rappa, G., Karbanová, J., Fontana, S., Bella, M.A.D., Pope, M.R., Parrino, B., Cascioferro, S.M., Vistoli, G., Diana, P., et al. (2021). Itraconazole inhibits nuclear delivery of extracellular vesicle cargo by disrupting the entry of late endosomes into the nucleoplasmic reticulum. J. Extracell. Vesicles *10*, e12132. https://doi.org/10.1002/jev2.12132.

Schindelin, J., Arganda-Carreras, I., Frise, E., Kaynig, V., Longair, M., Pietzsch, T., Preibisch, S., Rueden, C., Saalfeld, S., Schmid, B., et al. (2012). Fiji: an open-source platform for biological-image analysis. Nat. Methods *9*, 676. https://doi.org/10.1038/nmeth.2019.

Schindelin, J., Rueden, C.T., Hiner, M.C., and Eliceiri, K.W. (2015). The ImageJ ecosystem: An open platform for biomedical image analysis. Mol. Reprod. Dev. *82*, 518–529. https://doi.org/10.1002/mrd.22489.

Schirmer, E.C. (2003). Nuclear membrane proteins with potential disease links found by subtractive proteomics. Science *301*, 1380–1382. .

Schirmer, E.C., and Gerace, L. (2005). The nuclear membrane proteome: extending the envelope. Trends Biochem. Sci. *30*, 551–558. https://doi.org/10.1016/j.tibs.2005.08.003.

Schmidt, U., Weigert, M., Broaddus, C., and Myers, G. (2018). Cell Detection with Star-convex Polygons. ArXiv180603535 Cs *11071*, 265–273. https://doi.org/10.1007/978-3-030-00934-2_30.

Schoen, I., Aires, L., Ries, J., and Vogel, V. (2017). Nanoscale invaginations of the nuclear envelope: Shedding new light on wormholes with elusive function. Nucleus *0*, 1–9. https://doi.org/10.1080/19491034.2017.1337621.

Se, H., C, C., S, M., Lg, F., Sg, Y., and Ca, H. (2008). HIV-protease inhibitors block the enzymatic activity of purified Ste24p. Biochem. Biophys. Res. Commun. *374*. https://doi.org/10.1016/j.bbrc.2008.07.033.

Serebryannyy, L., and Misteli, T. (2017). Protein sequestration at the nuclear periphery as a potential regulatory mechanism in premature aging. J. Cell Biol. *217*, 21–37. https://doi.org/10.1083/jcb.201706061.

Shaner, N.C., Campbell, R.E., Steinbach, P.A., Giepmans, B.N.G., Palmer, A.E., and Tsien, R.Y. (2004). Improved monomeric red, orange and yellow fluorescent proteins derived from Discosoma sp. red fluorescent protein. Nat. Biotechnol. *22*, 1567–1572. https://doi.org/10.1038/nbt1037.

Shaner, N.C., Lambert, G.G., Chammas, A., Ni, Y., Cranfill, P.J., Baird, M.A., Sell, B.R., Allen, J.R., Day, R.N., Israelsson, M., et al. (2013). A bright monomeric green fluorescent protein derived from Branchiostoma lanceolatum. Nat. Methods *10*, 407–409. https://doi.org/10.1038/nmeth.2413.

Shigdel, U.K., Zhang, J., and He, C. (2008). Diazirine-Based DNA Photo-Cross-Linking Probes for the Study of Protein–DNA Interactions. Angew. Chem. Int. Ed. *47*, 90–93. https://doi.org/10.1002/anie.200703625.

Sinensky, M. (1994). The processing pathway of prelamin A. J Cell Sci *107*, 61–67. .

Stoimenov, I., and Helleday, T. (2009). PCNA on the crossroad of cancer. Biochem. Soc. Trans. *37*, 605–613. https://doi.org/10.1042/BST0370605.

Strickland, D., Lin, Y., Wagner, E., Hope, C.M., Zayner, J., Antoniou, C., Sosnick, T.R., Weiss, E.L., and Glotzer, M. (2012). TULIPs: tunable, light-controlled interacting protein tags for cell biology. Nat. Methods *9*, 379–384. https://doi.org/10.1038/nmeth.1904.

Stringer, C., Michaelos, M., and Pachitariu, M. (2020). Cellpose: a generalist algorithm for cellular segmentation. BioRxiv 2020.02.02.931238. https://doi.org/10.1101/2020.02.02.931238.

Szentpetery, Z., Várnai, P., and Balla, T. (2010). Acute manipulation of Golgi phosphoinositides to assess their importance in cellular trafficking and signaling. Proc. Natl. Acad. Sci. U. S. A. *107*, 8225–8230. https://doi.org/10.1073/pnas.1000157107.

Terzakis, J.A. (1965). The nucleolar channel system of the human endometrium. J. Cell Biol. *27*, 293–304. .

Thul, P.J., Åkesson, L., Wiking, M., Mahdessian, D., Geladaki, A., Blal, H.A., Alm, T., Asplund, A., Björk, L., Breckels, L.M., et al. (2017). A subcellular map of the human proteome. Science https://doi.org/10.1126/science.aal3321.

Tollis, S., Rizzotto, A., Pham, N.T., Koivukoski, S., Sivakumar, A., Shave, S., Wildenhain, J., Zuleger, N., Keys, J.T., Culley, J., et al. (2022). Chemical Interrogation of Nuclear Size Identifies Compounds with Cancer Cell Line-Specific Effects on Migration and Invasion. ACS Chem. Biol. *17*, 680–700. https://doi.org/10.1021/acschembio.2c00004.

Turgay, Y., Champion, L., Balazs, C., Held, M., Toso, A., Gerlich, D.W., Meraldi, P., and Kutay, U. (2014). SUN proteins facilitate the removal of membranes from chromatin during nuclear envelope breakdown. J Cell Biol *204*, 1099–1109. https://doi.org/10.1083/jcb.201310116.

Uhlén, M., Fagerberg, L., Hallström, B.M., Lindskog, C., Oksvold, P., Mardinoglu, A., Sivertsson, Å., Kampf, C., Sjöstedt, E., Asplund, A., et al. (2015). Tissue-based map of the human proteome. Science https://doi.org/10.1126/science.1260419.

Uhlén, M., Zhang, C., Lee, S., Sjöstedt, E., Fagerberg, L., Bidkhori, G., Benfeitas, R., Arif, M., Liu, Z., Edfors, F., et al. (2017). A pathology atlas of the human cancer transcriptome. Science https://doi.org/10.1126/science.aan2507.

Ulloa, G., Hamati, F., Dick, A., Fitzgerald, J., Mantell, J., Verkade, P., Collinson, L., Arkill, K., Larijani, B., and Poccia, D. (2019). Lipid species affect morphology of endoplasmic reticulum: a sea urchin oocyte model of reversible manipulation. J. Lipid Res. *60*, 1880–1891. https://doi.org/10.1194/jlr.RA119000210.

Vance, J.E. (2015). Phospholipid Synthesis and Transport in Mammalian Cells. Traffic *16*, 1–18. https://doi.org/10.1111/tra.12230.

Varnai, P., Thyagarajan, B., Rohacs, T., and Balla, T. (2006). Rapidly inducible changes in phosphatidylinositol 4,5-bisphosphate levels influence multiple regulatory functions of the lipid in intact living cells. J. Cell Biol. *175*, 377–382. https://doi.org/10.1083/jcb.200607116.

Vella, S., and Floridia, M. (1998). Saquinavir. Clinical pharmacology and efficacy. Clin. Pharmacokinet. *34*. https://doi.org/10.2165/00003088-199834030-00002.

Vigouroux, C., and Capeau, J. (2005). A-type lamin-linked lipodystrophies. Novartis Found. Symp. *264*, 166–177. .

Voeltz, G.K., Prinz, W.A., Shibata, Y., Rist, J.M., and Rapoport, T.A. (2006). A class of membrane proteins shaping the tubular endoplasmic reticulum. Cell *124*, 573–586. http://dx.doi.org/10.1016/j.cell.2005.11.047.

Vorkel, D., and Haase, R. (2020). GPU-accelerating ImageJ Macro image processing workflows using CLIJ. ArXiv200811799 Cs Q-Bio.

Vos, W.H.D., Houben, F., Kamps, M., Malhas, A., Verheyen, F., Cox, J., Manders, E.M.M., Verstraeten, V.L.R.M., Steensel, M.A.M. van, Marcelis, C.L.M., et al. (2011). Repetitive disruptions of the nuclear envelope invoke temporary loss of cellular compartmentalization in laminopathies. Hum. Mol. Genet. *20*, 4175–4186. https://doi.org/10.1093/hmg/ddr344.

Wang, N., and Rapoport, T.A. (2019). Reconstituting the reticular ER network – mechanistic implications and open questions. J. Cell Sci. *132*, jcs227611. https://doi.org/10.1242/jcs.227611.

Wang, A.S., Kundu, A., Fong, B., Fitzgerald, J., Larijani, B., and Poccia, D. (2013). A Structural Role for Lipids in Organelle Shaping. Biol. Bull. *224*, 218–226. https://doi.org/10.1086/BBLv224n3p218.

Wang, Y., Lichter-Konecki, U., Anyane-Yeboa, K., Shaw, J.E., Lu, J.T., Östlund, C., Shin, J.-Y., Clark, L.N., Gundersen, G.G., Nagy, P.L., et al. (2016). A mutation abolishing the ZMPSTE24 cleavage site in prelamin A causes a progeroid disorder. J. Cell Sci. *129*, 1975–1980. https://doi.org/10.1242/jcs.187302.

Weberruss, M., and Antonin, W. (2016). Perforating the nuclear boundary – how nuclear pore complexes assemble. J. Cell Sci. *129*, 4439–4447. https://doi.org/10.1242/jcs.194753.

Weigert, M., Schmidt, U., Boothe, T., Müller, A., Dibrov, A., Jain, A., Wilhelm, B., Schmidt, D., Broaddus, C., Culley, S., et al. (2018). Content-aware image restoration: pushing the limits of fluorescence microscopy. Nat. Methods 1. https://doi.org/10.1038/s41592-018-0216-7.

Weigert, M., Schmidt, U., Haase, R., Sugawara, K., and Myers, G. (2020). Star-convex Polyhedra for 3D Object Detection and Segmentation in Microscopy. In 2020 IEEE Winter Conference on Applications of Computer Vision (WACV), (Snowmass Village, CO, USA: IEEE), pp. 3655–3662.

Wong, X., Loo, T.-H., and Stewart, C.L. (2021). LINC complex regulation of genome organization and function. Curr. Opin. Genet. Dev. *67*, 130–141. https://doi.org/10.1016/j.gde.2020.12.007.

Worman, H.J. (2011). Nuclear lamins and laminopathies. J. Pathol. *226*, 316–325. https://doi.org/10.1002/path.2999.

Worman, H.J., and Schirmer, E.C. (2015). Nuclear membrane diversity: underlying tissue-specific pathologies in disease? Curr. Opin. Cell Biol. *34*, 101–112. http://dx.doi.org/10.1016/j.ceb.2015.06.003.

Worman, H.J., Östlund, C., and Wang, Y. (2010). Diseases of the Nuclear Envelope. Cold Spring Harb. Perspect. Biol. *2*. https://doi.org/10.1101/cshperspect.a000760.

Wynn, R.M. (1967). Intrauterine devices: effects on ultrastructure of human endometrium. Science *156*, 1508–1510. https://doi.org/10.2307/1722345.

Yang, Y.S., and Strittmatter, S.M. (2007). The reticulons: a family of proteins with diverse functions. Genome Biol. *8*, 234. https://doi.org/10.1186/gb-2007-8-12-234.

Ye, Q., and Worman, H.J. (1994). Primary structure analysis and lamin B and DNA binding of human LBR, an integral protein of the nuclear envelope inner membrane. J. Biol. Chem. *269*, 11306–11311. .

Zhang, H., Kho, A.T., Wu, Q., Halayko, A.J., Limbert Rempel, K., Chase, R.P., Sweezey, N.B., Weiss, S.T., and Kaplan, F. (2016). CRISPLD2 (LGL1) inhibits proinflammatory mediators in human fetal, adult, and COPD lung fibroblasts and epithelial cells. Physiol. Rep. *4*, e12942. https://doi.org/10.14814/phy2.12942.

Zhang, W., Lohman, A.W., Zhuravlova, Y., Lu, X., Wiens, M.D., Hoi, H., Yaganoglu, S., Mohr, M.A., Kitova, E.N., Klassen, J.S., et al. (2017). Optogenetic control with a photocleavable protein, PhoCl. Nat. Methods *advance online publication*. https://doi.org/10.1038/nmeth.4222.